Development of Nanoarrayed Surfaces for improved SPR detection of Biomolecular Recognition

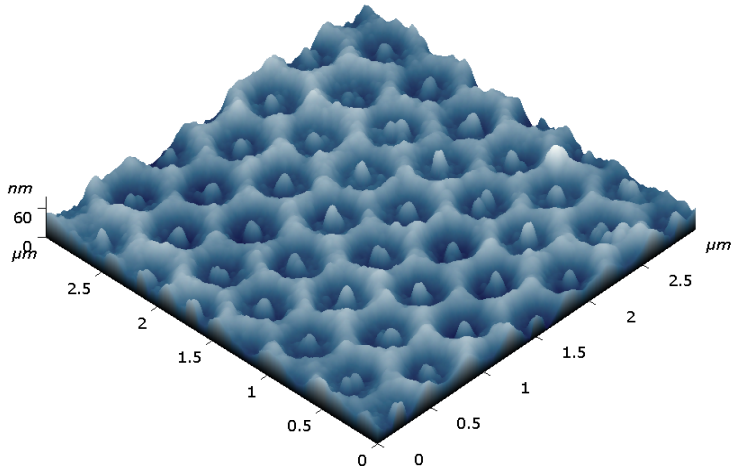

Patrícia Lisboa

Scienze Chimiche

Ciclo XXI
2008

Università degli Studi di Firenze

Table of Contents

Table of Contents

1 Introduction

1.1 Outline

The aim of the thesis concerns the development of nanoarrayed surfaces enabling to control spatially protein immobilisation at nanoscale on nano-areas and their application in SPRi detection of biomolecular recognition reactions.

In a first part is described the state of the art on biomolecular recognition and nanoarrays sensing platforms. The general aspects, such as materials, apparatus and procedures used in biomolecular recognition will be detailed and the different methodologies for the fabrication of nanoarrays and their application in biomolecular recognition are reported. Particularly the effect of optical gratings in optical detection will be described.

In a second part, the fabrication and characterisation of two different types of nanoarrays will be described; one being based on organothiols chemistry and the other based on polypyrrole (PPy) electropolymerisation.

Finally is reported the nanoarrayed surfaces as sensing platform for Surface Plasmon Resonance imaging (SPRi) will be studied to evaluate the effect of an optical grating on the detection of an immunoreaction.

1.2 Biomolecular Recognition and Biosensors Challenges

Topics related to healthcare system, security and environment are the main concerns of the citizens and their governments. Issues related to climate change are becoming more and more important for the Europeans citizens who consider that European policies should have as main priorities environmental issues together with territorial defence and scientific research (Eurobarometer 2008). These concerns give directions to the research of many institutions, among them; Biosensors and biomolecular recognition detection are becoming one of most popular research topics.

For instance, the traditional diagnosis techniques used for critical diseases like cancer, are often time consuming and therefore too slow and in many cases not enough sensitive for early diagnostic. This fact really evidenced the need to develop improved and innovative methods for screening dieses, providing earlier diagnosis and prognostics (Rasooly 2006). The successful development of such advanced detection methodologies will with no doubt improve the health care system, by improving the positive out comes of the patient and reducing therapy costs by treating diseases in their earlier stages.

Besides, in the field of food /agriculture there is an increased need to control the quality and safety of the products. The implementation of HACCP (Hazard Analysis Critical Control Point) systems enabling to identify and prevent specific hazards requires rapid, sensitive and accurate methods for the detection of contaminant (Ricci 2007). A recent concern is the detection of biohazards in the environment for protection against bioterrorism (Luong 2008; Rodriguez-Mozaz 2005) which requires the development of fast and precise detection systems.

Sensors based on biomolecular recognition (i.e. biosensors), are very promising to fulfil these requirements by developing high sensitive, fast and low cost devices.

The amount of publications and patents in the last years about this issue is enormous compared to the real commercial applications (Kissinger 2005). The first publications presenting a biosensor concept (Clark 1962; Guilbault 1969; Updike 1967) were the basis for the commercialisation of a glucose pen and still the glucose sensors are the most successful example of the few commercial achievements. The reason for the success of glucose sensors is related to the fact that the detection range of interest is high (milimolar) and as well because the oxidize enzymes used present high stability and specificity (Gramsbergen 2003; Parkin 2003; Wilson 2005; Yang 2001; Yu 2000). Not all the analytes present these favourable characteristics and this is why for many cases the biosensors developed in the laboratory have not sufficient performance and reliability to reach the market place.

.

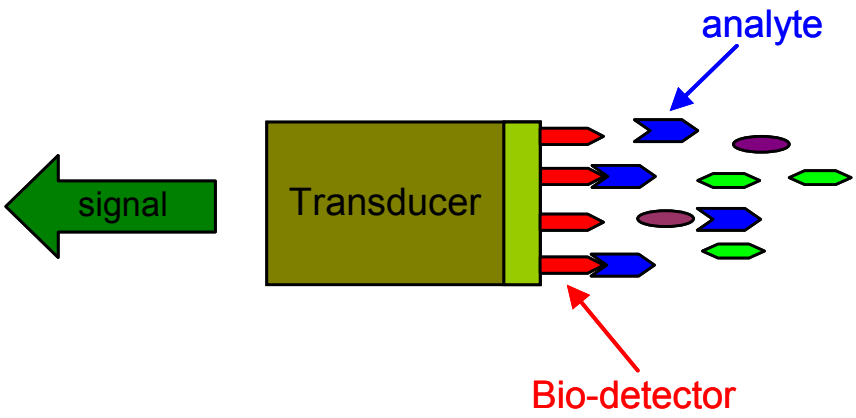

Figure 1.1- Schema of a Biosensor.

Many issues still need to be addressed to improve biosensor performance such as sensitivity, specificity and cross reaction control, for their practical application. In particular real clinical or environmental samples have a complexity far from the models used in the laboratory (Luppa 2001; Coughlin 2002; Luong 2008).

Biosensors are composed of three main parts (Figure 1.1), the bio-detector (enzyme, DNA, protein) that detects the analyte, the transducer that converts the biomolecular recognition into a measurable signal and a readout system that records and analyses the transduced signal (Raiteri 2002).

The transducers have inherent detection performance and must be chosen as a function of the better association between the type of detection (optical, electrochemical, and piezoelectric) and the biosensor format (biomolecular recognition system, surface modification) in order to ensure good sensing performance (Fan 2008).

Nevertheless one of the fundamental issues for the successful use of a biosensor is related to the so-called bio-interface. Bio-interface is the location where the biomolecules interact with the surface and where the biomolecular recognition process occurs. The main challenge is to design a well controlled bio-interface that allows the immobilisation of the bio-probes in an active state to promote efficient biomolecular recognition. The immobilisation of the bio-detector plays a fundamental role in the sensing performance. The bio-detector must be immobilised maintaining its reactivity on the transducer surface and promoting high affinity and specificity of the bio-detector/analyte reaction to guaranty good limit of detection and specificity.

Surfaces can be functionalised with a range of different reactive functional groups (amine, carboxyl, epoxide, polyethylene oxide) that are appropriate for the biodetector immobilisation. Then, the immobilisation of the bio-receptors on the surface can be carried out by different approaches from fast and less stable processes (physical

adsorption) to more complex and more robust ones (covalent binding, biological interactions) (Bilitewski 2006).

A recent promising approach to improve the detection of biomolecular recognition is the functionalisation of surfaces with chemical nano-contrasts (Agheli 2006; Frederix 2004 B; Rosi 2005; Valsesia 2006). These surfaces are characterised by nano-spots with bio-adhesive materials most commonly based on carboxylic, amine or epoxy chemistry distributed in a matrix of a non adhesive material commonly based in polyethylene oxide chemistry. This surface arrangement promotes the selective immobilisation of the bio-detector in the adhesive spots creating patterns of biomolecules distributed over the surface. Biomolecular recognition performed on this type of surfaces is improved by reduction of steric hindrance and better availability of the binding sites. Even if the reasons are not yet elucidated, the fact that the active area and the analyte (proteins) have comparable dimensions influence thermodynamically and kinetically the immobilisation mechanism resulting in an improvement of binding site availability for the biomolecular recognition (Valsesia 2008 B). Finally when the patterns are geometrically organised in the surface (nanoarrays) the surfaces present special optical and electric properties that can be use for improvements of optical and electrochemical detection (Arrigan 2004; Barnes 2003).

Surface Plasmon Resonance (SPR) is a label-free optical technique that allows quantitative analysis in real time and provides outstanding detection performances (Cooper 2006; Grosjean 2005; Löfås 1990; Rich 2007). In the last 5 years the SPR became one of the elected techniques for biomolecular recognition detection, being applied in biosensing for medical diagnosis, environmental monitoring and food safety (Schasfoort 2008). Optical detection systems like SPR are expected to be a future powerful tool in real time and high sensitivity detection, multiple analyte testing and integrated devices (Hoa 2007; Homola 2008).

The evolution of SPR bio-sensing performance is correlated with the type of surface chemistry applied in the system. A chemistry that avoids non-specific binding and that promotes good immobilisation of the bio-detector is essential for improving the SPR sensor performance. Nano-patterning the metallic thin films of the SPR interface with the adhesive/non-adhesive features distributed in a crystalline geometry not only contributes to achieve the improvements described before but also creates unique optical characteristics that can excite the surface plasmons, producing a detection signal enhancement (Barnes 2003; Cole 2007; Dintinger 2005).

1.3 Aim of the Thesis

The aim of the thesis concerns the development of nanoarrayed surfaces based on organothiols and PPy and their use in immunoreaction detection with SPRi.

The production of the organothiols nanoarray has the objective to create a surface with a geometrically organised bio-adhesive/non-adhesive nano-contrast able to induce selective immobilisation of proteins in the specific adhesive areas. The PPy nanoarray had the objective to create an array already modified with the bio-detector in specific spots of the surface creating an organised geometric distribution of proteins. The fabrication of the nanoarrays is based on colloidal lithography. In both types of surfaces polystyrene nano beads were used as nano-mask. The conditions of beads deposition and etching have been optimised in order to obtain the best surface coverage, a crystalline arrangement and well defined nano-areas.

The Thiolated PEO like films used as non-adhesive layer have been developed and synthesised during this thesis and combined with bio adhesive organothiols to produce

the nanoarrays. The two materials used in the nanoarray were characterised separately in order to determine their chemical, physical and bio-adhesive characteristics.

The PPy deposition was studied by electrospotting of pyrrole modified with proteins or peptides.

The nanoarrays have then been used as SPRi detection platform with two mains objectives: To improve the bioactivity of the bio-detectors on the surface by a better availability of the binding sites, induced by the confinement immobilisation in the nano-areas; and to improve the sensing sensitivity by creating an optical grating based on proteins at the interface of the SPRi chip. To evaluate the SPRi performance, the nanoarrays were produced on the SPRi chip surface and were used to study different immunoreaction formats. The performance of these surfaces was compared with uniformly functionalised surfaces and randomly organised nano-patterns.

1.4 Thesis Structure

The thesis is divided in 8 chapters and each of the chapters is briefly described below.

Chapter 1 (Introduction) provides the framing of this thesis studies starting with general presentation of the specific problems in biomolecular recognition detection.

Chapter 2 (State of the Art) explains the theory related with biomolecular recognition systems and applied transducers, surface functionalisation techniques, nanofabrication, nanoarrays in biomolecular recognition, surface plasmon resonance and optical gratings in SPRi detection.

Chapter 3 (Materials and Methods) gives the details related to the different materials, procedures, instruments and techniques used in the different studies of the thesis.

Chapter 4 (Production of Nanoarrays based in Organothiols) describes the synthesis and characterisation of the thiolated PEO used in the production of the nanoarray. In this chapter is also described the chemical, physical and bio-adhesive properties of a layer of thiolated PEO and carboxylic organothiols deposit on gold. Finally, the study of the production and characterisation of the organothiols nanoarrays is presented.

Chapter 5 (SPRi studies of an immunoreaction using Nanoarrayed organothiols surface) presents the study of nanoarrayed organothiols surface effect on SPRi detection performance. The study is based on the detection of an immunoreaction by using model immunoglobulin antibodies (Human IgG/anti-Human IgG). In a second part an AFM study simulating the SPRi experiments is described.

Chapter 6 (Production of Nanoarrays based in PPy) presents the production and characterisation of the PPy nanoarray. First the fabrication of a nano-template based in gold holes and SiOx matrix is described and second, the electrochemical growth of the PPy in the gold holes creating the PPy array is reported.

Chapter 7 (SPRi studies of an immunoreaction using Nanoarrayed PPy) is related to the study of nanoarrayed PPy surface effect on SPRi detection performance. The study is based on the detection of an immunoreaction based in proteins and peptide

detection models (Ovalbumin/anti-Ovalbumin, Casein/anti-Casein and peptide C131-150/anti-C131-150).

Chapter 8 (Conclusions) is dedicated to the general conclusions of the work developed within this thesis and to some future work proposals to develop and profit from the described study.

2 State of the Art

2.1 Biomolecular Recognition systems

Biomolecular recognition is the key issue for the reliability of a biosensor. The degree of specificity and affinity of the bio-recognition process is crucial for the performance of analyte detection. There are two main types of bio-systems applied in sensing, bio-catalytic and bio-affinity. The first type has been the most popular approach in the first generation of biosensors and still is the most sensitive and reliable device. Nevertheless, during the last 15 years the development of bio-affinity systems has been increasing due to their promising characteristics (Luong 2008).

2.1.1 Bio-catalytic sensors

These systems exploit catalysed bio-reaction by macromolecules that are immobilised on the surface detector and are continuously consuming a substrate. The most common bio-catalysts used are enzymes (Thévenot 2001) and are generally applied in electrochemical based transducers. Most of the enzyme systems used are based in oxidoreductases, glucose oxidase, horseradish peroxidase and alkaline phosphatase (Laschi 2000; Rogers 1998; Wang and 2000). The bio-reaction is based on a substrate (analyte) that reacts in the presence of an enzyme resulting in the production of one or several products that are proportional to the analyte concentration. The main problems associate with enzymes is their low stability and the difficulty in maintaining a long life activity (D'Orazio 2003). Electroactive interferences can as well become significant and create the need of finding additional strategies that will result in more complex systems. Until now Glucose oxidase is the most stable and specific enzyme and can be obtain easily and in high quantities (Luong 2008).

2.1.2 Bio-affinity sensors

Bio-affinity systems are mainly based on the binding reaction between antibodies and antigens (immunosensors) or in DNA hybridisation to complementary nucleic acid sequences (genosensors).

In genosensors the bio-detector is usually a short oligonucleotide (DNA probe) immobilised on the surface matrix that is complementary to the analyte (target DNA). The DNA probe is usually synthesised and variables like chemical composition and conformational arrangement can be achieved depending on the analytical purpose. Usually the sample is pre-treated by polymerase chain reaction (PCR) amplification in order to reduce its complexity and increase the target concentration (Lucarelli 2008). The most used detection methods for the detection of hybridisation reaction are SPR, piezoelectric and electrochemistry sensors (Lucarelli 2008; Luong 2008; Spangler 2001). The good stability of the probes and the efficient immobilisation together with successful sensor regeneration promote the continuous development of systems based on hybridisation reactions (Navani 2006). However it is still a challenge to develop methodologies that allow the detection of natural DNA present in organisms or human blood with high sensitivity (Drummond 2003; Mascini 2005; Minunni 2004; Paleček 2002).

Immunosensors have as bio-detector an antibody immobilised on the surface matrix that has high specificity for the analyte (antigen). The detection of the analyte is based in the antibody-antigen reaction output. Figure 2.1 Shows the typical Y-shape structure of a conventional Immunoglobulin (IgG) antibody, where is represented the light and heavy chains and the Fc (fragment crystallised) and Fab (fragment antibody). The Fab fragment has the two binding sites which present the combination of amino acids that are specific for the recognition of the antigen(Silverton 1977).

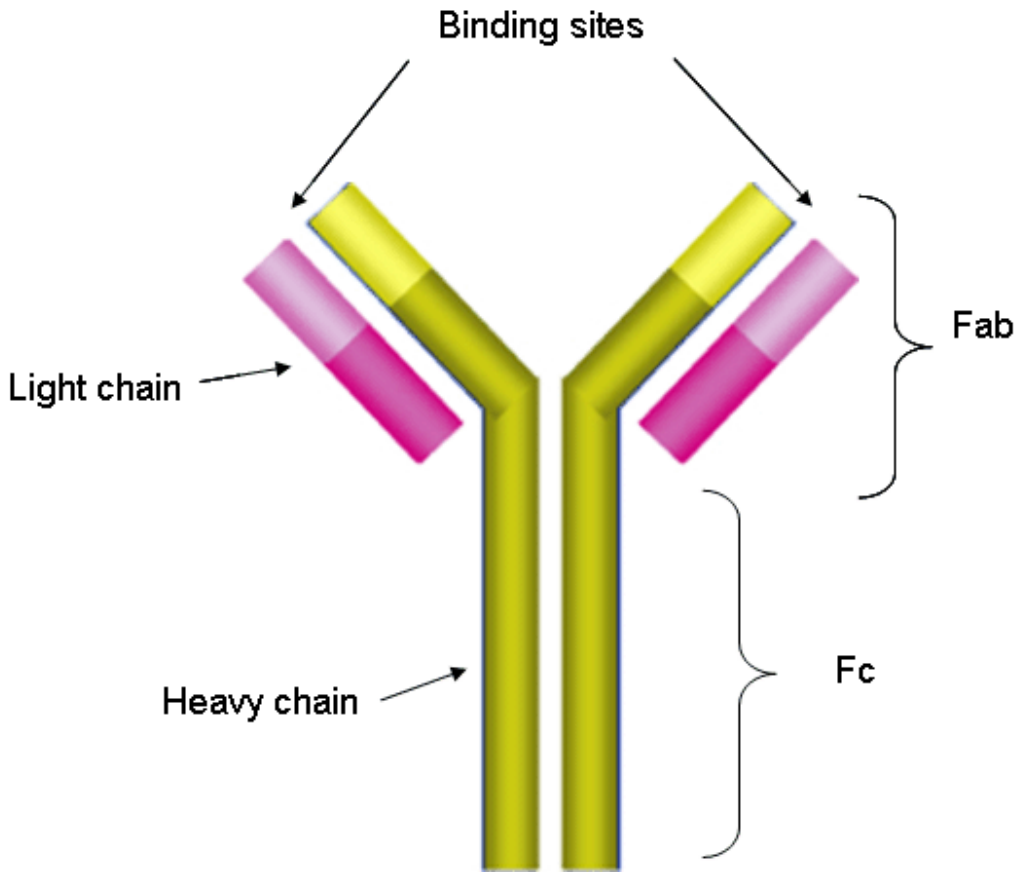

Figure 2.1- Scheme of a conventional IgG antibody.

Most of the immunosensors are based in labelled methods like competitive and sandwich assays, having in most cases an enzyme as label. Competitive assays have antibodies immobilised on the surface that will react with free antigens in competition with labelled antigens. The labelled and unlabeled antigens compete for a limited number of antibody binding sites (Figure 2.2). A Sandwich Immunoassay is a method using two antibodies, which bind to different sites on the antigen. The highly specific antibody in immobilised in the surface and the then the antigen is added followed by addition of a second labelled antibody. As a result the antigen is 'sandwiched' between the two antibodies (Figure 2.2).

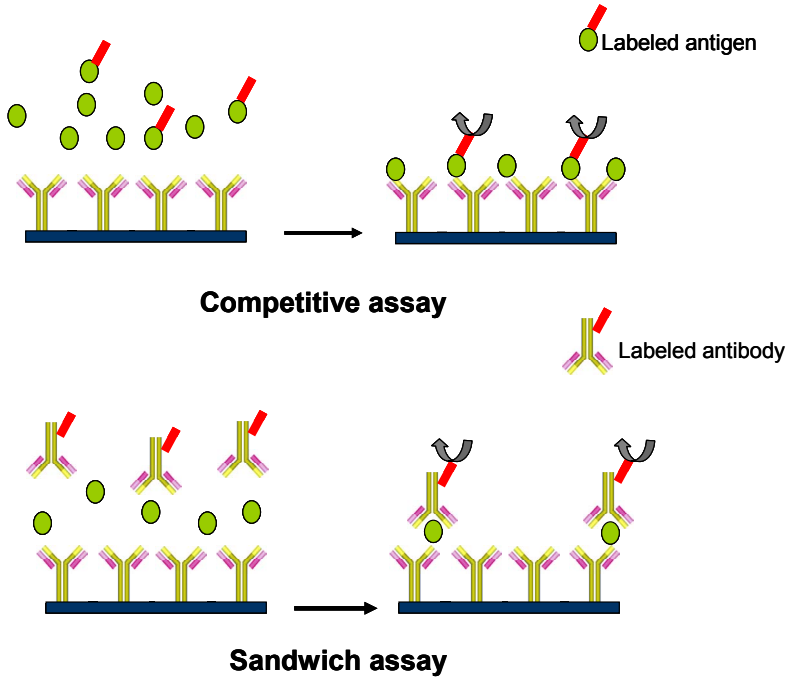

Figure 2.2- Schema representing the most common immunoassays applied in bio-sensing.

Label free immunosensors are mostly associated with SPR and Quartz Crystal Microbalance (QCM) transducers, methods where is possible to follow the physical changes and the reaction kinetics of the immune complex formation (Luppa 2001). Even if labelled immunosensors are more sensitive, the label-free approach has been intensively study as a potential alternative to due to its simplicity.

The immobilisation of the antibody on the surface is a crucial step for the success of the biomolecular interaction with the antigens. The immobilisation should favour the reactivity of the antibody by optimizing the availability of the recognition sites by avoiding bad orientation, steric hindrance and denaturation. High stability is also an issue in the regeneration of the system. Different approaches for controlling the correct immobilisation of antibodies on a surface have been developed. Techniques such as binding the antibody to Fc receptors immobilised on the surface (protein A or G) binding

labelled antibodies in Fc fragment to a surface with the correspondent binder immobilised on the surface (biotin/streptavidin) and coupling an oxidised carbohydrate moiety from Fc fragment on the surface, have been successfully used (Luppa 2001). Another recent approach is the application of surfaces functionalised with chemical nano contrasts, which influence thermodynamically and kinetically the immobilisation of the antibodies by improving their availability for biomolecular recognition (Valsesia 2006; Valsesia 2008 B; Agheli 2006; Krishnamoorthy 2008).

Immunosensors have the advantage of being cheap and highly specific but, in the other hand issues like, lack of reproducibility low linear range, random antibody orientation, instability of the antibody and difficulty in regeneration put the immunosensors in a lower development stage as compared with biocatalyst-systems (Thévenot 2001).

2.2 Transducers in Biomolecular Recognition detection

The main transducer techniques used in biomolecular recognition detection are electrochemical, optical and piezoelectric (Luong 2008). Half of the applications are based in electrochemical transducers due to their good sensitivity, low cost and simplicity (Meadows 1996). Optical sensors are promising for multiple analyte detection, label free analysis and integrated devices (Fan 2008). Piezoelectric detection can be one alternative to optical detection once is as well a label free technique, but the lower sensitivity makes it less common in bio-sensing. Optical transducers technology is becoming very popular in sensing devices and the achieved advances are promising in replacing electrochemical systems.

2.1.2 Electrochemical

Electrochemical detection is based in the monitoring of electric changes associated to an interaction of chemicals with an electrode sensing surface. There are three main types of electrochemical transducers applied in bio-analytical detection.

Potentiometric transducers measure the change in voltage between two electrodes related to analyte activity. This type of transducer associated with selective ion membranes results in sensors based in enzyme systems that can monitor substrates, inhibitors or enzyme modulators (Rogers 1998).

Amperometric techniques are the most used electrochemical transducers and are based in the measurement of current obtained at a certain potential, resulting in a reduction or oxidation of the electroactive specie producing a current that is proportional to the analyte in study. In the last years disposable screen-printed electrodes have been developed for this type of transduction avoiding regeneration problems and reducing reagent consumption. These electrodes can be produced in high number and with low cost (Cagnini 1995; Ricci 2007).

Conductometric transducers are based on the changes of ability of charge transport in a sensing matrix due to enzymatic ionic consumptions that change with analyte concentration. These transducers are available as disposable interdigitated electrodes that represent together with the reproducibility and low cost the main advantages of the technique (Thévenot 2001; Zhylyak 1995).

2.1.3 Acoustic

Acoustic based detectors are based in the propagation of acoustic shear waves in piezoelectric crystals like quartz or zinc oxide. These materials present a resonant oscillation when excited by a electrical field (Sauerbrey 1959). The resonant frequency of the crystal is influenced by the total mass and physical properties of the biolayers at

the crystal surface; thus the adsorption of analyte on the crystal interface will induce a change in the resonant frequency that can be detected by the system (Minunni 1995).

Acoustic detectors can be divided in different categories depending on the methods of generating the acoustic wave (Rogers 1998). The most classical acoustic transducer is the quartz crystal microbalance (QCM) that operates with a quartz crystal and presents two gold electrodes in opposite sides for the application of the electric field. In this type of detector, the acoustic wave propagation is done under a thickness shear mode (TSM) inside the quartz, the oscillation frequency being dependent on the quartz thickness. When mass is adsorbed on the crystal surface, it is considered as an increase of thickness of the crystal itself creating changes in the oscillation frequency. This detection system is widely used, has a low cost and the mass produced quartz crystals. On the other hand the technique is limited to high molecular weight molecules (>1000 Da) due to the small frequency (5 and 10 MHz) (Bizet 1999; Luppa 2001)

Other types of acoustic detectors are based in surface acoustic waves (SAW) of a piezoelectric material placed between two interdigitized electrodes. In this case the signal of detection is based in changes in the propagation rate of the surface wave due to the increase in the surface mass. This type of transducers present a larger and higher work frequency range which increases the sensitivity of the system, but they are not suited for liquid applications once the liquid induces loss of radiation on the surface wave (Kurosawa. 2006) (Tom-Moy 1995).

2.1.4 Optical

Optical transducers are based on the measurement of optical signals like light absorbance, fluorescence, chemiluminescence, light reflectivity, light polarisation and rotation. The main methods of optical detection are divided in florescence based labelled detection and label free detection(Fan 2008).

Florescence based detection is based in labelling the bio-detector or target molecules with a florescent tag. The obtained florescence signal is related with to the bimolecular recognition intensity once associated with the presence of analyte on the transducer interface. These labelled assays present unique sensitivity and limit of detection and have been used since the earlier works on drug screening approaches. Nevertheless these techniques are time consuming, interfere with the biomolecules activity due to the labelling generating false negatives and have problems with background interferences (Cooper 2006; Cox 2004; Moerner 2007; Ricci 2007).

Within the optical label-free detection category are present methods based on optical absorption detection, Raman spectroscopy (Fan 2008), and mainly based in refractive index changes like SPR or Optical dielectric (Baird 2001; Mullett 2000; Myszka 1997; Myszka 1999; Rich 2005) The label free detection has the advantage of not altering the biomolecules activity, is faster and allow kinetics study of the biomolecular interactions.

The Optical waveguides are made of materials with high refractive index (glass, quartz, fibbers) surrounded by materials with lower refractive index. The sensing is based on the interaction of a laser light wave with the high refractive index material at n angle that induces confinement of the light in the waveguide. At this point an evanescent field is created inducing multiple reflections. Some of the light penetrates the adsorbed layer and is reflected back in the waveguide, interfering with the transmitted light. The changes in the layer properties will affect the transmitted light (Luppa 2001). Waveguides are mostly made of fibbers since this type of material is adequate for analysis of hazardous materials, is cheap and provides a good quality signal of detection (Bosch 2007; Udd 1995).

SPR systems are widely used in biomolecular recognition detection (Chinowsky 2007; Kim 2006; Law 2007; Rich 2005; Shankaran 2006; Tombelli 2005; Yu 2005) applied in analytical studies for in medical diagnosis, food control and environmental

monitoring(Kim 2006; Shankaran 2006; Yu 2005). The detection principle of the SPR instrument is based on changes in the refractive index at the interface between gold and dielectric substrate due to the presence of immobilised biomolecules on the gold surface. The typical configuration of the SPR detection presents a glass prism coated with a metal film (usually gold or silver) where the biomolecules binding occurs. An incident light is reflected from the internal face of the prism. At certain wavelengths or angles the incident light matches with the Surface Plasmon Polariton (SPP) at the interface between gold and the dielectric over layer resulting in a resonance coupling of the electrons. Changes in refractive index cause a shift of the SPP momentum, which is detected by the angular detection of reflected light at the surface (Barnes 2003; Hoa 2007; Homola 1999; Homola 2006; Homola 2008). SPR imaging is a promising technique to improve multianalyte detection once the imaging system permits the simultaneous analysis of different reactions with the microarrays spotted in the surface. This technique will be widely described in chapter 2.5 once is the main technique applied in this thesis studies.

2.3 Surface Functionalisation

The correct bio-receptor immobilisation on the transducer surface is crucial for the efficiency of biomolecular recognition and detection. A good strategy of immobilisation coupled to the adapted surface chemistry is the solution to ensure stability, correct orientation and retention of biological activity. Immobilisation can be done via entrapment in polymeric matrices, specific biological reactions, electrostatic hydrophobic interaction or covalent binding. For all cases the immobilisation can be performed by modifying the surfaces with different functional groups (e.g. amine, carboxyl, epoxy, aldehyde, polyethylene oxide (PEO)). There is no universal approach for the surface

modification but more a set of methods which depend on the type of biomolecular recognition system, transducer method and type of immobilisation.

2.3.1 Bio-detector immobilisation

The immobilisation of the bio-detector on the surface can be done by different approaches from fast and less stable processes to more time consuming and more robust ones.

Entrapment on polymeric matrices such as agar gel, sol gels or conductive polymers increase the amount of immobilised bio-detectors due to matrices tridimensionality. In some cases the bio-detector is added to the polymerisation medium and is entrapped in the matrix (Song 2006). In other cases the bio-detector is covalently bonded to the polymer monomer, growing with the polymer matrix. Pyrrole molecules can be modified by covalent binding of antibodies, DNA or enzimes. The copolymerisation of the modified pyrrole together unmodified pyrrole results in a polymeric stable matrix with the bio-detector immobilised and thus ready to be applied in biomolecular recognition experiments (Grosjean 2005; Haddour 2005;Guedon 2000). This approach has problems related to low diffusion of analyte on to the bio-detector and sensitivity problems. On the other hand the use of such polymers can improve the detection signal when associated with adequate transducer system, induces stable bio-detector immobilisation and allows several regenerations.

Immobilisation by specific biological reactions is an alternative approach that consists in immobilising the bio-detector on the surface via a biospecific interaction. For instance the binding of an antibody to Fc receptors immobilised on the surface (protein A or G) (has already described in chapter 2.1.2). This approach has the advantage of immobilising the bio-receptor with a good availability of the binding sites but use of high

amounts of biological material, produces complex biologic systems and induces diffusion problems (Collings 1997).

Covalent immobilisation of the bio-receptors is a frequently used method that creates more stable systems allowing multiple regenerations of the surface. The bio-detector is immobilised by covalent binding of residue amino acids (most commonly lysine amine groups) with functional groups present on the surface. The biomolecules can be immobilised by direct reaction with aldehyde and epoxide groups or through an activation process (carbodiimide or glutaraldehyde linkers) with carboxylic or amine groups. Surfaces functionalised with glutaraldehyde and epoxide react with the primary amine groups of lysine (Chen 2003; Polzius 1996). Amine surfaces are mostly obtained by organosinalisation and need to be activated in order to covalently immobilise the biomolecules. The activation is done with glutaraldehyde creating Schiff bases and free aldehyde groups. The surface becomes chemically activated with aldehyde groups that easily react with the amine groups of the residue amino acids. Surfaces modified with carboxylic organothiols or carboxylate dextran gels are similarly activated to achieve the covalent reaction (Mannelli 2005; Oh 2004; Tombelli 2002).In this case the biomolecules are covalently immobilised by using a carbodiimide, usually 1-ethyl-3- (3-dimethylaminopropyl) carbodiimide hydrochloride (EDAC) combined with N-hydroxysuccinimide (NHS). The surface remains activated with hydroxysuccinimide that is a stable leaving group favouring the reaction with of the biomolecule amine groups. There are several commercially available l pre-treated chips with the different specific activation chemistries allowing direct immobilisation of the biomolecules on the chip surface (Biacore, Arrayit, Shott) Bilitewski 2006). The covalent bonding can occur closely to the binding sites thus reducing biomolecules activity. This problem can be overcome with techniques that insert functional groups with high reactivity with the surface functionality on locations of the bio-receptor that are far from the binding sites

(Wilchek 2003). Even if this method involves a complex sequence of steps and has problems to maintain the biomolecules biological activity, its stability makes it a base for robust sensing systems.

Physical adsorption on the solid surface is the most simple and fastest approach (no reagents or antibody modifications are evolved). This method is based in weak interactions like Van der Waals, hydrogen bonding, hydrophobic or electrostatic interactions (Figure 2.3) (Bilitewski 2006; Goddard 2007).

Van der Waals interactions are based in dipole-dipole attractions. Biomolecules can create positive or negative dipoles in originally non polar areas due to intramolecular interactions that disturb the electron clouds. When the biomolecule are immobilised, their dipoles align to maximize the interaction with the electric dipoles of the molecules in the surface.

Hydrogen bonding occurs when a hydrogen atom covalently bound to an electronegative element (oxygen, nitrogen) is attracted by another electronegative element creating a relatively strong interaction. The residue amino acids that present amine, hydroxyl or carbonyl groups can have this type of interaction with the proper surface chemistry.

The hydrophobic interactions are related to the presence of amino acids as phenylalanine and leucine that are non polar and hence interact poorly with polar molecules like water. For this reason, most of the non polar residues are directed toward the interior of the molecule whereas such polar groups as aspartic acid and lysine are on the surface exposed to the solvent.

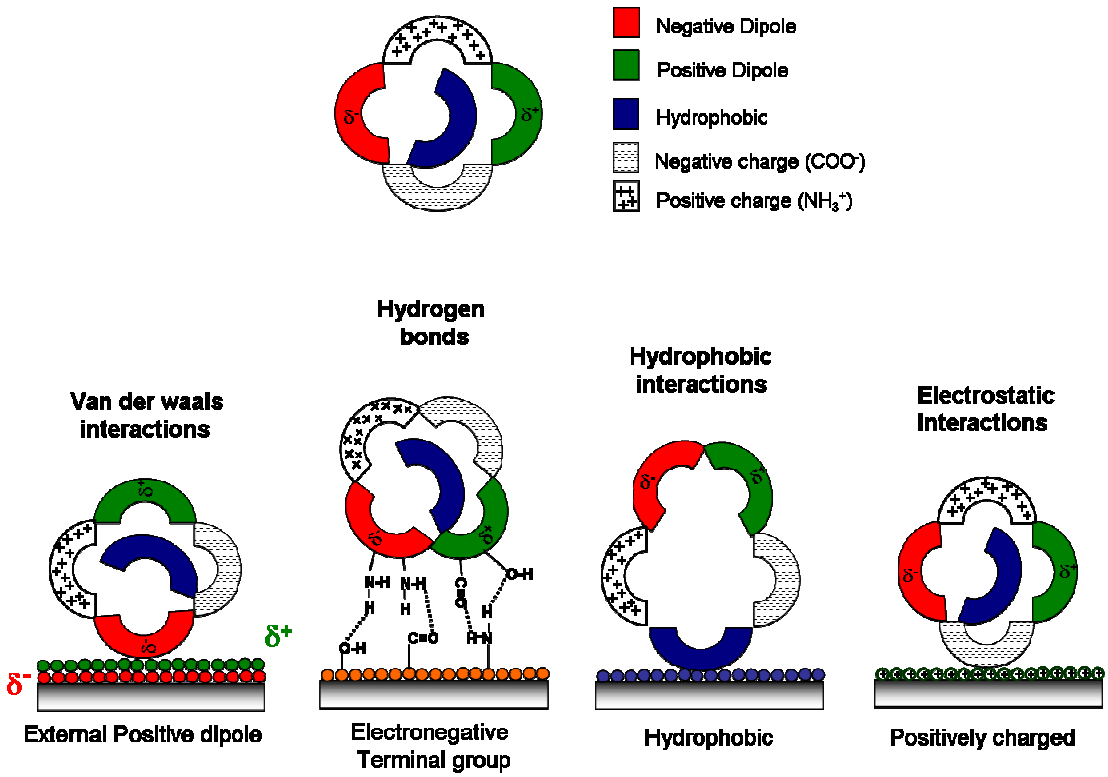

Figure 2.3- Different phenomena involved in physical adsorption of proteins in functionalised surfaces.

When the surface is functionalised with a hydrophobic layer, it is energetically more favourable for the non polar residues to approach the surface creating a hydrophobic interaction.

Finally, electrostatic interactions are based on the affinity of the biomolecules charged groups with charged groups in the functionalised surface. The negatively-charged carboxyl groups on aspartic acid (Asp) and glutamic acid (Glu) are attracted to positively charged amine groups and positively-charged free amino groups on lysine(Lys) and arginine (Arg) residues are attracted by carboxylic negatively charged groups. In physical adsorption the immobilisation is a combination of the different phenomena

described above, and the biomolecules conformation changes to maximise the interaction with the surface depending on the type of chemistry.

Physical adsorption results in a random orientation of the biomolecules since the orientation of the binding sites is not controlled. Moreover the biomolecules immobilisation can be disturbed by pH or temperature changes, and so this method should be used when the environment of the experiment is stable. Nevertheless when the conditions are stable the biomolecules self-arrange to achieve interaction maximisation with the surface creating a stability that allows surface regeneration (Shankaran 2007). This method is simple and induces high antibody binding capacity. Moreover it is used in sensitive immuno-detection based in nanoarrays (Lee 2004) and in the most popular clinical assay , the ELISA test (enzyme-linked immunosorbent assay).

2.3.2 Self assembled Monolayers

Self Assembled Monolayers (SAMs) are based in the spontaneous self organisation of organic molecules on specific surfaces into well ordered arrays (Bain 1989; Folkers; 1992 (Flink 2000; Smith 2004). It is a simple and fast methodology to change the surface properties. The wide range of end groups available (COOH, NH_2, PEO, CH_3) make this technique widely used in recent years. There are two main types of SAMs: organosilanes that are mainly used in self assembly on SiO_2 surfaces and organothiols that are mostly used on gold and silver surfaces.

SAMs based in organothiols form generally well ordered and crystalline monolayers (Figure 2.4). When exposed to the gold surface, normally in a ethanolic solution, the sulphur-gold bond is immediately formed, but it takes several hours to reach the crystalline close parking of the layer (Smith 2004).

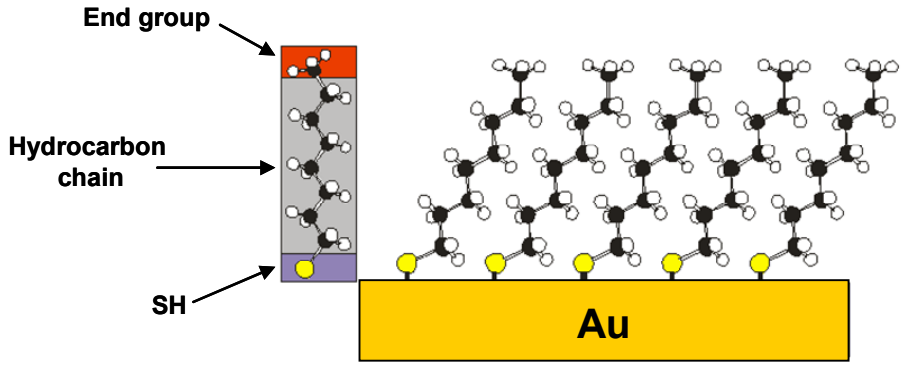

Figure 2.4- Scheme of Organothiols organised on a gold surface.

Better order of SAMs on gold surfaces is normally obtained on (111) planes, but other orientations can also be applied (Love 2005). The reaction of sulphur-gold formation is still a controversial issue, but is generally considered that it starts with an oxidation of the S-H bond followed by a reduction of the hydrogen bond (Love 2005). The chain length is very important for the monolayer quality. Organothiols with more than 10 methylene groups give better protection to the sulphur-gold bond and avoid oxidation, thus creating stable and reproducible monolayers (Frederix 2004 A). Organothiols have been applied with success on the production of nanoarrays and for biomolecular recognition detection systems (Baralia 2006; Frederix 2003; Love 2005; Prime 1991; Prime 1993; Zhao 1997).

2.3.3 Electrochemical polymerisation

Electrochemical polymerisation is the most appropriate method for fabricating conductive polymers films for biosensing applications (Ramanavičius 2006). In this method the substrate to be coated forms the working electrode of a two or three electrode electrochemical cell containing an electrolyte solution of the desired monomer plus additives or dopants. When the working electrode is positively polarised, oxidation of monomer molecules can occur at the surface of the electrode resulting on the formation

of a reactive radical which initiates a polymerisation reaction (Wang and 2006). The electrochemical oxidation process may be performed galvanostatically (constant current), potentistatically (constant applied voltage) or potentiodynamically (scanning voltage). The most important general feature of the electrochemical deposition method is the relative simplicity in incorporating biomolecules into the polymer film. Adding biomolecules to the electrolyte solution during deposition or previously modify the monomer with biomolecules, allows the physical entrapment of the bio-receptor in the growing film (Chaubey 2000; Grosjean 2005; Haddour 2005; Reiter 2001; Yasuzawa 2000).The most common conductive polymers used for sensing includes polypyrrole, polyaniline, polythiophene, poly (paraphenylene) and polyacetylene (Figure 2.5) (Guimard 2007; Lange 2008).

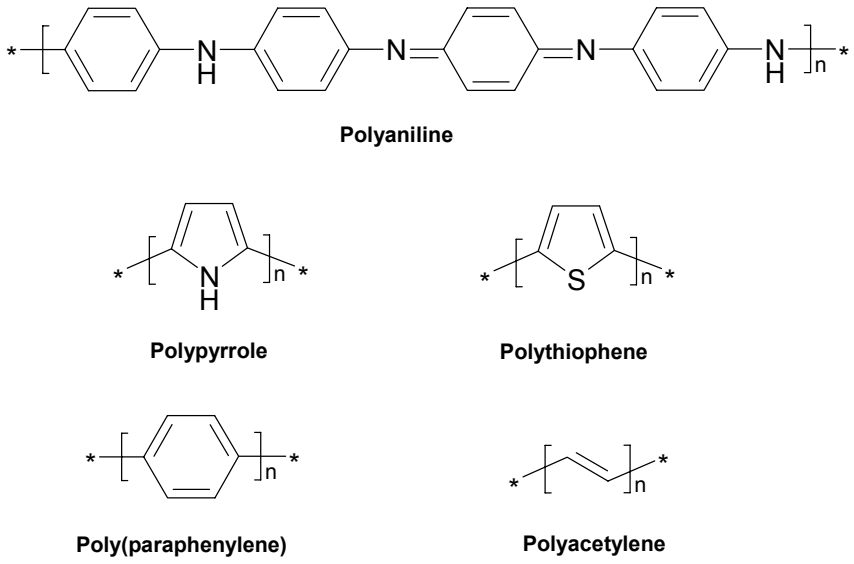

Figure 2.5- Chemical structure of main conductive polymers.

Commonly conductive polymers are applied in electrochemical transducers (Gerard 2002; Guimard 2007; Lange 2008) but lately polypyrrole and polyaniline have been used as base matrix for optical detection (Grosjean 2005; Guedon 2000; Lange 2008).

2.3.4 Plasma processes

One ever increasing technique for surface functionalisation is plasma assisted polymerisation (D'Agostino 2005; D'Agostino 2005; Goddard 2007; Yasuda 1982). Plasma is a partially ionised gas containing free electrons. The free movement of the positive and negative charges makes the plasma electrically conductive so that it responds strongly to electromagnetic fields. Plasma therefore has properties quite unlike those of solids, liquids or gases and is considered to be a distinct state of matter. Plasma processes can be used for etching, oxidisation, chemically activation of surfaces or for deposition of polymer layers with specific properties on a surface (Ratner 1995). The nature of the process gas or precursor are chosen depending on the type of desired surface modification and the operating parameters (pressure, power, time and gas flow rate) and can be tuned to optimised the final product properties. When the goal is to activate the surface for subsequent graft copolymerisation an inert gas is used to create radicals on the matrix.

Plasma Enhanced Chemical Vapour Deposition (PE-CVD) is a specific plasma technique to functionalize surfaces with functional polymers (Yasuda 1982; Yasuda 2005). In this technique the discharge is produced by using the precursor monomers of interest mixed with an inert gas. The discharged creates gas-phase radicals inducing a radical reaction that recombines the exited species into a film on the surface (Hegemann 2006). This type of surface functionalisation can achieve a large spectrum of surface chemistries (e.g. carboxylic, amine, PEO, Teflon like films). Plasma polymerisation has many advantage as compared to other processes e.g. it allows the deposition of

conformal films on a wide range of material, with a rather good stability and low contamination and is compatible with Industrial mass production (Ratner 1995).

2.3.5 Nano-patterned surfaces

Surface nano-patterning is receiving many interest nowadays thank to high potentiality to increase sensitivity and control in biomolecular recognition. First example of chemical nano-contrast used mixed SAMs (Bain 1989; Folkers 1992; Frederix 2003. Mixing different SAMs in solution results in a surface with a random nano contrast. Is possible to control the density of each component by controlling the stoichiometry of the mixing. This approach showed improved sensing performances

Nevertheless this technique has some limitation since it is difficult to control effectively the size and distance between bio-adhesive areas. New tools in nanotechnology have opened up new perspective to design nano-pattern surfaces where bio-adhesive domains can have well controlled sizes and distribution on the surface. Successful surface chemistry approach for improving the detection of biomolecular recognition have been reported (Agheli 2006; Frederix 2004 B; Rosi 2005; Valsesia 2006). When the nano-pattern has an organised geometry (nanoarray) it presents special optical and electric properties that can be use for improvements in optical and electrochemical detection (Arrigan 2004; Barnes 2003); (Lupu 2007). Many efforts have been made to develop nanoarrayed surfaces exploiting the different techniques available for the creation of nano-patterns (Blättler 2006; Gates 2004; Gates 2005; Geissler 2004; Ito 2000; Rosi 2005).

The techniques used for the creation of nano-patterns can be classified in top down and bottom up approaches (Vörös 2005).

2.3.5.1 Top down techniques

Top down methods are based on lithography techniques and can be divided in Series and Parallel approaches. Series techniques are those were the nanoarrays are produced in sequence processes like in the case of Scanning Probe Lithography (SPL) or Scanning Beam Lithography (SBL).

SPL includes Dip Pen nanolithography (DPN) and Chemical Nanolithography. The first method uses an AFM tip inked with a substance that is transferred with a nano-scale resolution. (Ginger, Zhang et al. 2003; Lee 2002). This technique has been used successfully in many applications resulting in a numerous publications. The second technique is based on chemical modification of resists or functional layers at the nanometric level. A sharp nano tool scans the surface reacting with it and creating a nano contrast. For instance a conductive AFM tip can be used oxidizes locally materials creating a nano-pattern (Krämer 2003). Near Field Scanning Optical Microscopy technique has been used to induce photochemical modification of SAMs to create nano-area of carboxylic groups (Krämer 2003; Leggett 2006).

The most used SBL technique is Electron Beam Lithography that is based on scanning an electron beam on a electron sensitive resist to modify it locally, thus creating high resolution nano-patterns (Bretagnol 2007; Lercel 1996; Sandison 2006; Zhang 2004).

These techniques allow the generation of very precise nano-patterned surfaces but have the disadvantage to be very slow.

Parallel approaches are those were the nanoarray is produced in a one step process.

Soft Lithography is considered as a parallel approach and includes techniques like Micro-contact printing. In the last years Micro-contact printing is been adapted for fabrication of nanoarrays (Sandison 2006; Whitesides 2001; Xia 1998; Zhao 1997). In this technique a nanostructured stamp (usually polydimethilsiloxane) is inked with a

substance and stamped in the surface. When stamping, the substance is transferred into the surface reproducing with conformity the nanostructured stamp design.

Top down techniques are compatible with massive production, but are dependent on the resolution of the tool used which can be as well very expensive and time-consuming.

2.3.5.2 Bottom up techniques

Bottom up techniques are based in self-assembly processes, meaning that the nano-pattern creation is based on the spontaneously organisation of materials at nanometric level.

Micelle lithography block-copolymers exploit the self assembled properties of block copolymers. In certain conditions is possible to mix two block-copolymers and form contrast nano-regions of the two types of blocks. One of the polymer can be removed by adapted solvent thus creating nano-pattern of the second polymer on the surface (Glass 2003; Hamley 2003 A; Hamley 2003B; Reviakine 2001).

Colloidal lithography is a bottom up method that is based on the capacity of colloid particles to form a two dimensional monolayer array on a surface. The colloidal monolayer is used as a mask for etching or sputtering process on a lithographic route (Choi 2006; Park 2006; Yang 2006).

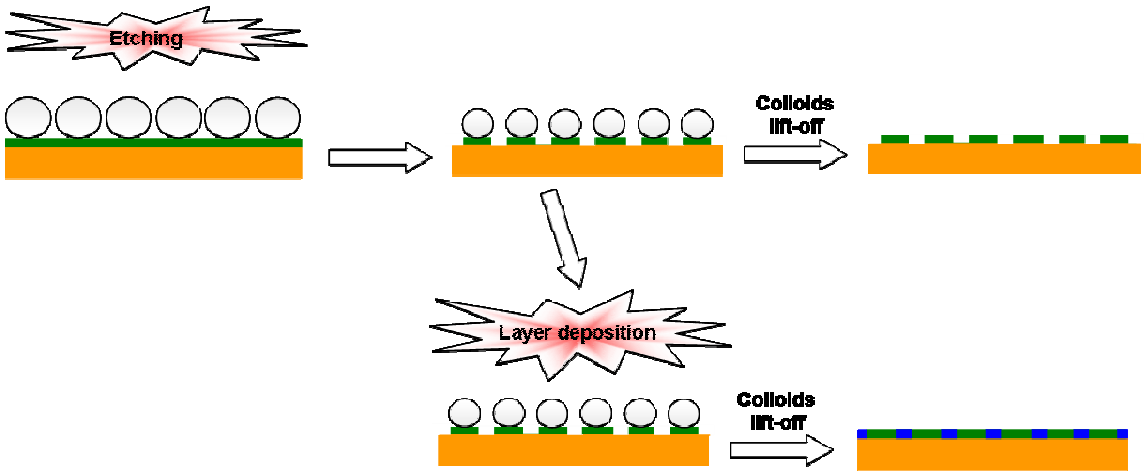

Figure 2.6- Production of nanoarrays by colloidal lithography.

Figure 2.6 illustrate the principle of nanoarrays production by colloidal lithography. The first step is the deposition of the particles on a functionalised surface which can be performed by (Yang 2006):

dip coating (capillary forces and evaporation induce the self organisation);

lifting up of a colloid layer from a interface using the substrate;

electrophoretic deposition (driven by electrical fields);

chemical or electrochemical deposition on a arrayed surface;

or spin coating on a wettable surface (the colloids solution is spread on the surface and forms a monolayer with hexagonal distribution).

After this step a second material is deposited on the particles and on the areas in between particles by metal evaporation, PECVD or wet chemistry. In some process, plasma etching is performed to reduce the particles size and to remove a first layer already deposited, in order to prepare the surface to a subsequent treatment. Finally the particles are removed by lift-off leaving a nano-pattern on the surface (Figure 2.6).

Colloidal Lithography present some advantages as compared to other lithography approaches it is a rather cheap in terms of equipment and materials, and is a technique with simple methodology enabling the controls the surface structures by simply changing the size of the particles. It has been demonstrated to be suitable for patterning biomaterial surfaces (Yang 2006).

2.4 Nano-patterned surfaces applied in Biomolecular Recognition

The development of nanopatterned surfaces for biomolecular recognition applications was motivated by the successes obtained with microarrays with multiplex detection of DNA and proteins (Rosi 2005). Nano-patterned surfaces are described as a promising approach to improve the magnitude of multiplex detection, miniaturisation of devices and decrease the volume of reagents and analyte. Moreover an improved sensitivity resulting from smaller analyte capture area is expected (Ekins 1998; Rosi 2005). The developed nano-patterned surfaces can present a random or organised geometry (nanoarrays). The application of nano-patterned surfaces in bio detection can be dived in four main approaches: nanoarrays where the binding event is monitored by AFM; nanoarrays with special conductivity contrast that work as nanoelectrodes in electrochemical detection; nano-patterns were the binding effect is detected by optical or acoustic transducers; and nanoarrays with special optical properties that are exploited in SPR detection. The first and the last approach are the most promising ones once theoretically, but the achievement of high sensitivities in nano-patterned approaches requires the use of methodologies where the performance is less linked with the analyte diffusion (Sheehan 2005)

The fabrication of nanoarrays with DNP for bimolecular recognition using AFM as readout method is been extensively studied (Demers 2001; Demers 2002; Lee 2002; Lee 2004; Lim 2003; Zhang 2004). In this technique is created an array of bio-detector is created, by direct immobilisation of the biomolecule on the metallic surface (Demers 2002) or by the creation of a nanoarray of functional material on the surface followed by biomolecule incubation (Lee 2004; Zhang 2003). The uncoated surface is afterwards passivated by PEO or hydrophobic chemistries (Demers 2002; Lee 2004; Zhang 2003). The analyte recognition is then detected by changes in height, shape or roughness by AFM measurements. This approach is very promising once, and presents high specificity due to the presence of the passive matrix (Demers 2001; Lee 2002), multiplex analyses (Demers 2002; Lim 2003) and high sensitivity due to miniaturisation of the biodetection system to a scale easily probed by AFM. The best achievement using this approach was obtained by combining this method with gold nanoparticle labelling for the detection of Human Immunodeficiency virus type 1 in plasma. The detection limit obtained with this method was better than the one obtained with conventional ELISA test (Lee 2004).

The use of Nano-Electrode Arrays (NEAs) for the electrochemical detection of biological or chemical species presents many advantages as compared to classical macro-electrodes. NEAs are based in arrays of nanometric conductive material (electrodes) distributed over an insulating matrix. The electrodes distance is optimised in order to have individual diffusion regimes on each spot. The use of the electrode array in sensing induces higher mass sensitivity, increased mass transport rate, lower background noise and a lower influence of the solution resistance (Arrigan 2004). The production of NEAs based on carbon nanotubes is widely used and results in high sensitivity detection with sensors based on DNA hybridisation (Andreu 2006; Koehne 2004; Li 2003). Most of the biosensors developed using NEAs are based on bio-catalytic reactions for glucose detection (Ekanayake 2007; Liu 2007; Yang 2006).

The creation of nano-patterns with adhesive functional areas surrounded by a non-adhesive matrix induces selective adsorption of biomolecules on the functional areas. When applied to biosensing, the bio-detector is immobilised on the adhesive nano areas and this confinement seems to create better availability of the binding sites and less biological denaturation. Another advantage is the decrease of cross-reactions. This effect has been studied by nano-patterning the interface of QCM and SPR chips used in the monitoring of immunoreactions (Agheli 2006; Krishnamoorthy 2008; Valsesia 2008 B). Even if the detection signals in absolute are lower than or similar than to common uniform surface modification, with e.g. protein A approach (Valsesia 2008 B), the efficiency of the bioreaction is comparatively higher on the nano-patterned surfaces. Indeed, the percentage of bio-detector on the surface able to recognize the analyte is improved on the nano-patterned surfaces. In this approach the geometry of the nano-pattern is not an issue, and the effect is detected on geometrically organised arrays (Valsesia 2008 B) as well as on random nano-patterns (Agheli 2006; Krishnamoorthy 2008).

The creation of nanoarrays at the SPR interface that creates periodic optical gratings is extensively studied due to their potentiality in originating high sensitive sensor devices. (Barnes 2003; Benahmed 2007; Park 2003; Stewart 2006). These gratings promote the coupling of the surface plasmon modes with the periodicity of the nanoarray modificating the plasmon behaviour. This effect creates systems more sensitive to refractive index changes. There are only few application reported were this effect is used in biomolecular-recognition detection (Benahmed 2007; Stewart 2006), probably because the phenomenon is not yet completely understood. The main purpose of this thesis is the study and application of this effect in the detection of bio-interactions. Chapter 2.6 presents a more complete description of the effect of nano-gratings in SPR detection.

2.5 Surface Plasmon resonance

SPR detection is becoming widely used in biomolecular recognition detection. This type of transducer is applied in analytical studies for medical diagnosis, food control and environmental monitoring (Chinowsky 2007; Kim 2006; Law 2007; Rich 2005; Shankaran 2006; Yu 2005). SPR is a label free technique, the analyte do not need any pre-treatment and the recognition is done in a one-step process. The SPR detector allows real time monitoring of biomolecular recognition reactions and gives information about affinity and kinetics. This chapter will focus in the fundamentals of SPR detection and in the different types of instrumentation.

2.5.1- Fundamentals

SPR is based on the principle of total internal reflectance (TIR). TIR occurs when a polarised light is passed through the interface between two materials with different refractive index (n1 > n2). In this condition an electromagnetic wave is created and propagates in the vicinity of the interface (evanescent field). SPR occurs when a thin conducting film is placed at the interface between the two optical media. At a specific incident angle, greater than the TIR angle, the surface Plasmon wave (oscillating electrons at the edges of the metal) in the conducting film resonantly couple with the evanescent field due to a matching of frequencies (Figure 2.7). The resonance condition that permits energy transfer from photons to plasmons depends on the energy and momentum of the photons and plasmons. Both the energy and momentum of the photons must match exactly the energy and momentum of the plasmons. Since energy is absorbed at this resonance, the reflected light intensity, decreases sharply and the angle were the maximum loss of reflected light is achieved is called the SPR angle. The SPR angle is dependent on the optical characteristics of the system. Refractive index

changes in the evanescent field induce changes in the SPR angle position (Schasfoort 2008).

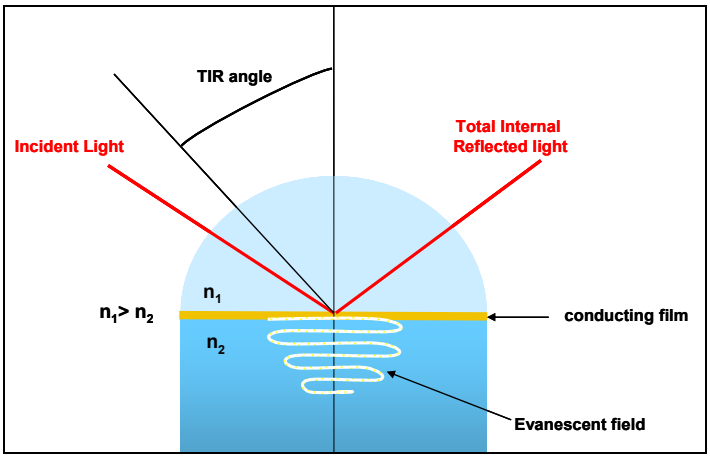

Figure 2.7– Principle of total internal reflectance in SPR.

For a flat metal surface, there is no wavelength of light that satisfies this constraint to create a surface plasmon resonance. To achieve this effect there are three general configurations of SPR devices that change the momentum of photons in a way that fulfils the resonance criterion: prisms, gratings and optical waveguides (Homola 1999).

Prism couplers are the most common in SPR sensors, and are based on the Kretschmann configuration (Homola 1999). In this configuration the light is passed through an optical dense medium (glass) and reaches the interface between this medium and the medium with lower optical density, and is totally reflected back to the dense medium. At this point an evanescent field is generated and penetrates the metal film. The evanescent wave propagates along the interface and can be adjusted to mach the surface Plasmon by controlling the angle of incidence (Schasfoort 2008).

SPR biosensors are based on the monitoring of the effect of changes of refractive index due to biomolecules immobilisation on the thin metal interface that produces a change of resonance condition i.e. SPR angle. The bio-detectors are immobilised on the metal thin

film and the followed binding of analyte will create increase in refractive index depending on the concentration. When the refractive index changes the angle of SPR shifts and the changes can be monitored in real time as a sensogram. The sensogram allows monitoring all the different steps involved in a bio-recognition assay (Figure 2.8).

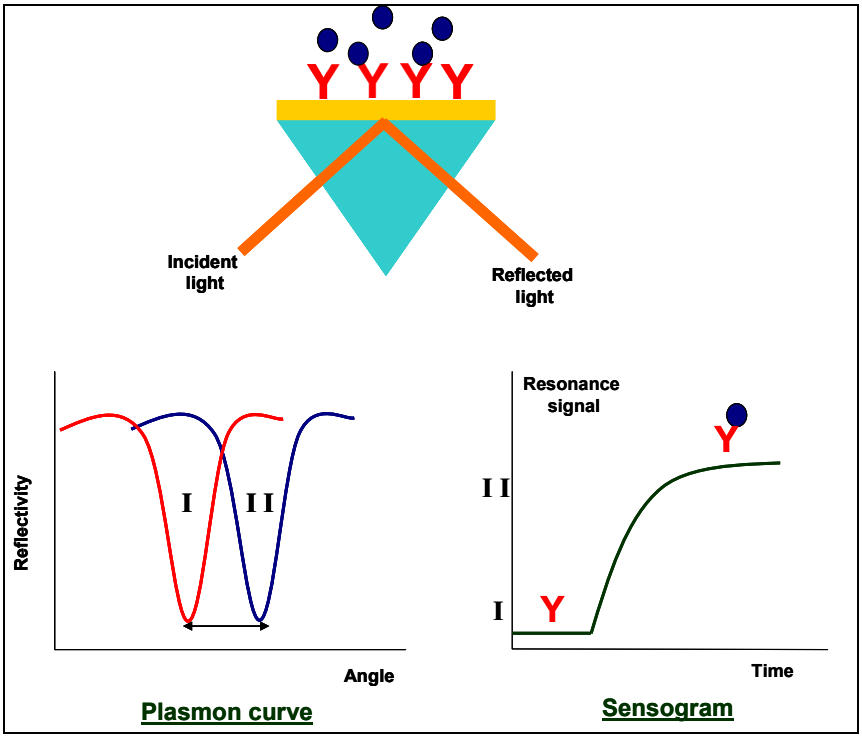

Figure 2.8 – Principle of SPR detection of Biomolecular interactions.

The SPR sensing is maximum and limited to the vicinity to the metal surface since the penetration of the evanescent field is limited to few hundred nanometer, so the surface modification must be done by low thickness films (Homola 1999; Schasfoort 2008)

2.5.2 Types of instrumentation

Most of the SPR instruments use a prism coupler which is the simplest and most conventional way of coupling the light with the surface Plasmon. In this chapter the two

main types of instrumentation based in prism couplers will be described: detectors based on spectroscopy of surface plasmons and detectors based on intensity modulation.

The first type of instrumentation is based in the measurement of angular or wavelength spectrum of the light coupled to the surface plasmon. The immobilisation of biomolecules changes the plasmon condition inducing changes in the angular or wavelength positions of the SPR angle. After each immobilisation the system detects the shift of the SPR angle which is proportional to the biomolecules concentration (Homola 1999). Biacore (GE Healthcare, USA), the commercial instrument that dominates the SPR market and publications, is based in this approach (Rich 2007). In the Biacore instrument a LED (light emitting diode) is focused on the prism/gold interface in a discrete range of angles and an array of photodiode is used to determine the SPR angle. During the measurement the SPR angle shift is determinate by a polynomial fit (Schasfoort 2008).

Most SPR imaging instruments are based on intensity modulation. In this type of instruments the sensogram is obtained by measuring changes in the reflected light at a fixed angle. To originate the coupling is used a beam of monochromatic light. The detector is usually a CCD (charged couple device) camera that collects the reflected light intensity in image format (Jordan 1997; Jordan 1997). Biomolecules immobilisation modify the refractive index distribution on the surface interfering with the Plasmon condition and consequently inducing changes in the intensity of the total reflectivity of light. These instruments allow the visualisation of the surface during the bio-reaction, by a live image, making possible to perform multiplex analysis by monitoring different biological reactions on an array of spots. The weakness of this technique is related to the fact that the reflectivity change is measured by changes on the refractive index on the evanescent field. To have precise kinetics analyses of the immobilised biomolecules it is necessary to use SPR angle monitoring that is directly proportional to the mass

change (Schasfoort 2008). Nevertheless the refractive index is dependent on the immobilised biomolecules, thus the SPRi results can be correctly used if the reflectivity change is perceived as a derivative parameter of the SPR angle. GenOptics (Orsay, France) is a laboratory instrumentation company that develops SPR imaging instruments using a rotating mirror that allows the selection of the optimised angle for achieving the best reflectivity monitoring (Schasfoort 2008). The SPRi instruments from GenOptics were used as main transducer method in this thesis and will be described in detail in chapter3.

2.6 Periodic optical Nano-pattern in SPR detection

This chapter is focused on the description of the effect of a periodic optical nanopattern in SPR detection using a prism to promote the surface plasmon coupling which is the approach used in this thesis to study the effect of nanoarrays in SPR detection.

The momentum matching of the incident light with the Surface Plasmon (k_{SPP}) at the interface between gold and the dielectric overlayer, using a glass prism as coupler, is based on the Kretschmann configuration. The condition for surface Plasmon matching with incident light in these conditions is expressed by the formula (Barnes 2003; Homola 2006):

$$k_{SPP} = \frac{2\pi}{\lambda_0}\left(\frac{\varepsilon_{Au}\varepsilon_d}{\varepsilon_{Au}+\varepsilon_d}\right)^{1/2} = \frac{2\pi}{\lambda_0} n_p \sin(\vartheta) \quad (2.1)$$

where λ_0 is the wavelength of the incident light , ε_{Au} is the dielectric function of the gold, ε_d is the dielectric constant of the dielectric interfacing the gold surface, n_p is the refractive index of the coupling prism and θ is the incident angle of light.

When the surface presents periodic nano-pattern of different optical properties and heights, with a lattice constant that is within the same order of magnitude as the wavelength of the surface plasmon, an interaction between the surface plasmon and the periodic structures occurs (Dintinger 2005; Hibbins 2002; Wedge 2007). The surface plasmon propagates following the surface periodicy (Figure 2.9) and the matching conditions for the Surface plasmon momentum change to (Wedge 2007):

$$k_{SPP} + i\frac{2\pi}{\vec{a}_1} = \frac{2\pi}{\lambda_0} n_p \sin(\vartheta) \quad (2.2)$$

where $\vec{a}_1$ is the lattice vector of the periodic structure.

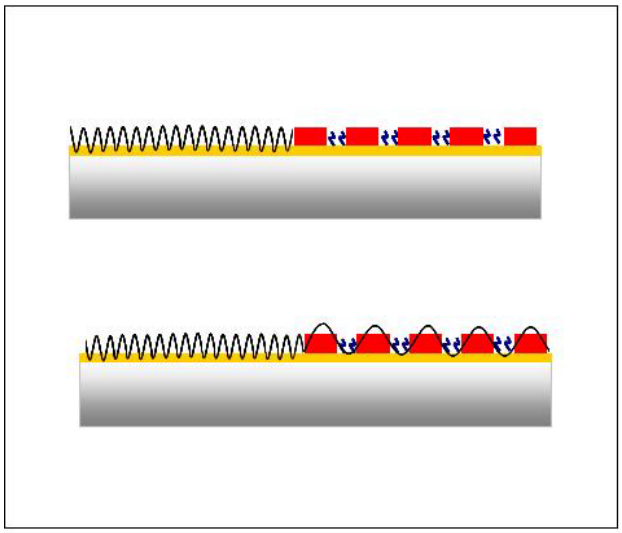

Figure 2.9- Surface Plasmon propagation in an optical nano-grating.

When the lattice periodicy is half of the surface plasmon wavelength, at some energy areas the surface plasmon is blocked creating a band gap. Figure 1.10 present a simulation of a reflectivity map originated by different combinations of angle and wavelength in a protein grating of 200nm lattice. The white colour indicates zones where the reflectivity is maximum, meaning that there is no plasmon resonance effect and the

dark areas indicate the energy levels where the resonance occurs. For a uniform surface the resonance effect takes place in a continuity of energies. From figure 1.10 is possible to see that compared to the uniform surface the energies where the resonance takes place are shifted in the grating surface. Moreover is clearly seen that at a certain point the resonance effect is highly disturbed originating the bad gap effect (A in Figure 2.10). The energies around the band gap (B in Figure 2.10) are as well disturbed leading to different behaviour as compared to a uniform surface.

The band gap effect is known to improve the sensitivity of SPR in detecting refractive index changes due to a more instable plasmon resonance effect (Barnes 1996; Benahmed 2007; Kitson 1996).

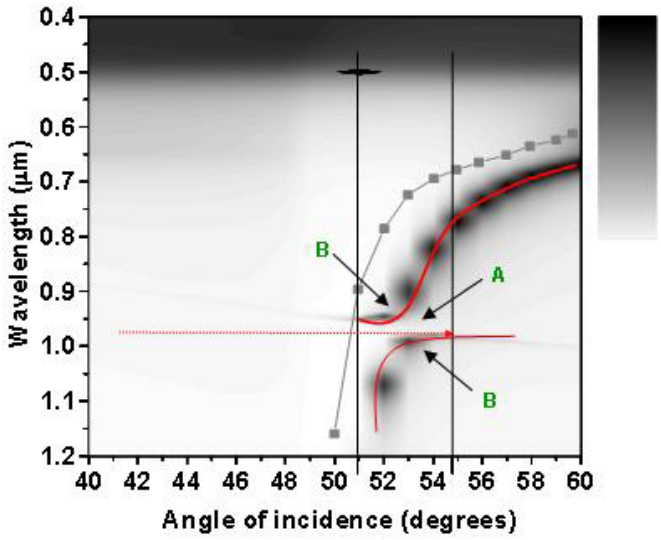

Figure 2.10- Simulation of reflected intensity versus angle and wavelength on 200nm lattice optical grating (water/protein) on a glass prism. The image describes the plasmon dispersion on a periodic structure (band gap effect) (red line) and the plasmon dispersion for bare gold with a layer of proteins (grey line). Is evidenced the energies relative to the bang gap effect (A) and relative to the vicinities of the band gap effect (B). The simulation was performed using the grating simulator from GSOLVER©.

Chapter 2

Periodic structures when used to detect biomolecular interactions can be developed so that the bio interaction to occur specifically on one of the features composing the pattern. This creates periodic optical contract between the biomaterials and the buffer, inducing the above described interferences on the surface plasmon, which can result in an improvement of the detection.

3-Methods and Techniques

3.1- Esterification reaction -Fischer and Speier method

The synthesis of thiolated PEO was performed following the Fischer and Speier method, which consists in the formation of an ester by the reaction between an acid and an alcohol using a inorganic acid as catalyst (Vogel 1961). The use of the acid activates the carboxylic group by forming a conjugate acidic ion (A in Figure 3.1) this induces the nucleophilic hydroxyl group to approach the dipole C-O^+ producing a water molecule (B in Figure 3.1) and finally the loss of a proton yields the ester (C in Figure 3.1). In this approach it is convenient to use an excess of acid to move the equilibrium towards the ester formation and thus with that achieve high yields of esterification. The reaction is done under reflux and in an organic solvent medium. To remove the acid, the reaction product has to be washed in a polar solvent where the ester is not soluble and ester precipitates.

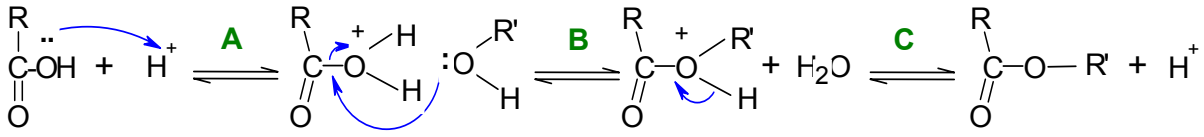

Figure 3.1- Esterification reaction mechanism - Fischer and Speier method.

3.2 Electrochemistry

3.2.1 Polymer deposition

Electrochemical polymerisation is the most appropriate method for fabricating conductive polymers films for biosensing applications (Ramanavičius 2006). In this method, the substrate to be coated forms the working electrode of a two or three electrode electrochemical cell containing an electrolyte solution of the desired monomer plus additives or dopants. When the working electrode is positively polarised, oxidation of monomer molecules can occur at the surface of the electrode resulting in the formation of a reactive radical which initiates a polymerisation reaction (Wang and 2006). In this thesis, two methods were used to electrochemically deposit PPy: gavalnostatic deposition and potentiosticaly deposition using a micro-spotter.

In galvanostatic deposition a constant current is applied to promote the polymerisation. Low currents density originate compact PPy films and the final thickness of the polymer can be controlled by the surface charge (Moreno 1999; West 1993).

The galvanostatic polymer deposition was performed with an Autolab-PGSTAT30 (Ecochemie) using a Teflon cell (7ml). A platinum wire was used as counter electrode and a saturated calomel electrode (SCE) as reference electrode. The surface used to deposit the polymer ($0.07cm^2$) plays the role of working electrode.

In potentiostatic deposition, a constant voltage is applied. The potential applied should correspond to the oxidation voltage of the monomer in order to start the polymerisation. The charge density in this approach is very important for the morphology and stability of the polymer obtained (Tietje-Girault 2007).

In this work, the potentiostatic deposition was performed using a micro-spotter. The system was based on a platinum needle (carrier of the monomer) used as counter electrode. The deposition was achieved by applying a pulse potential between the

needle and the surface (working electrode). The array was produced with a SPRi-spotting prototype (GenOptics) where the micro-spotting was performed by an x/y/z robot from Omnigrid Micro.

3.2.2 Cyclic Voltammetry

Cyclic Voltammetry is a technique adequate to characterize surface coverage and electron transfer properties. The typical setup is based on a three electrode cell : a counter electrode that compensates the cell resistance, a reference electrode that controls the potential versus the working electrode and a working electrode where the electronic exchange occurs (Wang and 2006). The cyclic voltammetry measurements are done by cycling the potential of the working electrode when exposed to a solution. From the measurement, a cyclic voltammogram of the current measured at the working electrode during the potential scan is obtained. This technique can be applied to characterise the surface coverage of organothiols on gold surfaces. When a redox couple like hexacyanoferrate (II/III) is added to the solution a faradaic current can be recorded resulting in a peak shaped voltammograms with oxidation and reduction peaks. The decrease of the peak shape and the increase of the peak separation is an indication of insulating character of the surface that is associated with good surface coverage by the organothiols (Frederix 2004 A) .

Another application is the characterisation of nanoarrays that present nano-electrode behaviour. In nanoelectrodes, configurationthe diffusion layer is much larger than the electrode size and so a maximum of mass transport is obtained by simple electrolysis. Consequently when the redox reactions take place, the maximum of current to the electrode is already achieved and so the typical redox peaks are not seen, and the voltammogram becomes sigmoid shaped (Wang and 2006).

The Cyclic Voltammetry measurements were performed with the same apparatus used for the galvanostatic deposition of the polymer.

3.3 Plasma Processes

To create and maintain a plasma discharge, energy must be provided to the system to reach ionisation of the atoms or molecules of the plasma volume; upon ionisation,these atoms or molecules produce charged particles, electrons and ions that move randomly in the discharge (Lieberman 1994). The energy is provided by an electromagnetic field that is applied by a set of electrodes. A plasma is composed of ionised material and neutral molecules that are majority in the mixture. It can be characterised by the charged particle density ($ni/\ \mathrm{cm}^3$) and by the fractional ionisation (X_{iz}) that indicates the ratio of between ionised particle and neutrals. Most of the plasmas used for material processing are cold plasma discharges that interact with the substrate surface without heating it. In this type of plasmas, the energy is added to the electrons instead of the ions and background gas molecules, and the electrons can attain energies of 1-10 eV, while the background gas remains at ambient temperature. These plasmas are normally produced at low pressures (around ± 1 Torr) and are characterised by a charged particle density from 10^8 to $10^{13}\mathrm{cm}^3$ and $Xiz << 1$.

3.3.1 Plasma Etching

This process induces the removal of organic material by atomic oxygen free radicals that oxidise the alkyl chains present in the surface leading to their removal (Egitto 1990). In this work, plasma etching was performed using an oxygen plasma producedcarried out in a Magnetic Pole Enhanced-Inductive Coupled Plasma (MaPE-ICP), a high density plasma source developed at the NMI surface processing laboratory at the Joint Research Centre in Ispra (Meziani 2001). The reactor is based on a stainless plasma

chamber with a cylindrical geometry. The water cooled inductive coil is powered by a 13.56 MHz RF generator via a matching network composed of two driven air capacitors (Advanced Energy RFX II generator 1.25kW, matching network AZ90). The substrate holder is biased by a secondary RF supply (Advanced Energy RFX 600). The distance between the substrate holder and the dielectric widow was 8cm. The gas is injected using a ring tube placed at the top of the chamber. The plasma ionic density is controlled by the current flowing in the inductive antenna while the kinetics energy is controlled by the bias.

3.3.2 Plasma Enhanced Chemical Vapour Deposition

Plasma Enhanced Chemical Vapour Deposition (PE-CVD) is one of the major plasma processes used most used to obtained functionalised surfaces applied forin biological - applications (D'Agostino 2005; Muguruma 2007). This technique permits the achievement of layers of different physical chemical properties, from chemical composition, to wettability or mechanical properties. To obtain the different layer characteristics, is controlled the chemical composition of the plasma phase is controlled (gas precursors) and processing parameter (power, pressure, electrodes configuration) (D'Agostino 2005).

Silicon Oxide (SiOx) was deposited using a homemade plasma reactor with the same characteristics of the reactor used in the etching process, but in this case the substrate holderplasma process is not biased (Meziani 2001). This layer is deposited from hexadimethilsiloxane (Ssigma) precursor mixed with O2 and Ar gases; and the gas mixture is controlled by MKS mass flow controllers. The working pressure was 50 mTorr and the power 450watts.

The Polyethylene Oxide (PEO) deposition was carried out in pulsed mode using a reactor developed in the laboratory (Bretagnol 2006). The reactor has a stainless plasma

chamber (300×300×150 cm^3) equipped with two symmetrical parallel plate electrodes (5cm diameter) separated by 140cm. A RF generator connected to the upper electrode ignites the plasma and the other electrode is used has sample holder. The flow rate of the gas mixture (argon and diethylene glycol monomethyl ether (DEGDME)) (Sigma Aldrich) is controlled by MKS mass flow controllers. The working pressure is constant (20mTorr) and the power is ranged from 1 to 15 watts.

3.4 Nuclear Magnetic Resonance (NMR)

NMR is based in the capability of some atoms to rotate in a magnetic field, thus creating a magnetic dipole due to the nucleus charge. These atoms present a characteristic magnetic spin that is related to the charge distribution. ^{1}H-NMR is based in the nuclear magnetic spin of the ^{1}H hydrogen isotope. When placed in a magnetic field these hydrogen atoms align in the direction of the field. If after the atoms are exposed to another magnetic radiation the atoms rotate again in the new magnetic field direction due to the absorption of resonant magnetic frequency. The intensity of the magnetic spin is dependent on the local chemical environment, and thus different hydrogen atoms in the same molecule resonate at slightly different frequencies. The different frequencies are represented as chemical shifts that are reported as a relative measure of reference atoms resonance frequencies. By understanding different chemical environments, the chemical shift can be used to obtain precise structural information about the molecule in a sample (Silverstein 1997).

^{1}H-NMR spectra were recorded at 500 MHz on a spectrometer Bruker (Rheinstetten, Germany) DRX 500. Measurements were made at 300 K using a 2.5 mm inverse Broad Band probe. The samples were dissolved in deuterated chloroform ($CDCl_3$ 99.9%

isotope purity, Aldrich). Chemical shifts are given in δ (ppm) referred to Tetramethylsilane (TMS).

3.5 Infra-Red Spectroscopy

Infrared spectroscopy is technique is based in the adsorption of Infrared radiation by organic molecules. The adsorbed radiation is converted into molecular vibration energy. The adsorbed wavelengths depend on the types of bonds present in the different functional groups of the sample (Silverstein 1997). It gives information about chemical groups and purity of the sample in analysis.

The Infra-red spectra of the reagents and product of the Esterification reaction were obtained with the solid state of the pure samples using a spectrometer Perkin-Elmer (Boston, MA, USA) Spectrum one FT-IR.

3.6 Size Exclusion Chromatography (SEC)

SEC is based on the use of porous particles to separate molecules of different sizes. It is generally used to separate biological molecules, and to determine molecular weights and molecular weight distributions of polymers. The elution time is dependent on the average residence time in the porous particles that depends on the molecules size and shape. SEC can be used as a measure of both the size and the polydispersity of a synthesised polymer (Mori 1999).

SEC was carried out by means of an Alliance 2690 chromatograph (Milford, MA, USA) using a differential refractometer as on-line detector. The eluent, 0.15M sodium chloride, flowed at 0.8 ml/min through two ultrahydrogel size exclusion columns (250 and 120 A ° of pores size from Waters), at 35 ^{0}C. The calibration of this size exclusion chromatographic system was performed with twelve polyethylene oxide (PEO) and polyethylene glycol (PEG) narrow standards with the molar mass in the range between

160 and 160,000 g/mol. The number (Mn) and weight (Mw) averages of molar masses and the polydispersity index (Ip = Mw/Mn) were calculated from the whole molar mass distribution obtained from the polymeric peak and the direct SEC calibration (PEO/PEG standards).

3.7 X-Ray Photoelectron Spectroscopy (XPS)

XPS is a quantitative spectroscopy that allows the determination of elemental composition and chemical functionalities of materials present on a surface. XPS is based in the irradiation of a material with x-rays causing photoelectron ejection. The photoelectron kinetic energy is dependent on the nature and environment of the elements on the material and the concentration is determined from the photoelectron intensities. The energy balance is given by:

$$BE = h\nu - KE \quad \textbf{(3.1)}$$

Where BE is the binding energy of an electron to an atom, KE is the kinetics energy of the emitted electron (measurded by the instrument) and $h\nu$ is the energy of the X-rays. The depth of analysis is around 10nm (Goldstein 1992).

XPS measurements have been performed with an AXIS ULTRA Spectrometer (KRATOS Analytical, UK). Instrument calibration was performed using a clean pure Au/Cu sample and pure Ag sample (99.99%). Measured values for electron binding energies (BE) of samples were respectively 84.00+/-0.02 eV and 932.00+/-0.02 eV. The samples were irradiated with monochromatic AlK X-rays ($h\nu$=1486.6eV) using X-ray spot size of 400μm x700μm with a take off angle (TOA) of 90° with respect to the sample surface. The data were processed using the Vision2 software (Kratos, UK). Chemical surface composition was obtained from the survey spectra after linear background subtraction and using the RSF (Relative Sensitivity Factors) included in the software derived from Scofield cross-

sections. The C1s envelope was fitted with Gaussian-Lorenztian function (G/L=30) and variable full width half maximum.

3.8 Ellipsometry

Ellipsometry is a powerful tool for the characterisation of refractive index and thickness of thin films. This technique measures the change in polarisation state of light reflected from the surface of a sample. The reflected light becomes elliptically polarised in two polarisation directions for which the reflected light is plane polarised (p-polarised light and s-polarised light). The ellipsometer will measure the ratio of the reflected p- and s-components and the phase difference between these two components (Hauge 1980). These two parameters are related to the optical properties of the reflecting surface such as refractive index and the thickness. The actual value of the surface properties is determined through the use of an interactive regression fitting computer algorithm.

Ellipsometry measurements were carried out with a variable angle multi-wavelength imaging ellipsometer, model EP^3 by Nanofilm Surface Analysis GmbH. The measurements reported here were performed in air at room temperature at a fixed wavelength of λ = 532 nm using a low-capacity laser as light source. The angle of incidence was varied between 42° and 78°, with a step-width of 0.5° (73 measurements for each run). A conventional polarizer-compensator-sample-analyzer null-ellipsometry procedure was used to obtain the values of the ellipsometric parameters Δ and Ψ as a function of the angle of incidence. The resulting data were then fitted using the EP^3

4- Production of Nanoarrays based in Organothiols

Organothiols have the property to spontaneously self organize on the gold surface creating Self Assembled Monolayers through the formation of a sulphur-gold bond. These molecules can have many end groups and therefore can be used in this context to create fouling/non-fouling chemical contrast at nanoscale on a gold surface. For adhesive non-adhesive contrast the adhesive material can be based on carboxylic, amine or epoxy terminated organothiols and the non-adhesive based on material such as for instance PEO or oligomer oxyde. PEO layers are known to offer resistance to protein and cell adhesion (Lee 1989; Nagaoka 1990), thanks to their non-fouling characteristic manly associated to steric repulsion and hydratation mechanisms (Morra 2000; Vermette 2003). In this chapter, we will describe the methodology used for the production and characterisation of nanoarrays based on 16-Mercaptohexadecanoic acid (MHD) and thiolated PEO to produce the nano-contrast.

4.1- Synthesis and characterisation of Thiolated PEO

Thiolated PEO was synthesised using MHD, a sixteen chain organothiol that creates stable layers on the gold surface (Frederix 2004). The reaction of MHD with a polymeric PEO (polyethylene glycol mono methyl ether) produces a thiolated PEO with a long carbon chain between the PEO units and the sulphur atom (Figure 4.1). This characteristic contributes to the stability of the sulphur-gold bond and creates a good quality layer on the gold surface.

Thiolation of the PEO was based in a procedure described elsewhere (Du 2003). Briefly, 5 g (approximately 1mM) of polyethylene glycol mono methyl ether (MW=5000) (Fluka) was mixed with 144mg (5mM)of MHD (Aldrich) and some drops of sulphuric acid in 25ml of toluene preheated to 80ºC. The reaction proceeded for 16h with continuous stirring. The product of the reaction was then purified by removing the unreacted MHD by precipitation in isopropyl-ether (3 times). Finally the thiolated PEO was dried in vacuum for 3 days.

The reaction product, together with the reagents, were characterised by NMR and FT-IR.

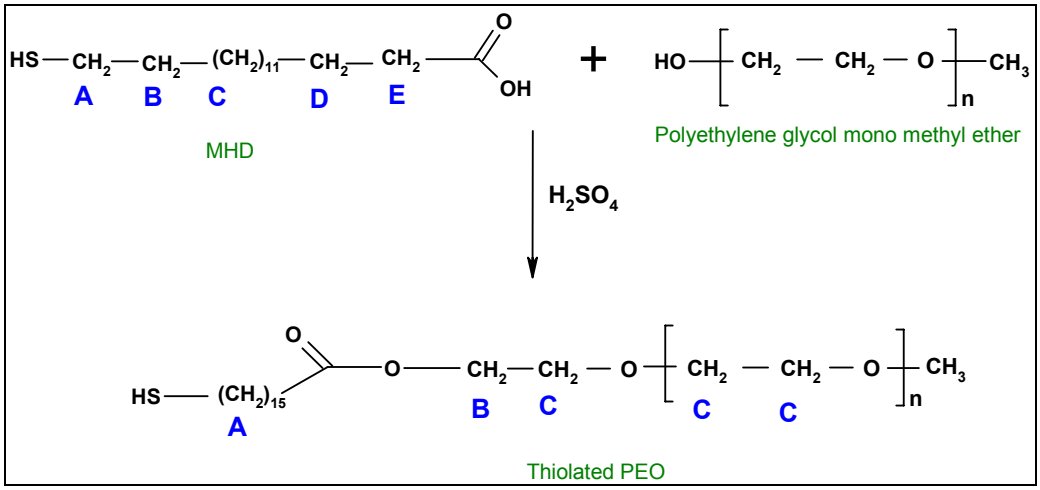

Figure 4.1 - Schema of Thiolated PEG-CH_3 synthesis.

The NMR spectrum of the PEO polymer reagent is shown in Figure 4.2. The spectrum presents the expected peaks for this type of polymers. At 3.3ppm is present a peak integrating 3 protons that is attributed to the CH3 protons and the large band at 2,6ppm is attributed to the hydroxyl proton. The multiplet at 3.6ppm corresponds to the protons from the CH2 groups. This peak integrates 450 protons which is in agreement with the molecular weight of the polymer (MW 5000)(Malmsten 1998):

$$5000 = Mw\,(CH3+OH) + Mw(CH2\text{-}CH2\text{-}O)n \Leftrightarrow 5000 = 32 + Mw(CH2\text{-}CH2\text{-}O)n \Leftrightarrow$$

$$\Leftrightarrow Mw(CH2\text{-}CH2\text{-}O)n = 4968$$

For, $Mw(CH2\text{-}CH2\text{-}O) = 44$ we obtain $n = 4968/44 = 112.9$

There are 4×n protons of CH2 type on the polymer, which means:

$$4 \times n = 452 \approx 450$$

The NMR analysis of MHD reagent shown in Figure 4.3 shows the S-H proton on the spectra by the triplet at 2,7ppm whereas a quartet peak that can be attributed to the protons on the carbon neighbouring to the S-H group at 2.6ppm (protons A in Figure 4.1). These protons are deshielded by inductive effect by the Sulphur resulting in peaks at lower field

(Pretsch 1985). The triplet at 2.4ppm integrating for 2 protons corresponds to the protons of the carbon adjacent to the carboxylic group (protons E in Figure 4.1), that are also deshielded by inductive effect by the carboxylic function.

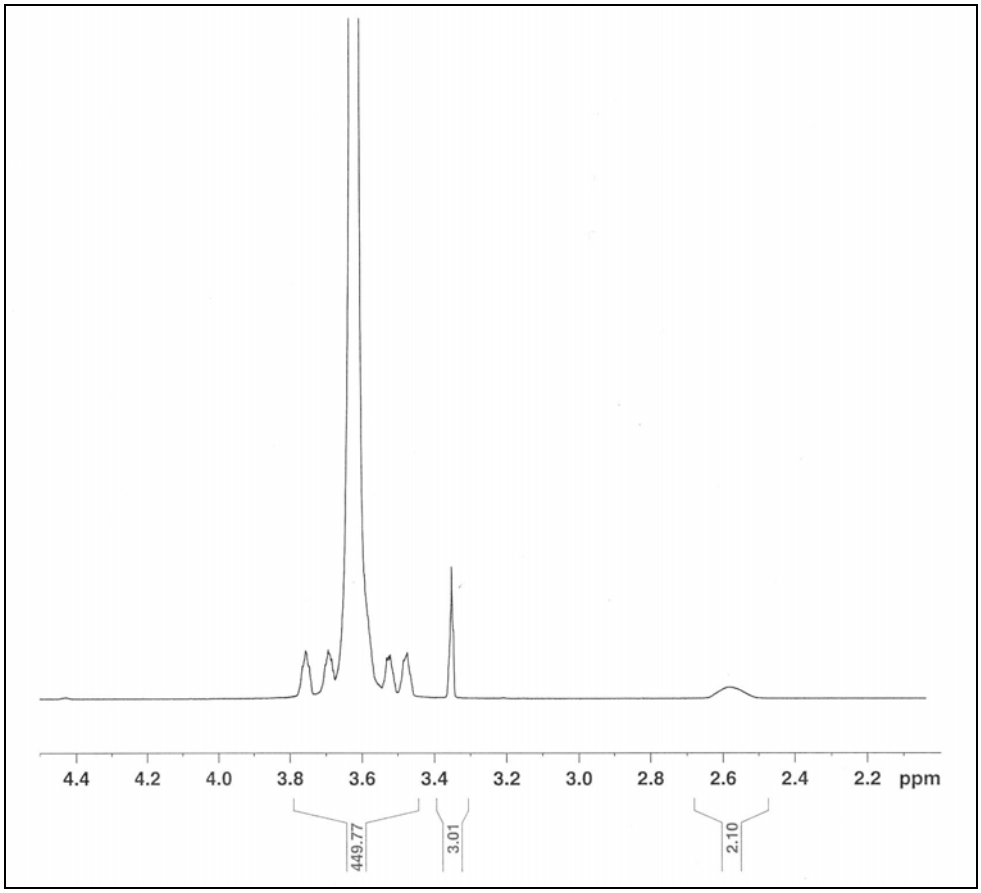

Figure 4.2 - NMR PEO reagent.

The multiplet at 1.65ppm integrates 4 protons and can be attributed to the protons represented in figure 1 as B and D. Even thought the effect is lower, these protons are as well exposed to an inductive deshielding. Finally at 1.3 ppm a multiplet that integrates for 26 protons is present and can be attributed to the other methylene protons (protons C in Figure 4.1). These protons are only 22 but even from the other peak integration is possible to conclude that this reagent presents some impurities.

The NMR spectrum of the thiolated PEO product (Figure 4.4) confirms the success of the reaction, in particular the peak at 4.3 ppm a (triplet) that corresponds to protons of

methylene group directly bonded to the ester group (protons B in Figure 4.1). The signals in the range 3.9 – 3.5 ppm are attributed to the methylene groups of PEO (protons C in Figure 1), in particular the signal at 3.65 ppm. The singlet at 2.4ppm is attributed to the CH_3 protons and includes the protons from the unreacted PEO reagent. The peak at 2.35 ppm can be attributed to the SH proton while the peaks between 1 and 2ppm correspond to the methylene groups of MHD (protons A in Figure 4.1).

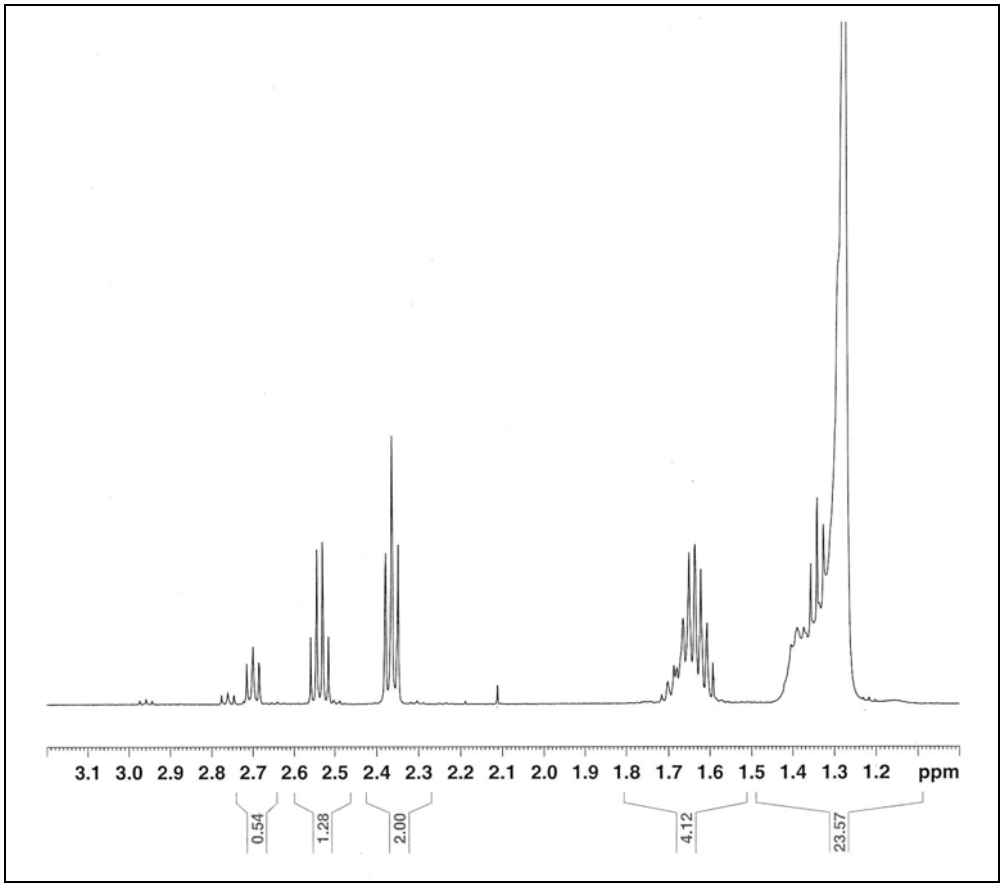

Figure 4.3 - NMR MHD reagent.

To calculate the yield of the reaction using NMR results, it was compared the integral of the signal at 4.3ppm with that of the signal at 3.4ppm related with CH_2 protons of the carbon bonded to the ester group and with the CH_3 protons, respectively. The final product is most probably a mixture of Thiolated PEO and the polymer reagent, thus the number of CH_2 protons is proportional to the total reacted OH groups and the CH_3 related with the total

reacted and unreacted OH groups. The measured integral ratio is found to be 1.86/2.99, very close to the theoretical maximum yield 2/3 (CH_2/CH_3), leading to a calculated reaction yield of about 93%.

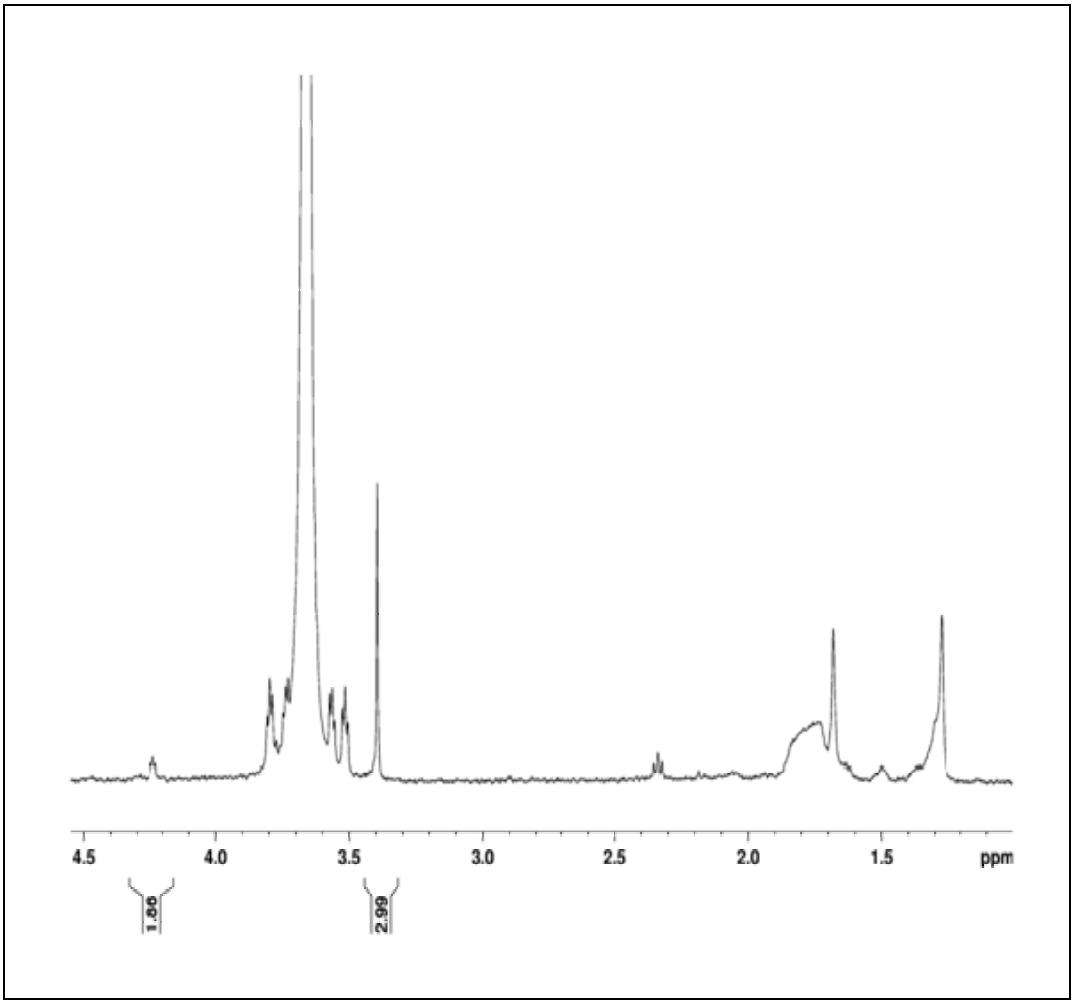

Figure 4.4 - NMR Thiolated PEO.

The FT-IR spectrum of the thiolated PEO (Figure 4.5) confirms as well the success of the reaction. Figure 4.5 shows a peak at 1735cm^{-1} that is characteristic of an ester carbonyl (C=O) bond. This band indicates that the PEO has reacted with the MHD, forming an ester bond and producing the thiolated PEO. The FT-IR spectrum of the PEO reagent (Figure 4.6) is very similar with the thiolated PEO product, even if the ester band is not present in the PEO reagent nor in the MHD reagent. The MHD spectrum (Figure 4.7) shows a C=O peak at

1692 cm^{-1} characteristic of carboxylic C=O which is not present in the FT-IR spectra of the thiolated PEO. This indicates that any unreacted MHD was correctly removed during the purification steps.

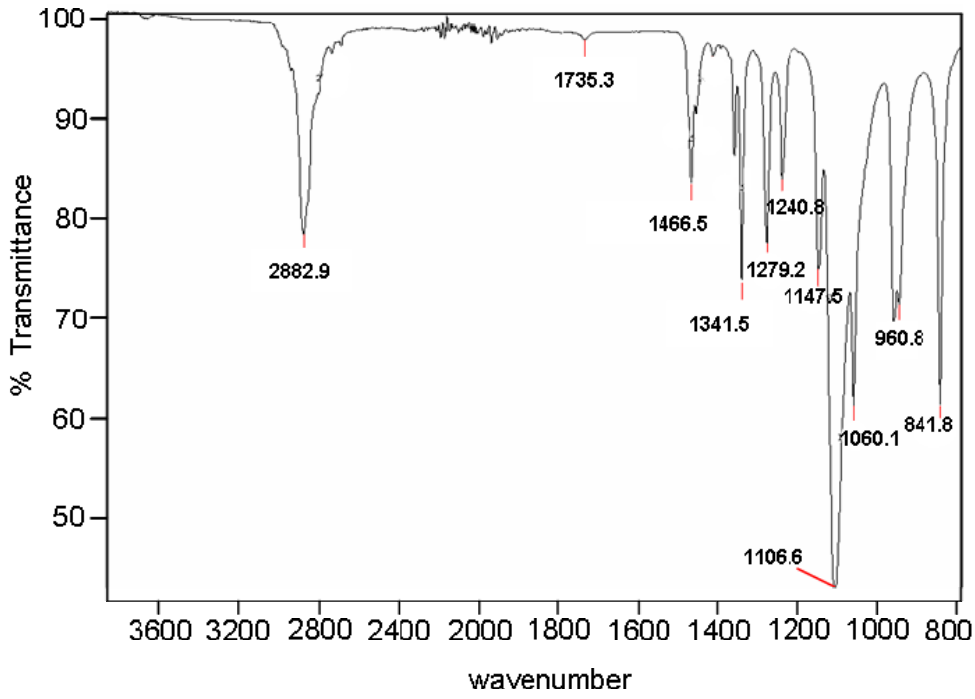

Figure 4.5 - Infra-red spectra of thiolated PEG.

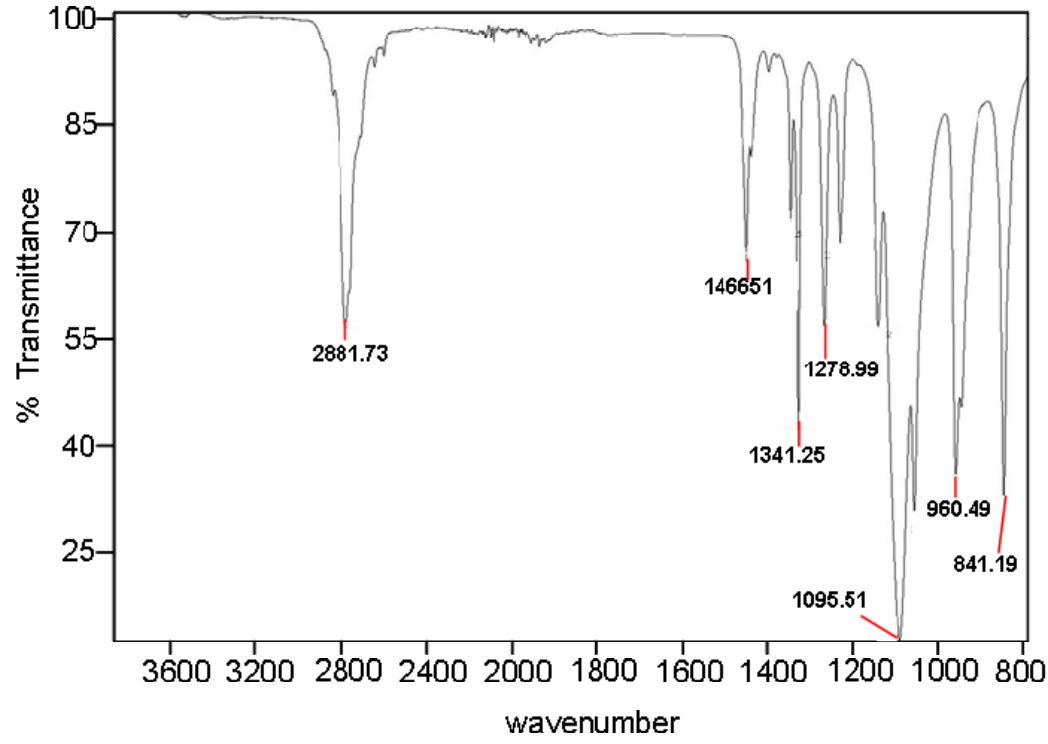

Figure 4.6 - Infra-red spectra of PEG (5000) (starting reagent).

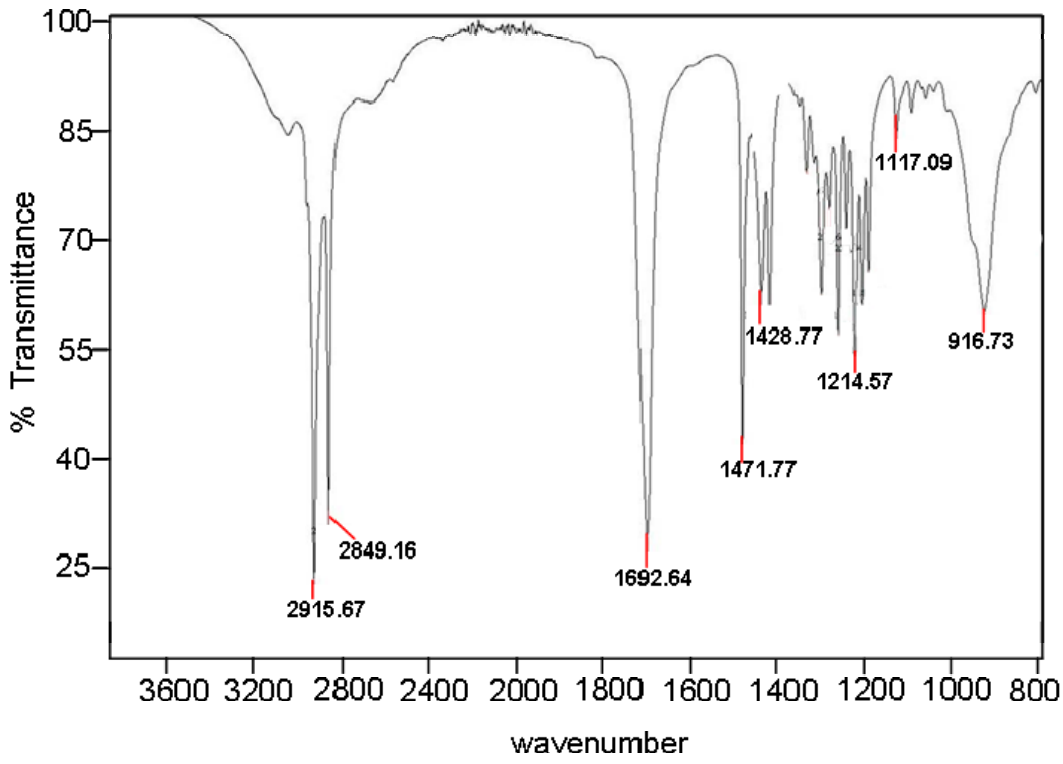

Figure 4.7- Infra-red spectra of MHD reagent.

The quality of the synthesised polymer was evaluated using SEC analysis. Figure 4.8 presents the comparison of the chromatograms of the PEO reagent and the thiolated PEO evidencing that the retention time is very similar. Nevertheless, the rifractometer signal presents some differences indicating small variations on the polymers nature.

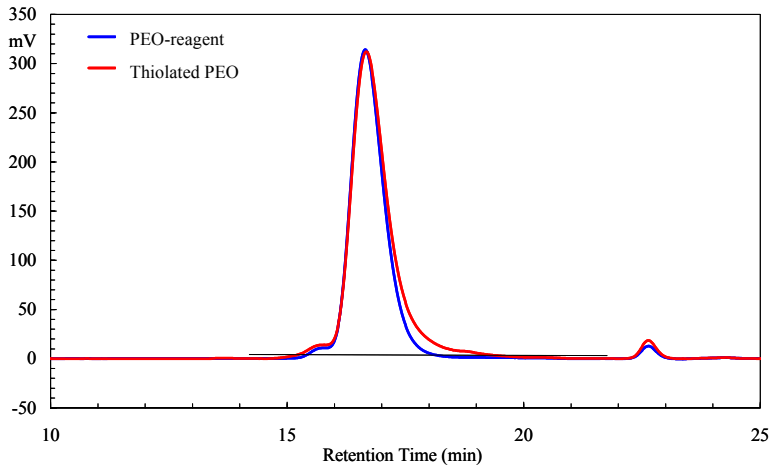

Figure 4.8 –Chromatograms of PEO reagent and thiolated PEO (rifractometer signal).

Table 4.1 presents the polydispersivity and molecular mass average of the two polymers. As expected, the average of the molar masses are similar for both polymers since the weight of the MHD chain grafted during the reaction is not significant compared to the total molecular weight of the polymer. The polydispersivity index (I_p) value for both samples is similar indicating that the thiolated PEO presents the same molecular weights distribution as the starting PEO. This result confirms that the reaction occurred without degradation of the polymer chain. SEC analysis demonstrates also that no disulphide formation occurred once no high molecular weight fractions were detected.

Sample	**M_n** g/mol	**M_w** g/mol	**I_p (M_w/M_n)**
PEO Reagent	4272	4596	1.08
Thiolated PEO	3810	4426	1.16

Table 4.1 - Molecular mass averages and polydispersivity index of the PEO reagent and thiolated PEO.

4.2 Characterisation of the two organothiols self assembled on gold

Before production of the nanoarray, the two different organothiols were separately self assembled on gold (previously deposited on silicon or on a quartz crystal chip of QCM) and the physico-chemical characteristics of the produced monolayer were assessed. The gold surfaces were cleaned with H_2O_2 (30%) /NH_3 (25%)/H_2O (1:1:5) for 10 minutes at 75ºC, followed by ethanol rinsing and immediately immersed in the organothiols solutions (5mM in ethanol) in the dark during 16 hours. After the chemisorption process, the samples were cleaned with ethanol in ultrasounds during 10 minutes and rinsed with ultra pure water. The chemical characteristics of the monolayers were evaluated by XPS, the thickness and refractive index by Ellipsometry and the fouling character by QCM measurements.

4.2.1 Chemical composition

Contamination of the layers by atmosphere elements, in particular oxygen and carbon containing compounds, were detected by XPS on the bare gold substrates even after an accurate cleaning process. showing that simple air exposure of the gold surface between the cleaning and the XPS measurement result in a re-contamination of the surface (Frederix 2004). To avoid gold contamination the chemisorption was performed immediately after the cleaning, transferring the surfaces from the ethanol immediately to the organothiols solution. As expected, the atomic composition of thiolated PEO and MHD modified surfaces (Table 4.2) show an increase of oxygen and carbon concentration and a correspondent decrease of the Au peak as compared to bare gold.

Sample	**Au** (84eV)	**C** (286eV)	**O** (532eV)	**S** (161 eV)	**C/Au**	**O/Au**
MHD	38.0 ± 1.7	53.12 ± 1.7	7.88 ± 0.36	1.55 ± 0.35	1.4	0.2
Thiolated PEO	16.1 ± 0.6	54.5 ± 2.2	28.9 ± 1.5	0.47 ± 0.2	3.4	1.7
Au	64.9 ± 0.5	33.9 ± 1.3	1.25 ± 0.6	n.d.	0.5	0.02

Table 4.2- Atomic composition (%) o MHD, thiolated PEO and gold surface. (n.d.= not detectable)

MHD C/O ratio (6.7) is slightly lower than the theoretical 16/2=8 probably due to a slight contamination of the surface. For the thiolated PEO the C/O ratio is 1.9, which is very close to the theoretical value of 2, thus demonstrating that the surface is most likely formed by PEO units (CH_2-CH_2-O).

In both cases the presence of sulphur is observed indicating the formation of a thiolated layer. Moreover the high-resolution S_{2p} core level spectrum of the two organothiols, illustrated in Figure 4.9, presents a main doublet structure with peaks at about 162eV and 163.2eV that can be assigned to the $S_{2p3/2}$ and $S_{2p1/2}$ spin orbit split levels. These results are in agreement with previous studies of organothiol adsorption on gold (Frederix 2004)

supporting that the sulphur is related to a thiolated chain. Moreover, sulphur signal above 166eV is not observed indicating that no oxidised sulphur is present at the surface which was expected from long chain organothiols (Evans 1991; Heister 2003).

The XPS C1s core level spectra before and after the organothiols chemisorption is presented in Figure 10. In the case of the cleaned gold, the carbon layer is mainly hydrocarbon (285eV), with a small contribution of C-O (286.5eV).

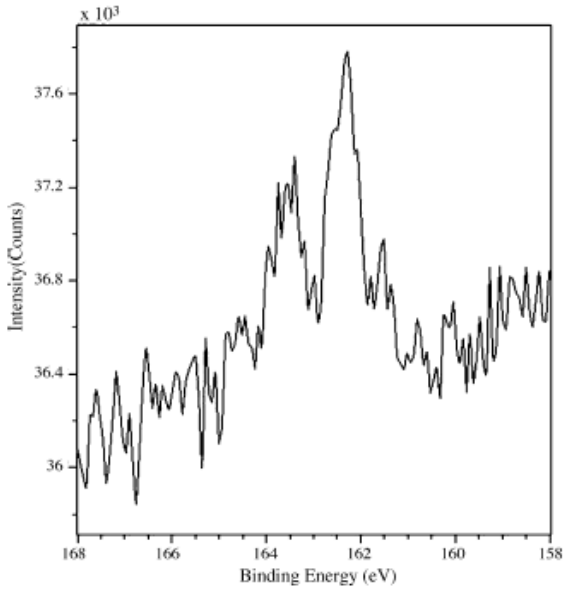

Figure 4.9 - S_{2p} XPS spectra of the thiolated surfaces

After MHD chemisorption three components are identified and can be attributed to CH_2 chain (284.9eV), to C-COOH (284.7eV) and finally to the most electrodeficient carbon (COOH) (289.6eV) (Whelan 2004). The intensity of each component is in agreement with the molecule structure (14:1:1). In the thiolated PEO spectrum three components were identified and attributed to C-O (286.7eV), C-C (285.0 eV) and finally C=O (287.9eV) that can be attributed to the ester bond created by the thiolation reaction (Beamson 1992). The C-O moiety is characteristic of the PEO-character (Sardella 2004) and gives an indication of the chain density. The thiolated PEO surfaces presented around 64 % of C-O component. This

result is comparable to the one obtained with plasma deposit PEO surfaces characterised by high protein and cell resistance (Bretagnol 2006).

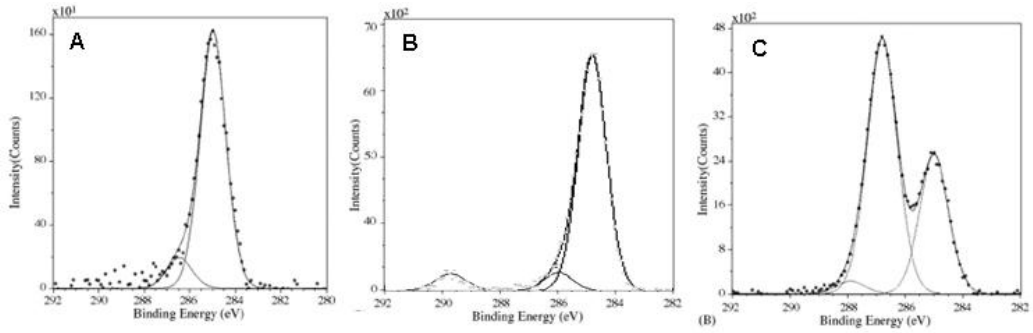

Figure 4.10 - C1s carbon peak of a) bare gold, b) MHD and c) thiolated PEO

4.2.2 Thickness and Density

The SAMS were deposit on 150 nm gold coated silicon wafer. To determine the complex refractive index $n_{Au} + ik_{Au}$ of the gold layer, variable-angle ellipsometry was used and n_{Au} = 0.4865 and k_{Au} = 2.0934 were calculated. After chemisorption, the effective thickness and the refractive index of the resulting layers were determined from angle-resolved measurements of Δ and Ψ, using a three-layer air-(organothiol)-gold model with fixed $n_{Au} + ik_{Au}$ as determined previously, and assuming a refractive index of the thiolated-PEO and MHD layer to be 1.47 and 1.45 respectively (Chien 2006; Tokumitsu 2002). Very good fits to the angle resolved measurements of Δ and Ψ were obtained over the entire angular region. Table 4.3 resumes the thickness values obtain for the monolayers, showing that the two layers have less than 1nm difference in thickness.

Sample	Thickness (nm)	*n*
MHD	2.4	1.45
Thiolated PEO	1.7	1.47

Table 4.3- Thickness and refractive index values of MHD and thiolated PEO, as measured by ellipsometry.

Additional information on chain density of the thiolated PEO surfaces can be extrapolated from the Ellipsometry measurements. The density of PEO layers is intrinsically connected with the level of protein resistance (Unsworth 2005).

Based on the Lorentz-Lorenz (Born 1965) relation for the refractive index (n) of a pure substance the adsorbed mass per area (μ) can be written as:

$$\mu = d \cdot \rho^0 = \frac{0.1 \cdot M_w \cdot d}{A} \frac{n^2 - 1}{n^2 + 2} \quad \textbf{(4.1)}$$

where A is the molar refractivity of the substance, ρ^0 is the film density, M_w is the molecular weight of the substance and d is the film thickness. For the thiolated PEO surfaces n = 1.47, d = 1.69 nm, as determined by Ellipsometry, and Mw = 5270 g/mole. A was calculated as 1336.2 cm^3/mole using the values of the molar refractivities of atoms and atom groups reported earlier (Cuypers 1983; Vogel 1954). Once the adsorbed mass is known, the chain density σ can be calculated from:

$$\sigma = \frac{N_a \cdot \mu \cdot 10^{-20}}{M_w} \quad \textbf{(4.2)},$$

where N_a is Avogadro's number. With μ = 0.19×10^{-6} g/cm^2 we obtain a value of 0.21± 0.03 chains per nm^2 for σ.

Alternatively, the chain density can be calculated using the equation proposed by Sofia et al. (Sofia 1998)for the average distance L between the chain attachment points:

$$L = \left(\frac{M_w}{\rho \cdot d \cdot N_a} \right)^{1/2} \quad \textbf{(4.3)}$$

with ρ^0 = 1.08g/cm^3 and d, n and Mw as above. The surface chain density can then be calculated as:

$$\sigma = \frac{1}{L^2} \quad \textbf{(4.4)}$$

With this method a value of 0.21±0.03 chains per nm^2 is obtained. The calculation of the chain density by the two methods leads to the same result and indicates that the thiolated PEO is in a brush regime since the estimated chain density of a mushroom regime should

have a much lower value (0.04chains/nm^2) (Unsworth 2005) The obtained chain density is lower than the estimated maximum for a brush regime (5.8 chains/nm^2)(Unsworth 2005) and is half of the reported ideal value to obtain an optimal hydration state that completely prevents protein adsorption (Unsworth 2005). Nevertheless, the fact that the thiolated PEO is in a brush regime and has a good surface coverage together with the high content of C-O component should guarantee good non-fouling characteristics as indicated by the increased protein resistance of these surfaces. (see chapter 4.2.3).

4.2.3 Bio-adhesive character

The protein resistance of chemisorbed thiolated PEO and MHD was studied by QCM-D, with two proteins, BSA and Lysozyme. The choice of these two proteins was made because they have different isoelectric points making possible to study the adsorption kinetics of two proteins of opposite charge at pH = 7 on the monolayer surfaces. Since the molecular weights of the two proteins are very different, it is possible to compare the effect of protein size on the adsorption. The properties of the BSA and Lysozyme are summarised in Table 4.4.

The sensor was equilibrated with PBS buffer (20mM pH7) to obtain a stable frequency and dissipation baseline signal. After that step, the buffer was replaced by a solution of BSA or Lysozyme (45µg/ml in PBS), and the monitoring was performed until the stability of the signal. Finally the buffer was again introduced and the frequency shift (Δf) between the two buffer steps was calculated. All measurements were performed at 25°C. The Δf was converted in mass change (Δm) using the Sauerbrey equation (Sauerbrey 1959) as follows:

$$\Delta m = \frac{-C\Delta f}{n} \quad \textbf{(4.5)}$$

Where C= 17.7ng Hz^{-1}cm^{-2} for a 5MHz crystal, and n= 1,3,5,7 correspondent to the overtone number.

Protein	Charge at pH=7	Mw (Da)	% reduction of adsorption by PEO surface	% increase of adsorption by MHD surface
Lysosyme	positive	14 500	53.3	55.1
BSA	negative	66 250	52.2	45.8

Table 4.4 - Protein characteristics and adsorption evaluation on the two monolayers.

Results shown in Figure 4.11 indicate that the protein adsorption on the thiolated PEO surface is reduced as compared to the gold surface. The adsorption on the carboxylic functionalised MHD surface is more than the double of the one obtained with the PEO surface, as expected from a fouling surface.

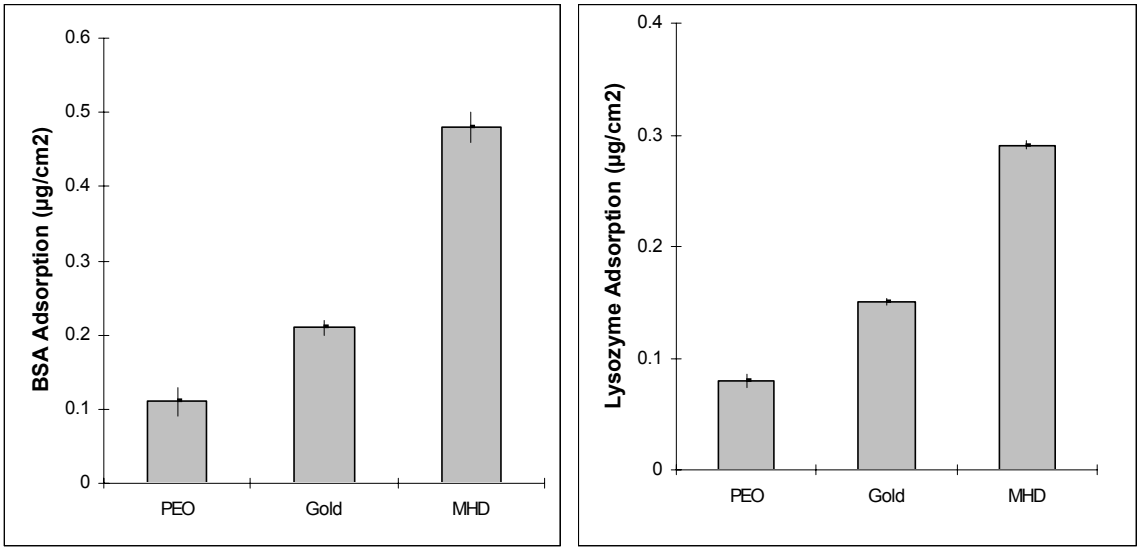

Figure 4.11 - Protein adsorption on bare gold, thiolated PEO and a carboxylic surface (MHD).

The percentage of reduction in protein adsorption for the PEO surface is similar for Lysozyme and BSA indicating a same resistance whether the protein has high or low molecular weight and whether it has positive or negative charge (Table 4.4). In the case of MHD surface the adsorption is highly increased in the case of Lysozyme which is related to

the positive charge of the protein that adsorbs more on the negatively charged MHD surface because of electrostatic interactions.

These results demonstrate clearly the non-adhesive character of the thiolated PEO developed in this work.

4.3- Nanoarray Production and Characterisation

The production of the nanoarrayed organothiols involves three main steps: gold uniform modification with MHD, creation of MHD nanopattern on gold by plasma colloidal lithography and finally gold functionalisation with PEO creating MHD/PEO nanoarray. The steps of production were controlled by Cyclic Voltammetry, AFM and SEM. The chemical nano-contrast was evidenced by selectively immobilised amine functionalised gold nanoparticles on the carboxylic nano areas.

4.3.1- Steps of production

The first step of the nanoarray production consists in the deposition of a self-assembled monolayer of MHD on the gold surface, as described in the chapter 4.2 which will constitute the bio adhesive spots after the nano-patterning. Then the 2D colloidal nano-mask consisting of Polystyrene (PS) nano beads (500nm diameter) functionalised with carboxylic groups (sigma-Aldrich) is self-assembled on the MHD functionalised gold surface by means of spin-coating using an approach previously described (Valsesia 2008). Water and surfactants (sodium bicarbonate and potassium sulphate) that stabilize the colloidal PS suspension, to avoid flocculation, were removed by centrifugation of the suspension (13500 rpm for 1minute). This step improves the hydrophilicity of the beads for a better adhesion on the carboxylic surface. The pellet was then re-suspended in a solution of 200:1 Methanol: Triton®-X100 a nonionic surfactant that reduces the surface tension of the liquid allowing the formation of the bead monolayer. The Methanol easily evaporates and being an organic

solvent the hydrophilic beads preferentially adsorb on the surface. After this process, the deposition parameters of the beads were optimised in order to obtain surface coverage over a large area. The spin coater velocity was maintained constant (800rpm) and the solution volume varied. Figure 4.12 shows the optical microscopy images of the beads monolayer for different volumes of beads solution deposited on the SPRi chips. Low solution volumes create large non covered areas whereas high solution volumes create double layers. The ideal volume for the deposition of the beads on the gold surface of the SPRi chip (rectangular surface: 7.8cm^2) was found to be 10µl leading to a surface coverage of 70% of a hexagonal poly-crystal bead layer. The same study was perform for 1cm^2 gold surfaces deposit on glass (used for AFM and SEM characterisation experiments) and in this case was found that 3µl was the ideal volume for the beads deposition.

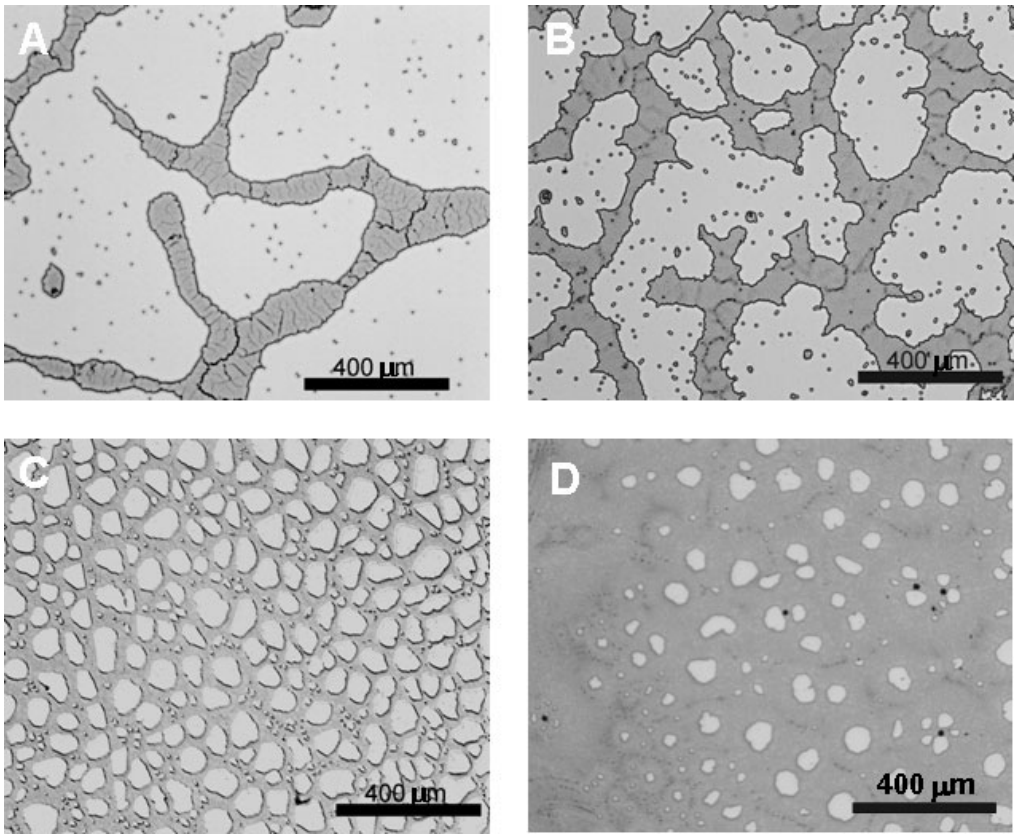

Figure 4.12 - Optical microscopy images (magnification 500 ×) of PS beads deposition on MHD functionalised gold surface (SPRi chip) with different solution volumes: A) 3µl; B) 5µl; C) 7µl and D) 10µl.

The calculation of surface coverage was done by a statistics histogram of the black and white version of the optical microscope images, using the NT-MDT software.

The next fabrication step is a plasma etching process to reduce the size of the beads and etch the unprotected MHD for subsequent thiolated PEO deposition on gold. The etching step was done with a High Density Inductively Coupled Plasma Reactor, using Oxygen as etching gas. The final size and shape of the beads is controlled by a fine tuning of the etching parameters such as operation pressure and inductive power. For instance, high working pressure induces isotropic etching that changes the beads geometry. High inductive power (P>180 W) and Voltage (|V|>150V) induce melting and consequent merging of the beads (Valsesia 2008). Process parameter i.e. lower pressure (10 mTorr) and milder plasma conditions (P= 150W and |V|= 100 v) allow to maintain the shape of the beads and control their final size by controlling the etching time.

Three different etching times (60s, 80s, and 90s) were studied. Figure 4.13 presents the SEM image of the beads after the different etching times and the correspondent AFM image of the surface after beads removal. The SEM images show that the bead diameter is reduced while maintaining the hexagonal poly-crystal distribution on the surface. The correspondent AFM images evidence a decrease in the MHD spot diameter with the increase of etching time. After 60 seconds of etching, a MHD spot of 180nm diameter is obtained and increasing the time to 80 seconds, 140nm spots are obtained. Longer etching time led to contamination of the sample and polystyrene re-deposition on the mask interstices (Figure 4.13 C1). It was found that 60 seconds was the ideal etching time to obtain reasonable dimension and separation of the carboxylic areas. These etching conditions were used in the followed study.

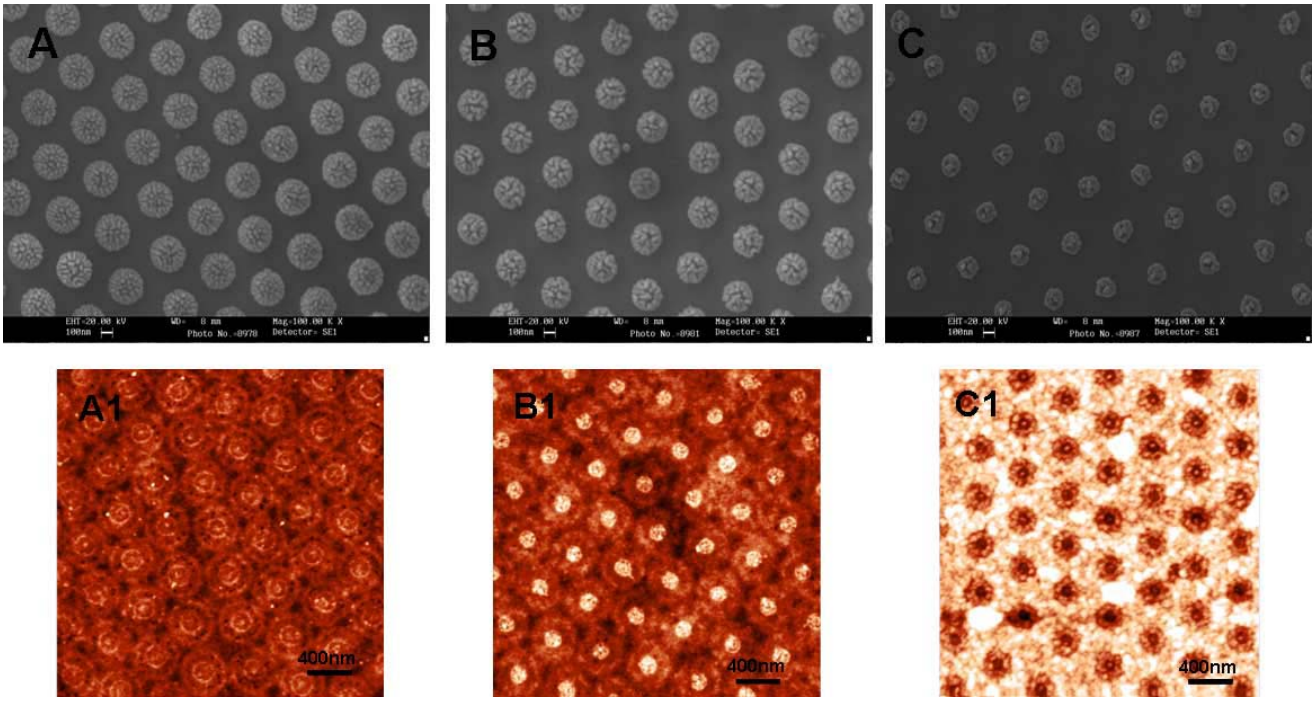

Figure 4.13 - Analysis after etching process with O_2 plasma (P= 150W an d |V|= 100). SEM images (field o view is 7×5 μm^2) of PS beads etched and correspondent AFM image (vertical scale 0-3 nm) of resulting MHD spots after the different etching times: A) 60s; B) 80s; C) 90s.

From the topography image obtained after 60 seconds etching (Figure 4.14), is can be seen that the MHD is not completely removed from the Au substrate. This is explained by the fact that the size of the nano mask varies with time and therefore the MHD plasma exposition is not constant in all locations. Nevertheless the presence of some MHD residues on the surface do not affect the quality of the thiolated PEO deposit afterwards as will be seen in the subsequently studies. The thickness of the MHD layer is estimated from the height profile shown in Figure 4.1.4, and a value of about 2.5 nm is obtained which is in agreement with the ellipsometry analysis in chapter 4.2.2.

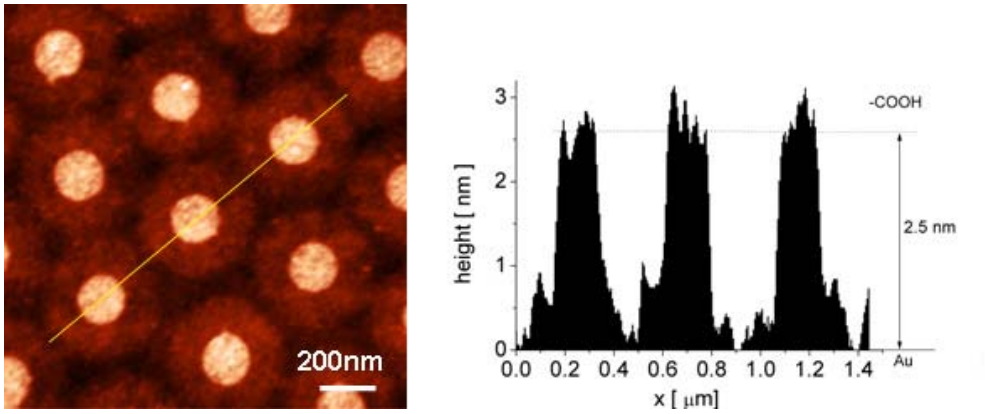

Figure 4.14 - AFM topographic image (vertical scale 0-3nm) of the surface after 60s etching and profile analysis along yellow line.

After the etching process the etched areas of the nanoarray of MHD spots are backfilled with thiolated PEO. The minimum chemisorption time to create a quality monolayer of organothiols on gold is usually 3h (Frederix 2004) but in this case such long time results in a complete coverage of the nano areas of MHD and loss of the surface patterning. It was found that to obtain a good quality nanopatterned surface the maximum time of chemisorption should be around 10 minutes. Finally the removal of the beads is done by sonicating the surface in water during 10 minutes.

The different optimised steps of fabrication were characterised by cyclic voltammetry. The redox reaction of the couple $Fe(CN)_6^{3-}$/ $Fe(CN)_6^{4-}$ was monitored using the modified surfaces as working electrode. The CV measurements were carried out with a graphite rod as counter electrode and a saturated calomel electrode (SCE) as reference. The electrolyte was an aqueous solution of KCl (1M) (Sigma-Aldrich) / C6FeK3N6 (5mM) (Fluka) degassed with nitrogen flow during 30 minutes. The measurements were done with a scan rate of 10mV/s at room temperature. The absence of interfering contaminants on the surfaces was verified by a pre-cycling the samples in KCl (1M). As expected in the presence of bare gold electrode, the voltammogram presents the typical peak shape (Figure 4.14)(Wang and 2006). The functionalisation with MHD creates an insulating layer on the gold electrode

reducing dramatically the collected current (no peaks present), thus indicating a good surface coverage (Figure 4.15 A).

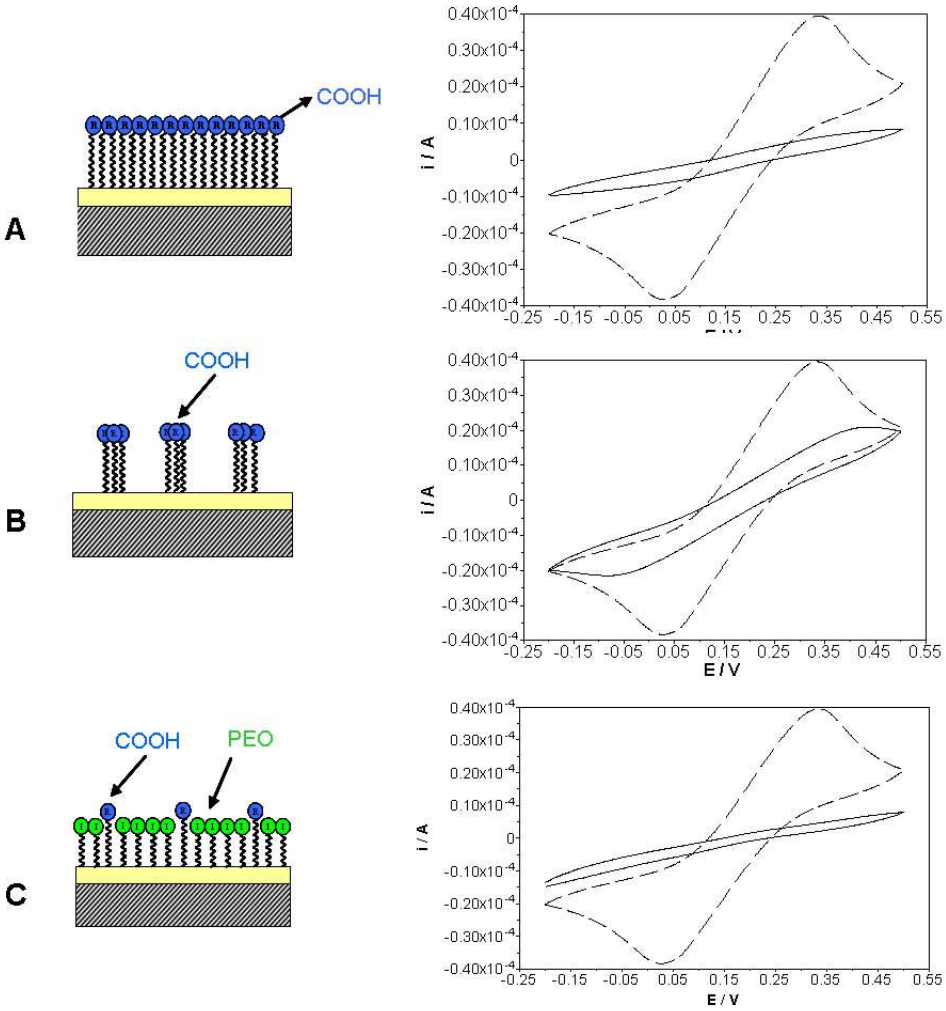

Figure 4.15 - Nanoarray fabrication steps and correspondent cyclic Voltammetry study comparing bare gold (dashed line) with the modified surfaces (solid line). (a) COOH functionalisation (b) Plasma etching through colloidal mask (c) COOH/PEO nanopattern.

After the polystyrene beads deposition, etching and removal, the voltammogram presents a peak shape with lower definition compared to the bare gold (Figure 4.15 B) due to the presence of the MHD nano-areas. Finally after the PEO chemisorption, the surface is again well covered as demonstrated by the non-peak shape voltammogram (Figure 4.15 C).

4.3.2- AFM analysis of the final Nanoarray

AFM analysis of the nano-arrayed surface produced on the SPRi chip presents a poorly distinguishable pattern from the topography image (Figure 1.16 A) due to the high RMS roughness of the gold substrate (~1nm) and the low difference of topography of the nanopattern (difference in height <1 nm between MHD and PEO SAMs) .

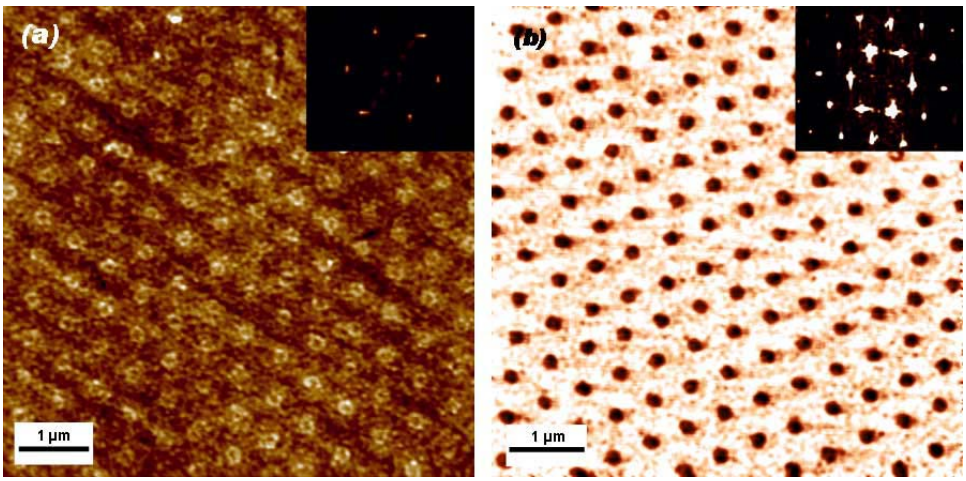

Figure 4.16 - AFM characterisation of the Nanoarray on the SPRi chip: A- topography image (vertical scale 0-5 nm), inset 2D-FFT; B- phase image (colour scale: -2^{o} to 1^{o}), inset 2D-FFT.

Nevertheless the hexagonal crystalline arrangement of organothiol nanoarray is confirmed by the 2-D Fast Fourier Transform (FFT) of the height function (Figure 1.16 A, inset) and by the phase contrast image (Figure 4.16 B) due to the different chemical properties of the two head groups present on the surface. The surface is characterised by a 2D hexagonal lattice of carboxylic spots surrounded by PEO.

In order to have a more accurate characterisation of the nanoarray smooth gold deposit on glass (RMS roughness of 0.15 nm) was used. The smooth gold permits to correctly characterise the different thicknesses between the two organothiols. Figure 4.17 presents a single MHD spot surrounded by the thiolated PEO showing that the border between the two materials is higher than the carboxylic spot. This effect is attributed to a mismatch of the two organothiol, due to incomplete etching of the MHD layer.

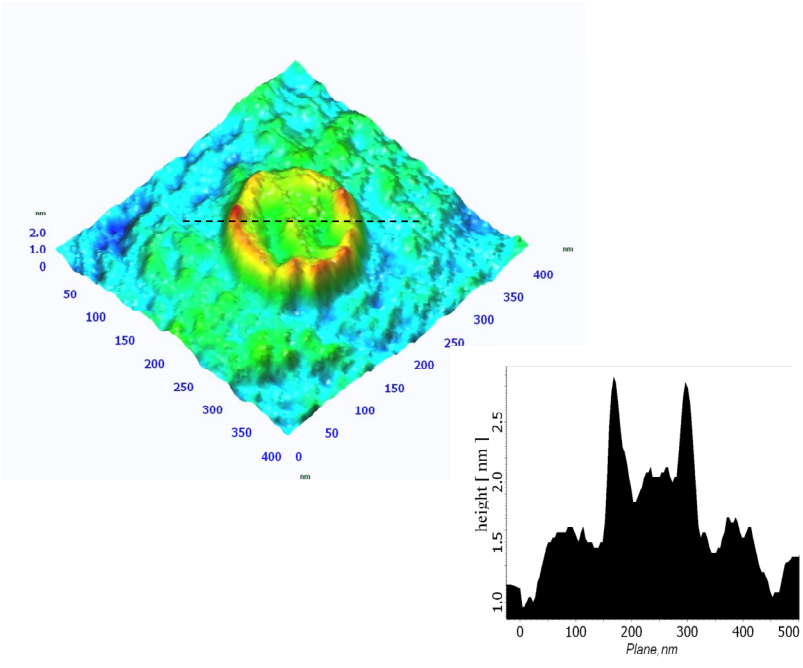

Figure 4.17 - 3D AFM image of a single MHD spot surrounded by thiolated PEO matrix and respective profile.

Figure 4.18 shows the contrast of MHD (white circles) and the thiolated PEO surrounding matrix. The height profile along a line with four carboxylic areas shows a difference in height of about 1 nm between the two organothiol layers (Figure 4.17.) It is thus possible to estimate the thickness of the thiolated PEO to be 1.5nm which is in agreement with the ellipsometry measurements.

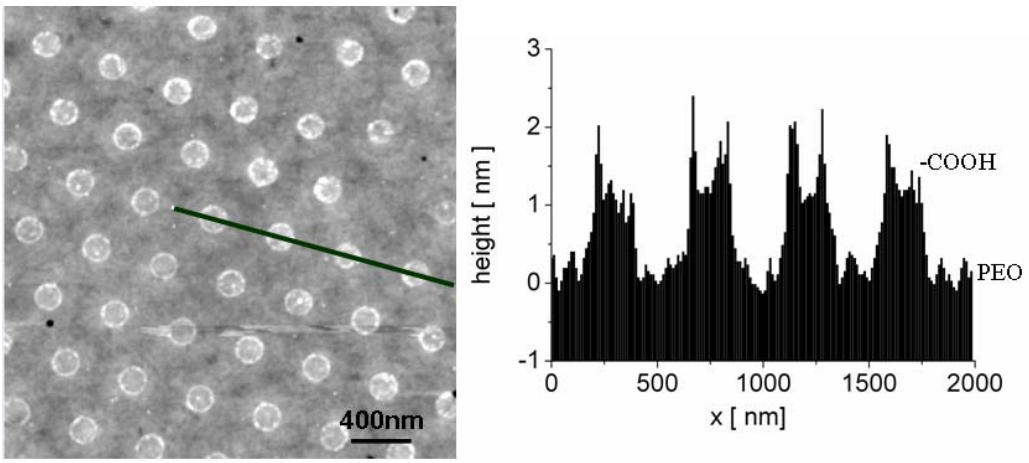

Figure 4.18 - AFM topographic image of the nanoarray (vertical scale 0-3 nm) and Height profile along the green line.

The carboxylic area present on the surface is calculated taking in account the beads surface coverage (70%) and the diameter of the carboxylic spots (180nm). Figure 4.18 presents a schematic of the hexagonal distribution of the carboxylic spots on the surface, showing the subdivision in parallelograms. The area of each parallelogram can be determined by the following expression:

$$A_{parallelogram} = h \times d \quad \textbf{(4.6)} \qquad \text{and} \qquad h = \sqrt{d^2 - \frac{d^2}{2}} \quad \textbf{(4.7)}$$

Taking ***d*** the lattice constant of the spots distribution as 500nm, the calculated area of the parallelogram is 0.216μm^2.

For a spot radius of 90nm, the calculated carboxylic area present in a parallelogram is 0,025 μm^2, which means that the carboxylic spot represents 12% of the parallelogram area and as well of the area covered by the nanoarray. Knowing that the area of the nanoarray is 70% of the total area is calculated that 8.4% of the surface presents carboxylic function.

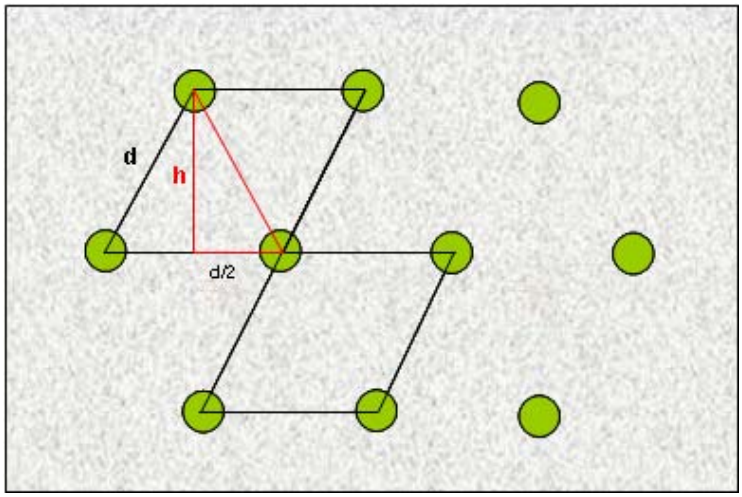

Figure 1.18 - Geometry of the nanoarray on the gold surface.

To compare the nanoarrayed surfaces with non crystalline nano-patterns, it was created in the SPRi chip some random nano-patters. The non crystalline nano-pattern was produced using colloidal lithography as performed for the nanoarray, but in this case the colloidal mask

was deposited by transferring the colloidal beads floating on the air/water interface to a MHD functionalised gold surface. Briefly, the PS suspension (Sigma-Aldrich, nominal bead size = 500 nm, 2% of solid content, dispersed in water and stabilised by salt, surfactants and PS) is centrifuged for 5 min at 6000 rpm, after removing the supernatant the PS are re-suspended in MeOH by keeping constant the original concentration. This operation is repeated 6 times. In this way, the surfactants stabilizing the colloid are removed from the PS surface and the beads can float on 0.1 M KCl solution in water. KCl solution is filling a transfer trough made of Teflon with the capacity of 10 ml. The PS suspension in MeOH is spread on the air/water interface by a micropipette, forming a monolayer. The PS monolayer is transferred to the MHD-functionalised gold substrate using the latter as a spoon. In this way a non-crystalline monolayer of beads is deposited on the substrate. After the patterning process, the carboxylic total area and spot dimensions were maintained similar to the crystalline array, as measured by AFM. The surface was characterised by nano spots of bioadhesive material distributed randomly on a PEO matrix.

4.3.3- Adsorption of Gold nanoparticles on the nanoarray

The presence of the chemical contrast between COOH nanospots and the PEO matrix was studied by exposing the nanoarray produced on the SPRi chip to a suspension of gold nanoparticles functionalised with aminothiophenol and thus presenting positively charged surfaces. The surface was in contact with the nanoparticles solution during 1 hour at pH7. At pH 7 the amine groups are positively charged and so the particles are expected to selectively adsorb onto the negatively charge carboxylic nanospots (PEO is neutral). The AFM analysis shows that the nanoparticles are absorbed on the negatively charged carboxylic groups of the MHD domains and not on the neutrally charged PEO covered areas (Figure 4.20 A). AFM height profiles (Figure 4.20 B) also show that the objects immobilised on the COOH areas are around 9 nm high, in agreement with the nominal diameter of the nanoparticles (10 nm). These results confirm the nanoscale chemical contrast with COOH spot size of 180 nm.

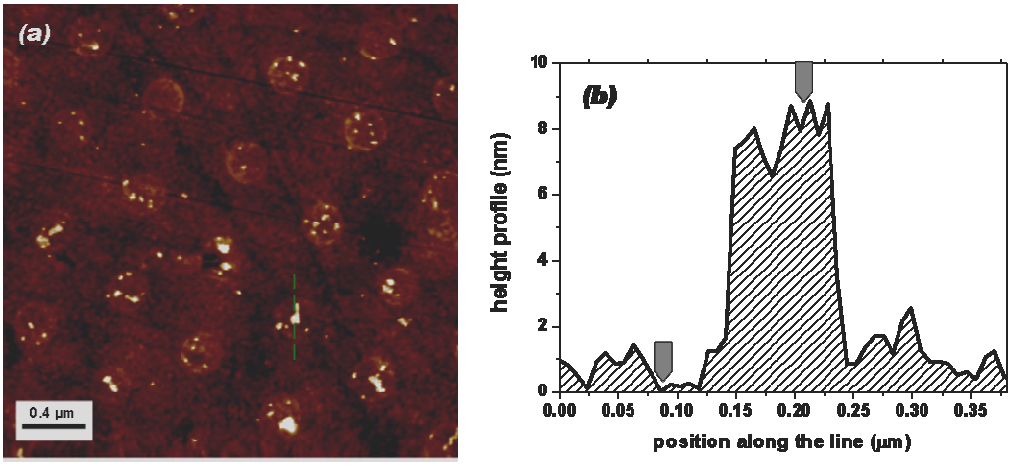

Figure 4.20 - A) Topography image after gold nanoparticles immobilisation (vertical scale 2-20nm) and B) Height profile along the dashed line in A.

5 SPRi studies of immunoreaction using nanoarrayed organothiols surface

This chapter presents the study of the effect of nanoarrayed surfaces on SPRi detection performance of immunoreaction by using immunoglobulin antibodies. The nanoarrayed surface presents organothiol based adhesive and non-adhesive areas to control the immobilisation of the proteins at nano-scale thus creating an optical grating thanks to the modulation of refractive index between the proteins and the buffer. The objective is to study the interaction of the grating with the surface plasmon wave for a potential SPRi detection signal improvement. In this study was monitored Human IgG/anti-Human IgG immunoreactions using a SPR chip modified with the nanoarray of organothiols (see chapter 4 for the fabrication). The results were compared with results obtained with uniformly functionalised carboxylic surfaces and as well with QCM measurements. AFM measurements of the immobilized proteins on the nanoarray were performed, in order to analyse in detail the mode of protein interactions with the nano patterned surfaces during SPRi experiments.

5.1 Signal enhancement by optical grating

To perform the comparison of SPRi performance in both surfaces simultaneously, the gold coated prism surface was divided in two adjacent areas, one being patterned with the nanoarray of two different organothiols (thiolated PEO and MHD) and the other uniformly coated with MHD.

The SPR measurements started by passing phosphate buffer saline (PBS) (10mM pH 7.4) with 12.5µl/min of flow rate until obtaining a stable signal as the initial baseline. All the protein solutions were prepared using the same PBS and added with the same flow

rate. The different solutions were injected in a 200µl loop and after were pulled into the cell chamber by the PBS buffer.

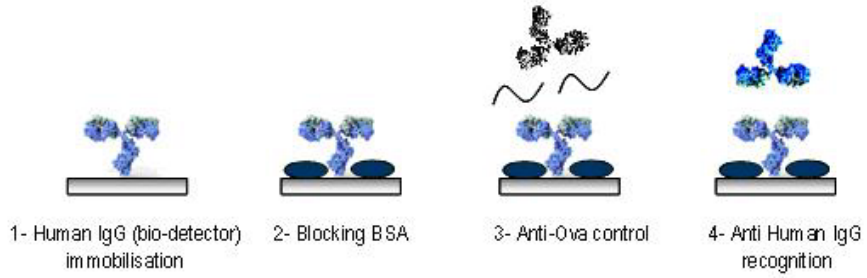

Figure 5.1 - Schema of the bio-assay monitorated by SPRi.

The various steps involved in the bio recognition assay are represented in figure 5.1.
The first step of the SPRi experiment was the immobilisation of the bio-detector (Human IgG, 50µg/ml, Sigma-Aldrich) in PBS onto the surface. This operation is performed for 32 minutes (two injections of 16 minutes). MHD acid is negatively charge at pH 7.4 thus Human IgG is adsorbed on the nano areas mainly by electrostatic interactions between the positively charged amine groups of the residue amino acids and the negatively charged carboxylic groups on the surface nano areas (Lee 2004; Leopold 2002). After, the unmodified MHD areas were passivated by a blocking step with BSA (Sigma-Aldrich) (200µg/ml in PBS, two injections of 16 minutes) to avoid unspecific binding. Then, a specificity control was performed by using anti-Ovalbumin (OVA) (Sigma-Aldrich) (25 µg/ml, 16 minutes). After the control steps, the recognition of the analyte (anti-Human IgG (Ab specific, 10µg/ml 16 minutes, Sigma-Aldrich) has been performed. The analyte being Ab specific ensure that the immunoreaction will take place only with the recognition sites of the immobilised Human IgG so can give some information on the orientation and activity of the antibody on the different surfaces.

Reflectivity curves of figure 5.2 show that the SPRi reflectivity relative change is higher for the nanoarrayed surfaces than for the uniform surface for all step of the assay. This is confirmed by the image contrast obtained after IgG and Anti IgG immobilization by the SPR CCD camera (Figure 5.3) where the brighter colour is a result of a higher change in reflectivity. For both surfaces, the signal produced by anti-OVA adsorption was less than 10% of the signal measured for Ab IgG recognition, indicating a good specificity.

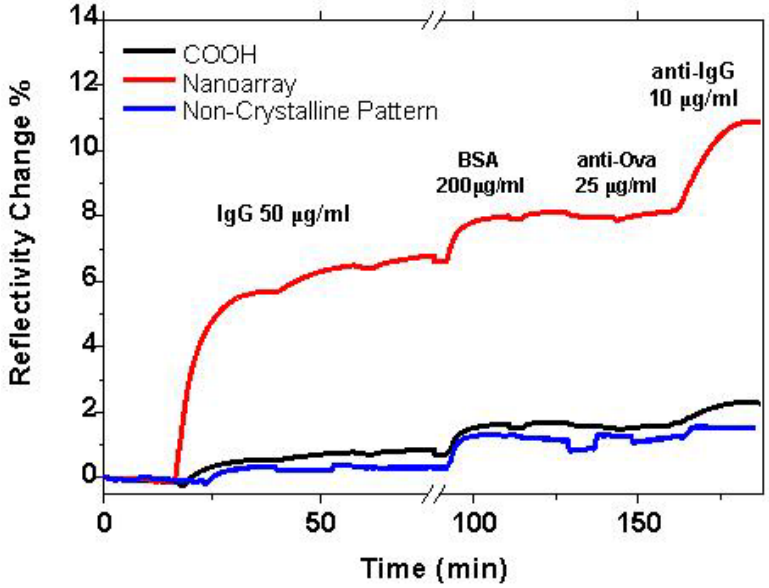

Figure 5.2- Kinetics of the SPRi immunoreaction experiments for the uniform, nanoarrayed and non-crystalline patterned COOH surface.

The active surface of the nanoarrayed MHD presenting only 8.4% of the total area, the expected the detection signal must be in the order of 9% of the signal obtained for the uniform MHD surface. On the contrary, the reflectivity changes associated to the nanoarrayed surface is amplified by a factor 5 as compared to the uniform surface and by a factor 60 if normalised by the active area.

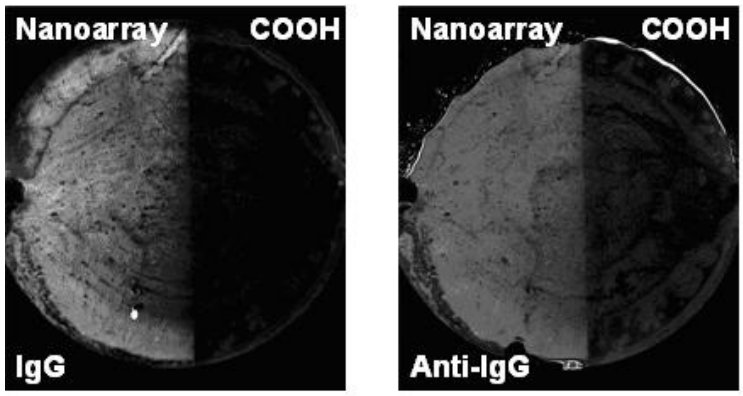

Figure 5.3-The SPR contrast images of the reflectance difference between the COOH region and the nanoarrayed region for the IgG absorption and the anti-IgG recognition.

Such amplification can not be only explained in terms of a higher efficiency of immobilisation of the bio-detector by the nano-patterned surface as shown by using equivalent nanopatterned surfaces and similar assay without observing such amplification (Agheli 2006; Hibbins 2002; Krishnamoorthy 2008; Valsesia 2006). For instance, organothiols based nano-patterned surfaces have been used in SPR detection leading to amplification only by normalizing by the active area (Krishnamoorthy 2008). Nevertheless the work used nanopatterned surfaces as well but with a random organisation without any periodicity.

This abnormal amplification of reflectivity can likely be attributed to the crystalline arrangement of our nanoarray that leads to the interaction between the surface plasmon modes and the regular spatial modulation of the optical constants of the nanoarray above the gold film.

The initial organothiols nanoarray cannot be the origin of this amplification since the refractive index (nMHD = 1.45 and nPEO = 1.47) and thickness of the two organothiols constituting the nanoarray are very similar so results in a plasmon effect similar to a

uniform surface (i.e. the reflectivity curves of the uniformly functionalised COOH surface and the nanoarray are similar).

The amplification is initiated by the selective immobilisation of Human IgG molecules on the organised nano areas (figure 5.2 a.). Proteins nanoareas create an optical grating by the modulation of the thickness and of the refractive index (nIgG = 1.55 and nPBS = 1.33) (Figure 5.4) at the gold interface. This leads to a perturbation of the surface plasmon modes at the interface leading to an amplification of the reflectivity change. The interaction between the surface plasmon and gratings has been observed by many authors and it is reported that the optical contrast when presenting a lattice constant that is half of the plasmon wavelength originates an energy band gap were no plasmon resonance occurs (Benahmed 2007; Dintinger 2005; Hibbins 2002; Wedge 2007).

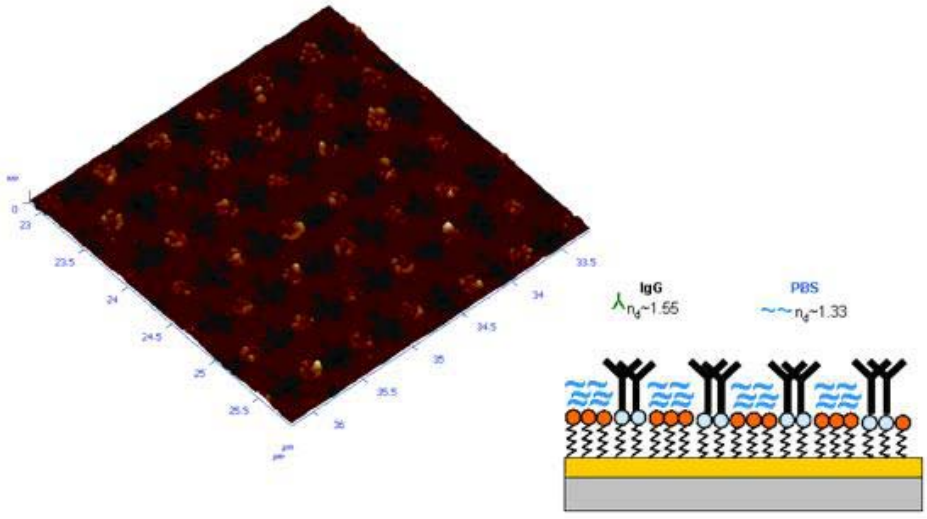

Figure 5.4 - Nanoarrayed surface after Human IgG immobilization. AFM topographic image (vertical scale 0-12 nm) and schematics illustrating the refractive index contrast.

Close to the bad gap conditions, the plasmon resonance takes place but suffers a perturbation that changes the plasmon wave. Nevertheless all the reported works were

based on pre-patterned polymeric surface that forms the optical grating. In our case the grating is created by the proteins themselves with a height that increases in all steps of the experiments.

The condition for momentum surface Plasmon wave matching condition with the incident light in a classical configuration is given by the formula (Barnes 2003; Homola 2006):

$$k_{SPP} = \frac{2\pi}{\lambda_0}\left(\frac{\varepsilon_{Au}\varepsilon_d}{\varepsilon_{Au}+\varepsilon_d}\right)^{1/2} = \frac{2\pi}{\lambda_0} n_p \sin(\vartheta) \quad \textbf{(5.1)}$$

This equation is valid at the beginning of our experiments when the grating effect is negligible due very similar optical properties of the organothiols. When the optical becomes efficient thanks to the localized Human IgG immobilisation, an interference between the Surface plasmon and the optical features of the grating occurs. This interference depends on the ratio between the grating lattice constant and the surface plasmon wavelength. The surface plasmon wavelength (λ_{SPP}) is given by (Barnes 2006):

$$\lambda_{SPP} = \frac{2\pi}{k_{SPP}} \quad \textbf{(5.2)}$$

Our conditions (λ_0 = 810nm, n_p= 1.77 and θ = ~50^0) and equation 2.1 (chapter2) lead to a surface plasmon wavelength $\lambda_{SPP\ of}$:

$$\lambda_{SPP} = \frac{2\pi}{k_{SPP}} = \frac{\lambda_0}{n_p \sin\vartheta} \approx 651nm \quad \textbf{(5.3)}$$

When the grating lattice constants and the initial wavelength are similar, the interaction induces an interference and the matching conditions for plasmon condition momentum is changed to(Wedge 2007):

$$k_{SPP} + i\frac{2\pi}{\vec{a}_1} + j\frac{2\pi}{\vec{a}_2} = \frac{2\pi}{\lambda_0} n_p \sin(\vartheta) \quad \textbf{(5.4)}$$

where $\vec{a}_1$ and $\vec{a}_2$ are the lattice vectors of the grating.

To promote the band gap effect the surface plasmon wavelength should be two fold the lattice constant of the grating (Barnes 2006).

In our conditions, the grating has an hexagonal geometry with lattice constants of a_1 = 500 nm and a_2 = 425nm so this corresponds to an incident light wavelength in the infra-red region (~1300nm) to achieve the band gap effect (Benahmed 2007). Nevertheless, the conditions used seem to be sufficient to observe amplification probably because it corresponds to an energy level neighbouring the band gap region. The contributions of the grating to the momentum matching conditions are reflected in a change of the reflectivity which is enhanced with respect to the one obtained on uniform surface. The SPRi system measures the change in reflectivity at a fixed angle where the derivative of the curve is maximum. A higher change of the angle position corresponding to the SPR induces a higher change of the reflectivity. Figure 5.5 presents the shift of SPRi external angle (θ_e) (see chapter 3.12) for both surfaces after Human IgG immobilisation. Uniform COOH surface leads to a small angle shift and gives rise to reflectivity changes lower than 1 whereas nanoarrayed surface results in a larger shift leading to higher variation in the reflectivity at a fixed angle. The result in the nanoarrayed surface is due to the coupling of the surface plasmon with the grating, during the IgG absorption.

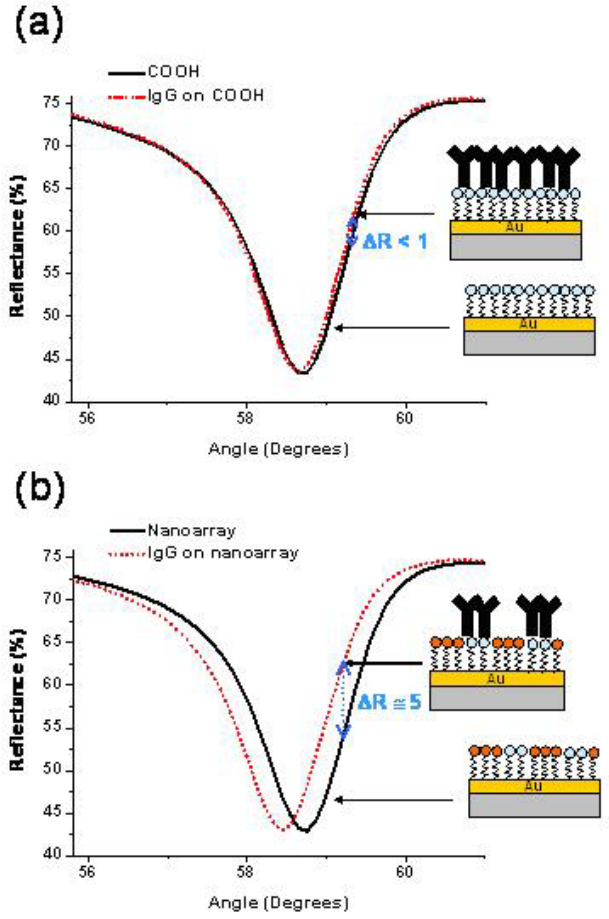

Figure 5.5 - (a) Plasmon resonance curves for the COOH surface before (solid line) and after (dashed line) IgG absorption. (b) Plasmon resonance curves for the nanoarrayed surface before (solid line) and after (dashed line) IgG absorption. Is plotted the external angle (θ_e).

Of course this effect has an influence on all the signal measure during the experiments. All the steps of the experiment have higher signal for the nanoarray which is probably related to the sensitivity improvement due to the presence of the grating. Furthermore adding proteins to the nano areas increases the thickness of the nanoarray, thus creating again disturbance of the surface plasmon modes resulting in a higher reflectivity

changes. The ratio between the signals of the different steps and COOH area is resumed in table 5.1. In all cases the ratio is higher for the nanoarray which indicates that the efficiency of the grating in detecting changes in the refractive index is better. But as already mentioned, in this case the good sensitivity is due to a combination of better availability of the bio-detector on the surface as well as to the optical signal amplification.

Step Signal	**Nanoarray**	**Uniform COOH**
Human IgG/ COOH area	0.68	0.008
BSA/ COOH area	0.15	0.01
anti-Human IgG/ COOH area	0.19	0.003

Table 5.1 - Ratio between the signals obtained during the different steps of the SPRi measurement and the active carboxylic surface.

The higher signal in the nanoarray does not mean that more proteins are adsorbed in the surface, indeed lower amounts of proteins are adsorbed once only 9% of the surface is active. The higher signal is mostly due to an optical amplification that improves the sensitivity of detection.

Another advantage of the nanoarrayed surface is the decrease in the signal to noise ratio (Table 5.2). The ratio anti-Human IgG/anti-OVA signal is reduced in the nanoarray to more than half of the signal of the uniform COOH.

Step Signal	**Nanoarray**	**Uniform COOH**
Anti-Ova/ anti-Human IgG	0.008	0.68

Table 5.2 - Ratio between the signals obtained during anti-Ova and anti-Human IgG steps.

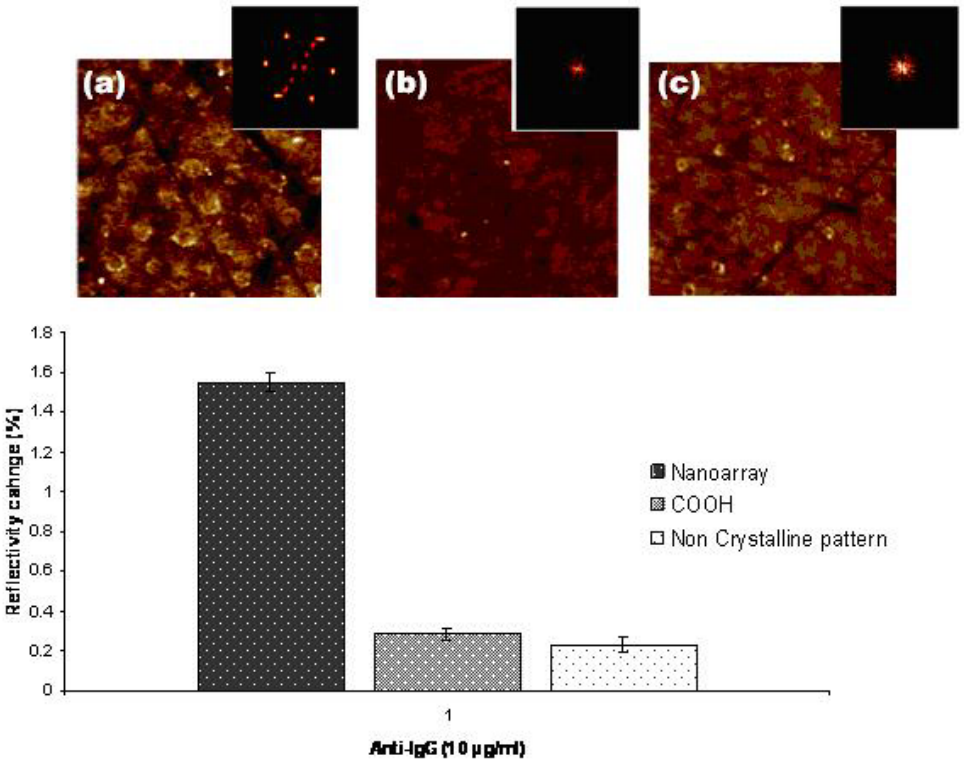

Figure 5.6 - Reflectivity change for the Anti-IgG recognition (10ug/ml) and AFM topography image and corresponding FFT after the recognition for: Nanoarray (A) (vertical scale 0-21 nm); COOH (B) (vertical scale 0-19 nm); Non Crystalline pattern (C) (vertical scale 0-22 nm).

To verify this assumption, the same experiment was performed by patterning the SPRi chip with a non crystalline nano-structured surface of organothiols (Figure 5.2). In this case the random organized nano-pattern should not interact with the optical detection since no periodic modulation of the refractive index is present. For this surface the observed signal related to the Human IgG immobilisation was only 10% of the signal obtained for the homogenous COOH surface but the anti-IgG recognition was 75% (Figure 5.6). The obtained signal is lower than both the crystalline nanoarrays and the uniform COOH. Nevertheless, the nano-pattern induces an improvement of signal/area

once the recognition signal is much higher than the expected 9%. This result is associated to an improved geometrical disposition of the capture element induced by the presence of nano-functional areas on a non adhesive matrix as it was already reported in disordered and geometrically organised nano-patterns (Krishnamoorthy 2008; Valsesia 2008 B). It can be clearly seen in these experiments that the presence of a geometric crystalline pattern is the main explanation for the amplification observed.

During the above described SPRi assays, the adsorptions of proteins on the different surfaces have been analysed by using Atomic Force Microscopy. The proteins are preferentially absorbed on the COOH nano areas both in the disordered and the crystalline nano-patterns. In the case of the ordered nanoarrays, a pattern was clearly observable by the FFT of the height AFM image (Figure 5.6), while the FFT for the disordered nano-pattern and the uniformly functionalised surface (Figure 5.6) did not show any particular pattern, as expected.

The optical amplification explanation has been confirmed as well by performing similar experiments using QCM-D, by comparing the uniform MHD surface and the nanoarrayed surfaces. These experiments had the objective to test the nanoarrays on a transducer with different detection principle. Detection in the QCM-D is based in frequency changes due to mass adsorption in the QCM crystal, thus in this case there is no optical interaction with the nanoarray. The measurements were performed with the same flow rate, same incubation times and same protein concentrations as in SPRi experiments. The signals related to Human IgG immobilisation present higher values for the uniform MHD surface and the nanoarray signal is about 20% of the uniform one (Figure 5.7). The BSA signal is much higher on the uniform surface which is related to the fact that in the nanoarray most of the surface is passivated with the thiolated PEO.

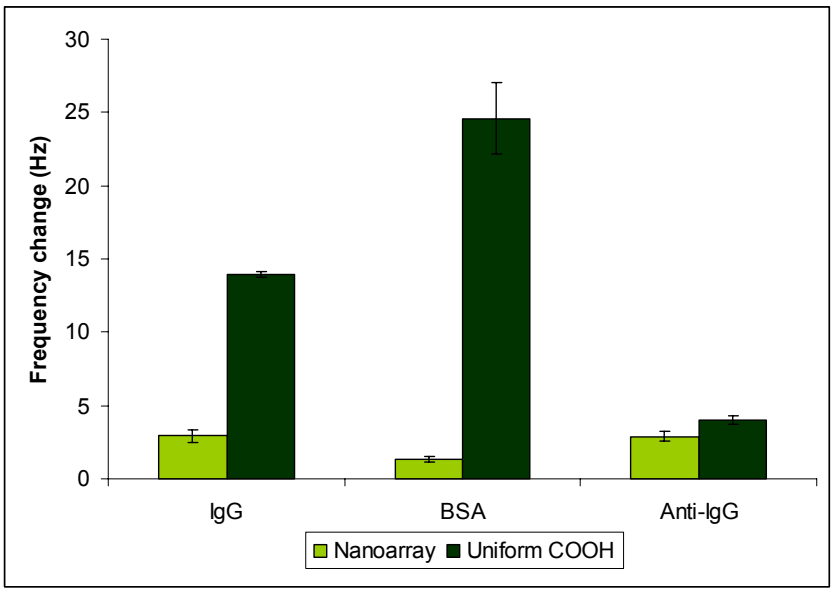

Figure 5.7- Frequency change for different steps of the immunoreaction monitored by QCM-D.

Finally the anti-Human IgG recognition on the nanoarray gave rise to 73% of the signal of the uniform surfaces, which is in agreement with the expected improved availability of the bio-detector on the nanoarrayed surface (Figure 5.7). The QCM-D results confirm that the amplification of the SPRi signal is directly correlated with the interaction of the grating present on the sensor patterned surface with the optical detection.

This chapter showed that SPRi detection performance can be improved by the rational functionalisation of the prism surface with nanoscale arrays, characterised by spacing of the order of magnitude of the wavelength of the surface plasmon wave. Moreover the SPRi experiments performed with the adhesive/non-adhesive random patterns and with the QCM-D confirmed the ability of these platforms in improving the immobilisation of the biomolecules on the surfaces. The combination of the nanoarray with SPRi detection improves the signal by a better bio-detector immobilisation and by an optical amplification of the signal.

5.2 Calibration Curve

In order to evaluate the performance of the differently functionalised surfaces, calibration curves were produced with different anti-Human IgG concentrations (Figure 5.8). The goal of these experiments was to study the sensitivity of the different systems in the linear range.

The SPRi chip was divided again in two adjacent areas, one being patterned with the nanoarray and the other being uniformly coated with MHD. The sensor surface was incubated with Human IgG and blocked with BSA with the same concentration as in, the previous experiments. For the same chips it was tested at least twice the four concentrations (1, 3, 5 and 10µg/ml) of anti-Human IgG. Before each tested concentration. Anti-OVA was used to verify the specificity of the recognition and after each recognition the surface was regenerated by Glycine hydrochloride (0,1M pH= 2,3).

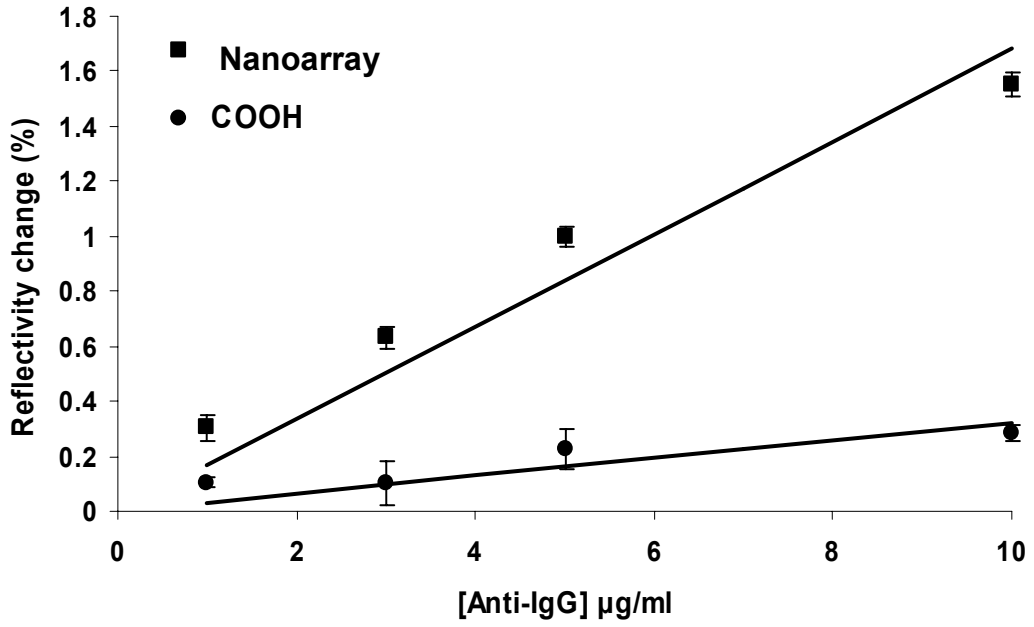

Figure 5.8 Calibration curves for the nanoarrayed and COOH functionalised surface.

For all concentrations the detection signal was higher in the case of the nanostructured surfaces. The control signal (anti-OVA) was in all cases less than 10%of the anti Human IgG signal, demonstrating that the sensor kept the specificity even after the regeneration cycles.

In the range of concentration explored the sensor response is linear for both the nano-patterned and the COOH functionalised surfaces. The sensitivity of detection (S) (defined as the variation of signal produced by an increment in the concentration of the analyte) can be calculated as the derivative of the calibration curve in the linear regime (Table 5.3) (Saah 1997). In this case the sensitivity is expressed as the variation of the signal due an increment of 1 μg/ml in the concentration of anti Human IgG. The sensitivity is enhanced by a factor 5 in the nanoarrayed surface with respect to the uniform one.

Surface	Sensitivity (a.u. × ml/μg)
Uniform COOH	**0.032**
Nanoarray	**0.168**

Table 5.3 - Sensitivity of the calibration curve obtained with the two surfaces.

The regeneration of the sensor was possible for several steps of detections. The Glycine HCl acts on the system removing only the recognised anti-IgG, leaving the sensor free to recognise new concentrations of analyte. After the regeneration steps the value of the base line was similar to the one of the first base line (before the fists recognition step). Figure 5.9 shows the difference between the base line after regeneration and first base line for a chip were several regeneration cycles were done. For all the regeneration cycles a difference lower than 1% of reflectivity change was obtained and the

reproducibility of the signals for the same anti Human IgG concentrations were good (0.5-1% of error) which indicates that the regeneration with the Glycine HCL was an adequate regeneration method for this system.

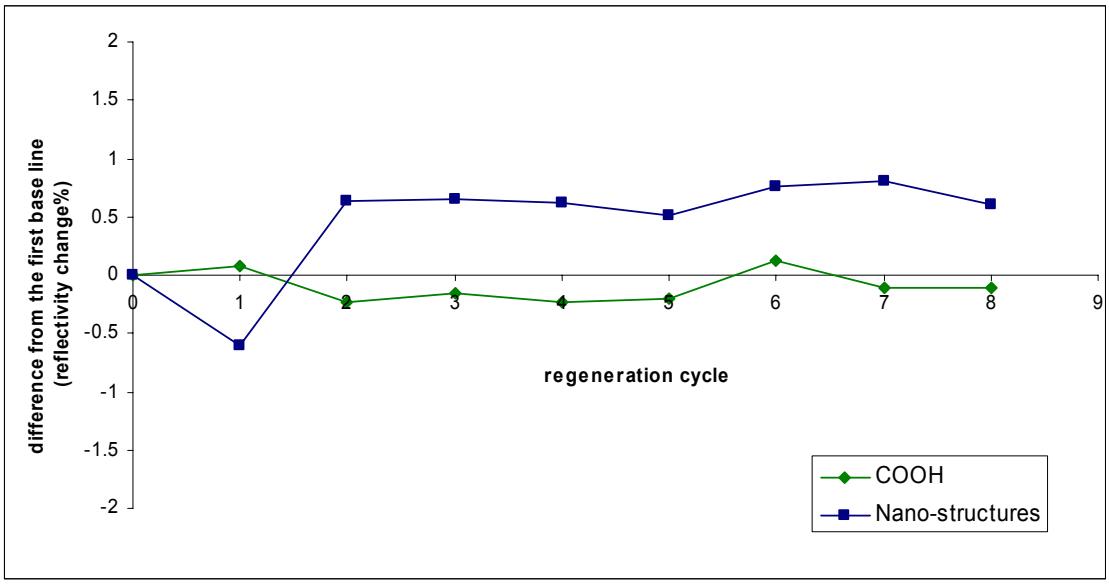

Figure 5.9 - Trend of the base line during different regeneration cycles.

The calibration curve results indicate that coupling of a commercial SPRi system with nanoarrayed surfaces, characterised by adhesive motives on a non-adhesive matrix, improves the sensing properties as compared to uniform chemistry surfaces.

5.3 AFM studies simulating SPRi measurements

In order to study the mode of interaction between proteins and the nano-arrayed surfaces during SPRi experiments AFM analysis was performed after Human IgG immobilisation and anti-Human IgG recognition steps. The protein solutions had the same concentrations as used in SPRi experiments.

To have a more accurate characterisation of the surfaces very flat gold coated glass (RMS roughness of 0.15 nm) was used. The nanoarray was incubated with IgG solution (32 min) and after rinsed with PBS. The topography images (Figure 5.8 A, B) show clearly an increase of height in the nano areas after the immobilisation of the Human IgG. The initial carboxylic nano area presents a higher border between the two organothiols. As already discuss in chapter 4.3, this effect is a result of a mismatch of the two organothiols, due to incomplete etching of the MHD layer. Analysis of the height profiles indicates that the height of bound Human IgG molecules is about 6 to 9nm. IgG has a globular Y shape molecule with height of about 12 nm (Silverton 1977), which means that the antibodies may have an orientation between prone and upright position on the surface.

The AFM image demonstrates that IgG molecules are adsorbed mainly on the border between the two organothiols. The preferential disposition of proteins on the borders of 2 different materials with hydrophobic and hydrophilic groups was already reported and associated to the fact that the proteins tend to adsorb where they can find better accommodation (Li 2006). In our case this effect can be explained by the fact that having the MHD spots with hydrophilic character the IgG hydrophobic groups are better accommodated on the border between the two materials, leading to higher adsorption on the boundaries between the two domains.

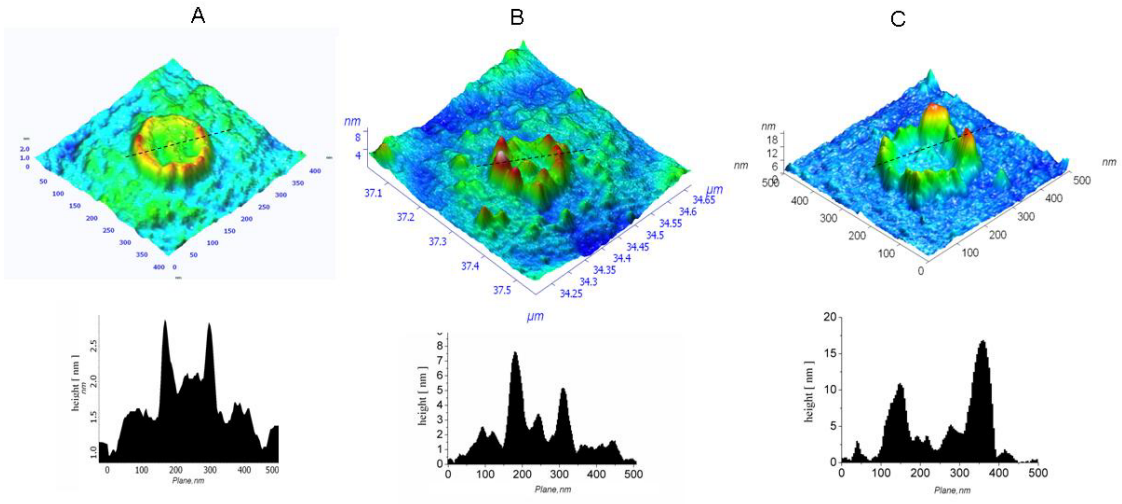

Figure 5.10- AFM topography images and correspondent profile analysis. A) nano COOH area, B) nano COOH area +Human IgG and C) nano COOH area +Human IgG + anti Human IgG.

After the Human IgG incubation, the surface was blocked with BSA (32 minutes) and rinsed with PBS. The following step consisted in the immobilisation of anti-Human IgG (16 minutes) and PBS rinsing. After this step, a height increase on the border of the COOH nano area is detected in the AFM analysis. The increase is about the double of the initial with Human IgG. This is an indication that the anti Human IgG binds specifically with the Human IgG already on the surface. The BSA does not block the central area of the nano-area and most probably the few molecules adsorbed are placed as well in the borders. It can be notice that the diameter covered by biomolecules increases in the last AFM profile which probably is associated with BSA deposition in the areas where is present the mix of the two organothiolis present.

These results confirm that the binding of the proteins in the nanoarray during the SPRi experiment is specifically done in the COOH spots and explaining the better availability of the proteins in this type of surfaces. The distribution on the borders of the nano area

can explain the better efficiency of the nano-patterns in biomolecular recognition in the QCM measurements (chapter 5.1) and described by different groups (Agheli 2006; Lee 2004; Li 2006; Rosi 2005; Valsesia 2006). The preferential proteins immobilization on the nano areas boundaries seems to improve the binding site availability of the immobilised Human IgG bio-detector.

These results are in agreement with the explanations given for the better bio-sensing efficiency of nanoarrays or non-crystalline nano-patterns based on adhesive/non-adhesive surfaces. The Immobilisation of the proteins on the nano-patterns is limited to the nano-area and this confinement influences the thermodynamic and kinetics of adsorption. The final conformation and distribution of the proteins in the surface change as compared to uniform surfaces. On a uniform surface the proteins have space to move and spread freely and these results in a random orientation once there is space to adopt any type of conformation in the surface (Figure 5.10)

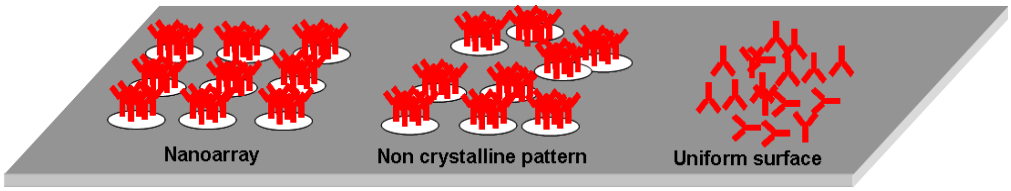

Figure 5.11- Schema of IgG immobilisation on the different surfaces.

On the nano-patterned surfaces the nano-areas are surrounded by an non-adhesive material which reduces the mobility and spreading of the proteins and induces a tendency to avoid prone configuration (in the case of IgG molecule) in order to avoid contact with the non-adhesive matrix. This configuration improves the availability of the binding sites (Figure 5.10). Another issue is the reduction of steric hindrance by the separation of the adhesive areas by the non-adhesive matrix which improves the bio-

recognition process. The steric interaction is as well improved by the distribution of the proteins on the boundaries of the nano COOH areas.

This chapter elucidates the behaviour of the proteins during the SPRi experiment, confirming the selective immobilisation of the proteins in the COOH areas and at the same time confirm some of the explanations associated with better availability of biomolecules in nano-patterned surfaces.

6 Production of Nanoarrays based on PPY

6.1 Nanoarray Production and Characterisation

In this chapter is described the fabrication of polypyrrole nanoarrays. PPy is a material of choice for bio-analytical sensors because of its good environmental stability and excellent biocompatibility, together with the possibility of being functionalised with biological relevant functional groups (Grosjean 2005; Lisboa 2006). The PPY nanoarray is produced by using of a gold nanotemplate over a silicon oxide (SiOx) matrix by using colloidal lithography. The nanotemplate is characterised by electrically conductive nano-areas (gold) distributed in an insulating matrix (SiOx). The insulting matrix is used as fabricated or covered by plasma polymerised PEO- like film in order to have a non-fouling background. Once the nanoarray is formed the electrochemical growth of PPy functionalised with biomolecules of is performed. The polymer grows selectively on the gold nano areas thus creating a nanoarray of PPy. The production steps of the nanoarray were followed by AFM and cyclic voltammetry.

6.1.1 Nanotemplate Fabrication

To produce the gold/SiOx nanotemplate four main steps are involved: 1) creation of a monolayer of polystyrene nano-beads on the gold surface; 2) etching of the beads by oxygen plasma; 3) deposition of a layer of insulating SiOx; and finally 4) removal of the beads. The process of fabrication of the nano-template is illustrated in Figure 6.1.

The 500nm P.S beads deposition was performed as described in chapter 4.3.1, but in this case the beads were deposited on bare gold (cleaned with H_2O_2 (30%) /NH_3 (25%)/H_2O (1:1:5) for 10 minutes at 75ºC, followed by 30 minutes in ethanol). The beads deposition conditions used in this chapter were those described in chapter 4 for the carboxylic surface.

Similar conditions were used since gold hydrophilic character was close to carboxylic surface due to air contamination (Frederix 2004).

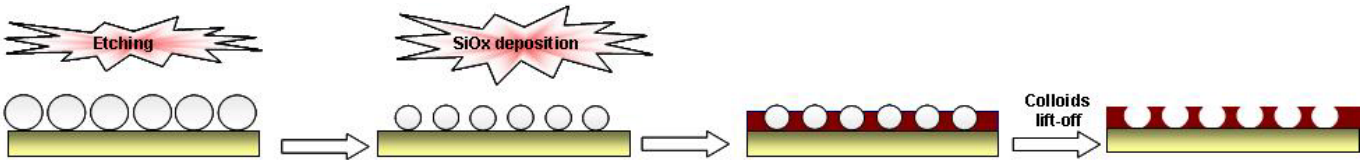

Figure 6.1. Scheme of the production of the gold/SiOx nano-template (a) Plasma etching of the PS beads (b) PE-CVD deposition of SiO_x layer (c) lift-off of the beads.

The etching step was performed as described in chapter 4.3.1, but with an exposure time of 80 seconds in order to increase the space in between the beads for the deposition of the matrix layer. Lower etching times were producing a rupture of the SiOx layer during the lift-off operation due to the large size of the beads.

The following step was the deposition of the SiOx by PE-CVD plasma deposition onto the surface with the etched PS mask. The reactor used for the deposition of SiOx was an inductively coupled plasma reactor described and characterised in (Valsesia 2006). The SiOx layer was deposited from hexadimethilsiloxane precursor (Sigma Aldrich) mixed with oxygen and argon to control the molecular fragmentation of the precursor. The deposition rate was approximately of 1nm/second and the process conditions lead to an isotropic filling of the areas located between the bead and the gold (Figure 6.2).

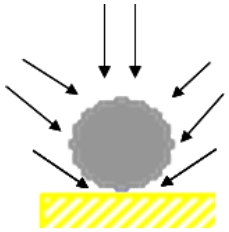

Figure 6.2- Schema of isotropic deposition of SiO_x by PE-CVD.

The verify the insulating character of the 5 nm SiOx film deposited on a gold working electrode was made by cyclic Voltammetry by studying the electrochemical reaction of the couple $Fe(CN)_6^{3-}$/ $Fe(CN)_6^{4-}$, and comparing it with bare gold (Figure 6.3). The cyclic voltammetry measurements were carried out as described in chapter 4.3.1. The results demonstrate that no peaks are present in the voltammogram of SiOx, indicating that the ions cannot reach the electrode. This demonstrates that the SiOx layer is insulating for thicknesses as low as 5 nm.

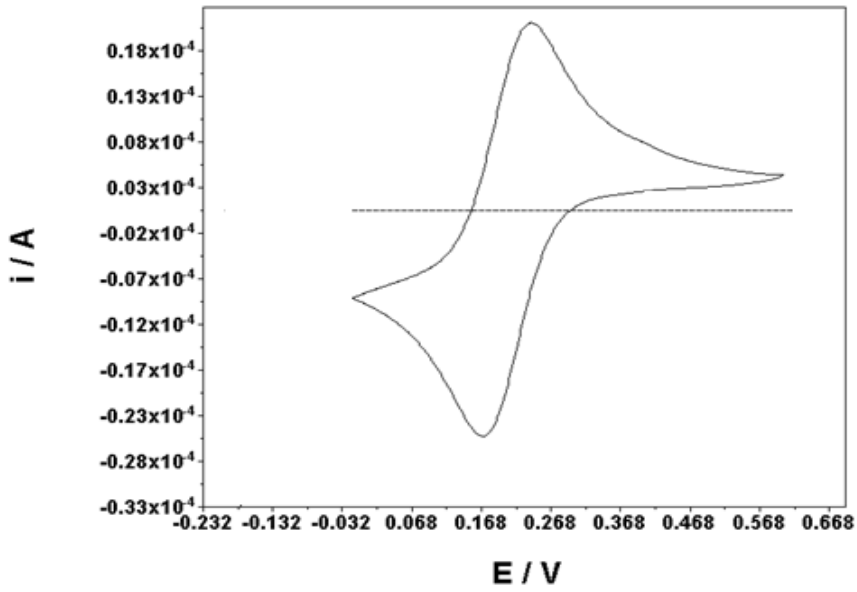

Figure 6.3- Cyclic Voltammograms in $K_3Fe(CN)_6$ with bare gold (solid line) and 5nm SiOx layer (dot line). Scan rate of 10mv/s.

After the SiOx deposition, the etched beads are mechanically removed by an ultrasonic bath leaving gold nano-holes in the SiOx layer.

In a second approach, after SiOx deposition a layer of PEO (10nm) was deposit by RF-plasma PE-CVD. The deposition was done in a home-made plasma reactor using a mixture of diethylene glycol monomethyl ether (DEGDME) (Sigma Aldrich) and argon following the

optimisation procedure described in (Bretagnol 2006). After the PEO deposition the beads were removed to obtain the nano-template on the surface.

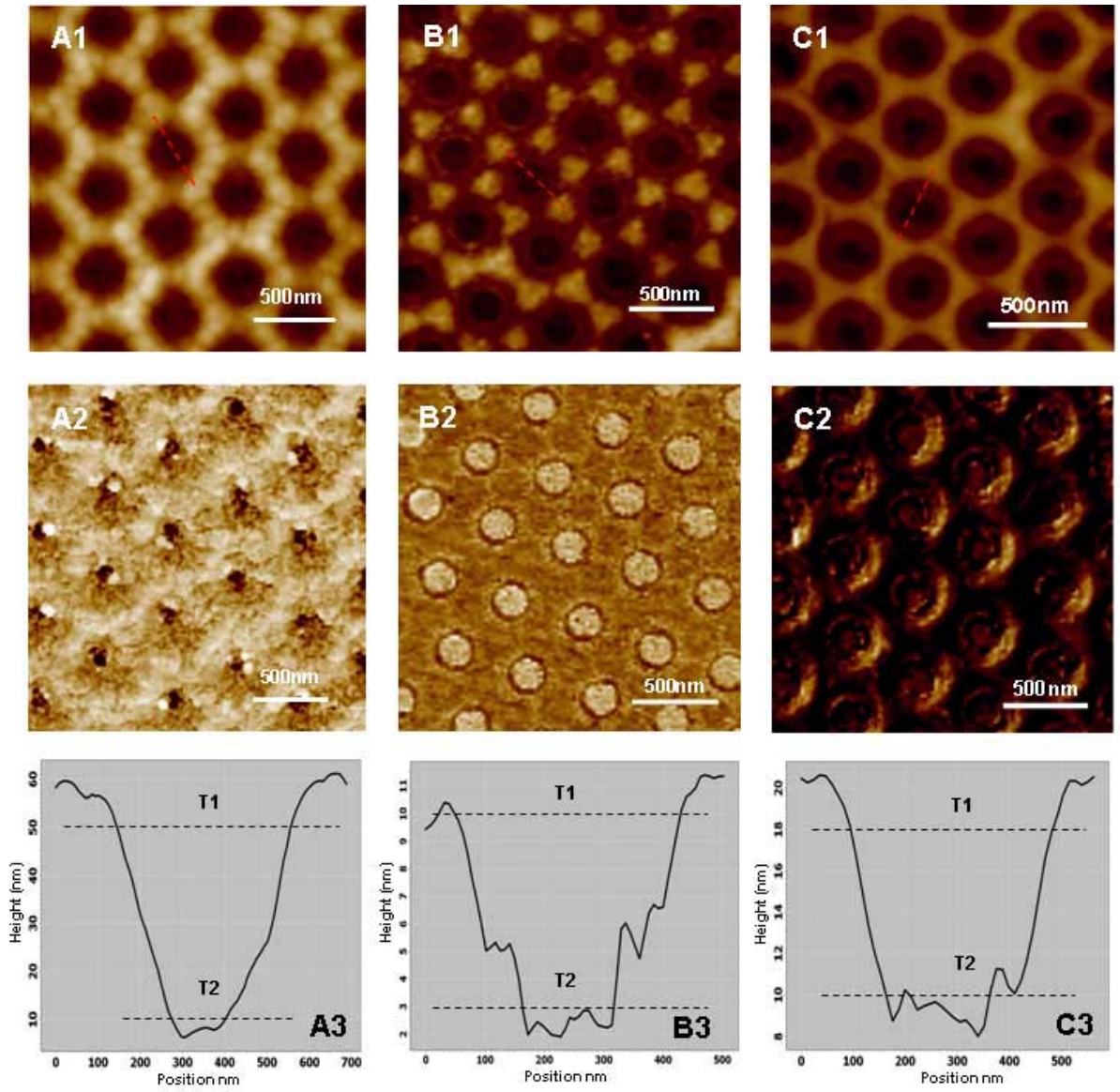

Figure 6.4- AFM analysis of the nano-templates: A) 60seconds SiOx deposition B) 10 seconds SiOx deposition and C) 10seconds SiOx deposition plus 10nm of PEO; 1) topographic image 2) corresponding phase image and 3) height profile along the line. A1) vertical scale 0-80 nm; A2) colour scale: -58^{o} to 28^{o}; B1) vertical scale 0-20 nm; B2) colour scale: -8^{o} to 10^{o}; C1) vertical scale 0-25 nm; C2) colour scale: -1^{o} to 0^{o}.

The AFM analyses of the SiOx nanoarray (Figure 6.4_1) evidence the presence of the fingerprint of the beads after the plasma etching. The profile of the nano-hole is characterised by a conical shape with the bottom side smaller than the upper one due to the isotropic SiOx deposition (Figure 6.4_3). The bottom and the top side size of the holes of the truncated cone is dependent on the matrix thickness (Table 6.1) and influences the final gold area on the surface (calculated as described in chapter 4.3.2.).

The contrast of the two materials is confirmed by the phase image (Figure 6.4_2), evidencing the presence of spots with a different phase located at the centre of the holes. Such an evident phase contrast is plausibly due to the presence of gold only at the central part of the bottom of the nano-hole, while the surrounding areas are made by SiOx or PEO layer.

	60 sec SiOx	***10 sec SiOx***	***10 sec SiOx + 10nm PEO***
Hole Height (nm)	58.6 ± 3.1	11.7 ± 1.2	22.4 ± 1.9
Hole Top side (nm)	446.3 ± 27.4	363 ± 14.9	359.4 ± 51.9
Hole Bottom (nm)	60.5 ± 12.4	179.1 ± 10.6	155.6 ± 22.6
Gold area on the surface	*0.9%*	*8%*	*6%*

Table 6.1 - Topographic characteristics of the nano-holes and total gold area on the surface. The size of the top side and bottom were calculated by averaging the diameter at a threshold T1 and T2 in Figure 6.4.

The nanotemplate has an organised geometric distribution of nano-areas of conductive material (gold) surrounded by an insulating matrix (SiOx) which is the typical geometry of nano electrode arrays. The electrochemical behaviour of these type of arrays is characterised by sigmoid shaped voltammogram due to steady state current creation in the presence of redox mediators with fast electrode kinetics like hexacyanoferrate (II/III) (Arrigan 2004; Tu 2005). A macroscopic electrode has a large area impeding the diffusion layer of electrolysis (rate of mass transport) to reach the maximum of current. When the redox

reaction occurs the diffusion layer is greatly increased resulting in an increasing of current (peaks). In the case of a nanoelectrode arrangement, the diffusion layer is much larger than the electrode size and so a maximum of mass transport rate is obtained during simple electrolysis, consequently a maximum of current is achieved. When the redox reactions take place the mass transport to the electrode is maximum and so the typical redox peaks are not seen (Wang and 2006).

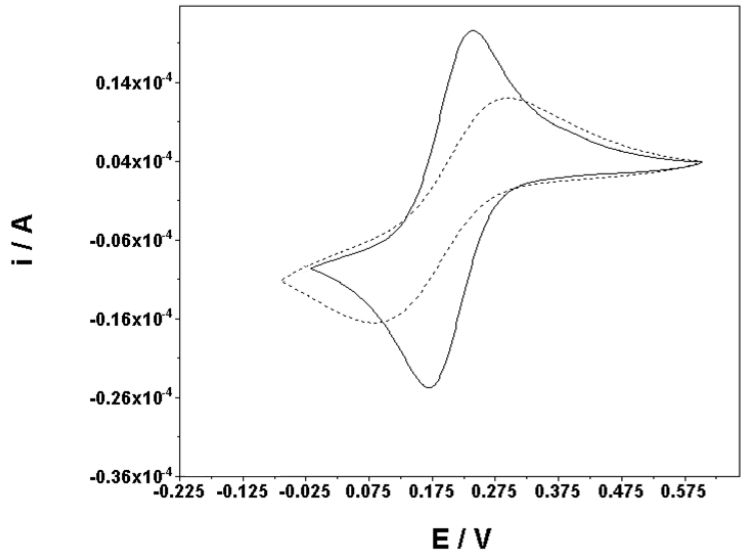

Figure 6.5 - Cyclic Voltammograms in $K_3Fe(CN)_6$ with bare gold (solid line) and Au-SiO_x (60nm) nanoarray (dot line). Scan rate of 10mv/s.

In order to verify the effective insulating character of SiOx and conductivity of the gold nano-holes, which are fundamental conditions for growing a nanoarray of PPY, cyclic voltammetry with $Fe(CN)_6^{3-}$/ $Fe(CN)_6^{4-}$ was performed using the conditions described above. The bare gold surface presents the typical voltammogram with redox peaks whereas the nano-structured surface voltammogram is characterised by the sigmoidal shape (Figure 6.5) typical of nanoelectrode arrays behaviour.

These results indicate that the nano-template presents the ideal electrochemical character to growth selectively the PPy on the gold areas, thus creating a nanoarray of PPy.

6.2 PPy growth

The goal of this part of the studies was to create a nanostructured microarray of PPy modified with biomolecules. Pyrrole modified with proteins is a valuable material (time consuming production and expensive) thus before using it on the nanostructured nanoarray, it was tested the capability of the array to electrochemically grow PPy selectively on the gold nano-areas. The microarray of nanostructured PPy modified with biomolecules was produced by electrospotting. Electrospotting o PPy modified with biomolecules is a methodology well established originating good performances in sensing systems (Grosjean 2005; Guedon 2000; Livache 1998; Livache 2001).

6.2.1 Nano- template as a base to create PPY nanoarray

The growth process has been carried out in the same apparatus described in chapter 6.1.1 using the nanostructured Au/SiO_x surface as working electrode. The deposition of the PPY was done under galvanostatic control (0.2mA) from an aqueous electrolyte solution of Pyrrole (Fluka) (0.05M) and Lithium Perchlorate (0.05M) (Fluka) that works as electrolyte and final salt dopant. This approach is commonly used to grow PPy in uniform and nanostructured films (Li 2008; Lisboa 2006; Moreno 1999; West 1993).The mechanism of polymerisation (Figure 6.6) starts with the oxidation of the pyrrole at the electrode surface, resulting in a radical formation. The radical react with other monomers creating a chain reaction and forming the polymer. During and after the reaction the polymer is stabilised by the doped salt.

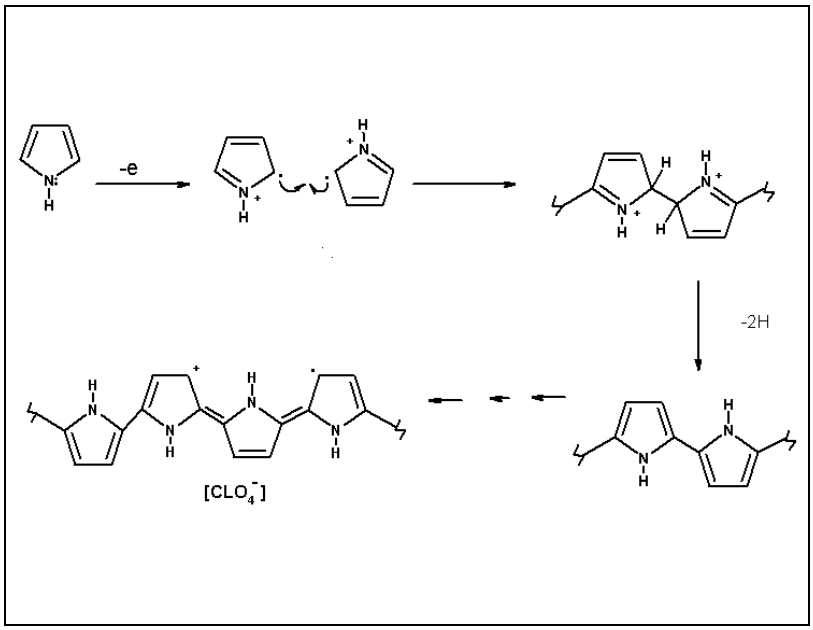

Figure 6.6- Electrochemical Polymerisation of PPy.

The thickness of the PPy grown on the surface is controlled by the deposition time. For low deposition time (t < 3 min), the growth is driven by the current flowing through the gold nano-areas, resulting in PPy growth exclusively inside the nano-hole to form isolated nano-pillars. With longer deposition time (t >> 3 min) the PPy pillars tend to merge by bridging over the SiOx matrix to form PPy homogenous films. The isolated PPy nano-pillars were grown on the nanotemplate areas as shown in the AFM picture in Figure 6.7. The average dimensions of the PPy nano-pillars have been extracted from the AFM pictures by the object analysis tool provided by the SPIP software: the average radius of the nano-pillars was calculated to be 60 ± 3 nm The values for the radius of the nano-pillars are in agreement with the estimated size of the Gold nano-holes.

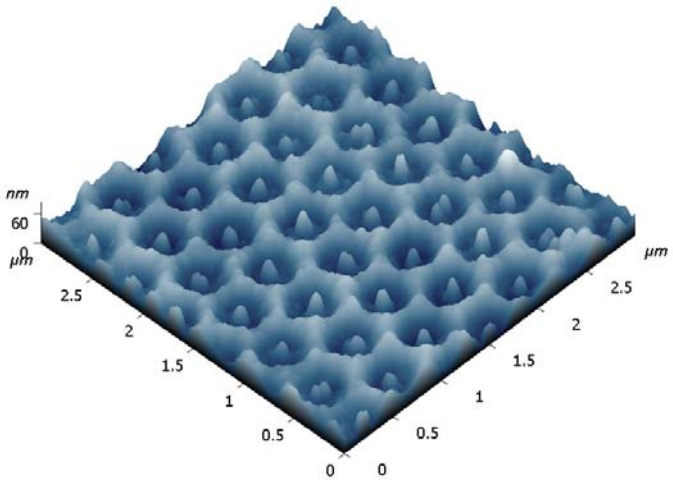

Figure 6.7 AFM picture of the nano-pillars of PPy grown inside the nano-template.

To confirm that PPy grows only on the gold holes thus maintaining the nanoelectrode behaviour of the surface, the electrochemical characteristics of the PPy nano-pillars array were evaluated and compared with a uniform PPy surface by cyclic voltammetry using the same experimental conditions as described above. The uniform PPy was deposited on a nanotemplate using the same galvanostatic conditions during 6 minutes, leading to complete coverage of the holes and the creation of a uniform polymer layer. The uniform surface presents the typical voltammogram with redox shape, whereas the PPy nano pillars surface present a sigmoidal shape (Figure 6.8).

The results show that the nanotemplate is suitable for the selective grow of PPy on the gold areas of the array and maintains the insulating characteristics of SiOx.

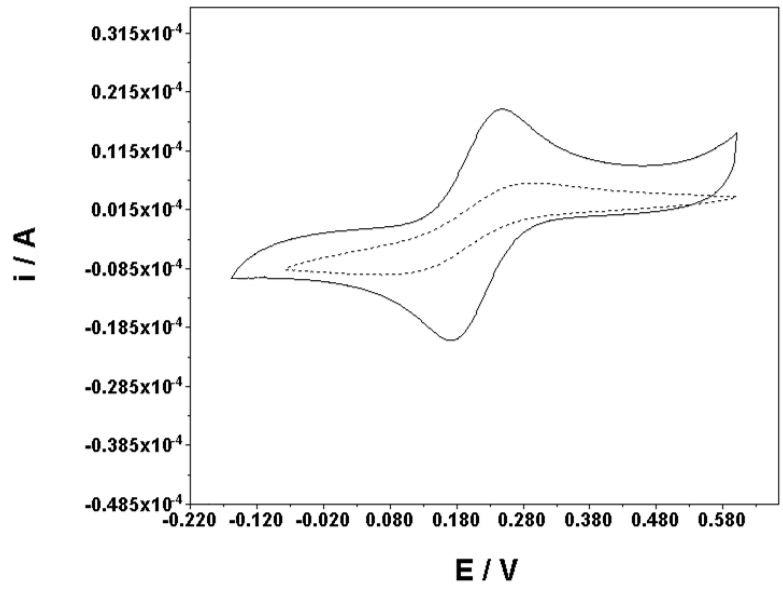

Figure 6.8- Cyclic Voltammograms in $K_3Fe(CN)_6$ with uniform PPy (solid line), PPy nano pillars (dot line) Scan rate of 10mv/s.

6.2.2 – Micro arrayed Electrocopolymerisation

The gold nanoarray produced on the SPR chip was used to grow PPy modified with proteins or peptides by electrochemical copolymerisation using a microarrayer (Figure 6.9). The solutions used in the spotting were based in 50mM sodium phosphate buffer (pH6.8) with 10% of glycerol, containing 20mM of free pyrrole. The spots were created using only free pyrrole or free pyrrole with pyrrole modified with proteins or peptides (10 to 300μM). The electrocopolymerisation was carried out by controlled potentiostatic conditions applying a short 100ms pulse (0.6V vs SCE) between the gold surface and the platinum wire localised on the pipette tip that was carrying the solution. The pipette tip was rinsed between each spotting on the gold surface. The chip was rinsed with PBS, Tween 20 1% (w/v) after the spotting in order to clean the surface and remove any non-grafted material. The electrochemical copolymerisation of the PPy was performed as well in an unmodified gold chip to use as comparison in the SPRi measurements. For the SPRi experiments was used only the templates produced with 10 seconds deposition of SiOX and the templates with

PEO, since larger thickness of the matrix would reduce the SPR sensitivity. At the same time the low SiOx promotes a better availability of the biomolecules grafted on the PPY once the microspotting deposition produces PPy with 5 to 10nm thickness. The deposition on the bare gold surface creates a uniform PPy layer of 10nm with 400 to 500nm diameter.

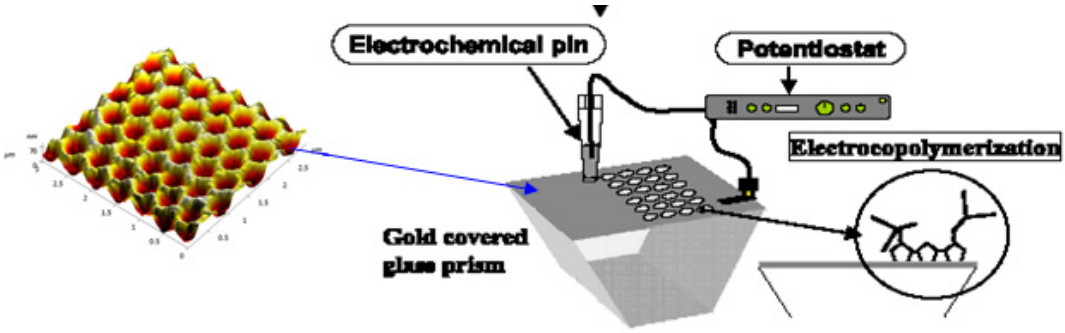

Figure 6.9- Scheme of the microarray electrocopolymerisation process with a 3D AFM topographic image of the nanotemplate.

The growth of the modified PPy on the nanotemplate takes place only on the gold nano-areas as can be seen by AFM analysis, but in this case grows in the side areas of the holes, creating a ring like geometry (Figure 6.10) with height of about 10nm. The difference of shape as compare to galvanostatic deposition and with the uniform deposition is related to the type of electrochemical deposition conditions. In galvanostatic deposition low current density originates compact PPy films and the controlled deposition time determines the thickness (Moreno 1999; West 1993). In potentiostatic deposition the same potential conditions can originate smooth films or spike shape depending on the charge density (Tietje-Girault 2007). The gold surface area on the nanoarray is less than 10% of the uniform surface, which increases more than 10 times the surface charge. This increase of charge density induces less uniformity on the PPy growth. This can explain why with a uniform gold surface the films are homogenous and on the nanoarray the films have non-uniform cylindrical shape. The reason for using such type of electrochemical deposition conditions is

justified by the fact that these conditions are known not to damage the biomolecules grafted on the PPy (Grosjean 2005; Guedon 2000; Livache 1998; Livache 2001).

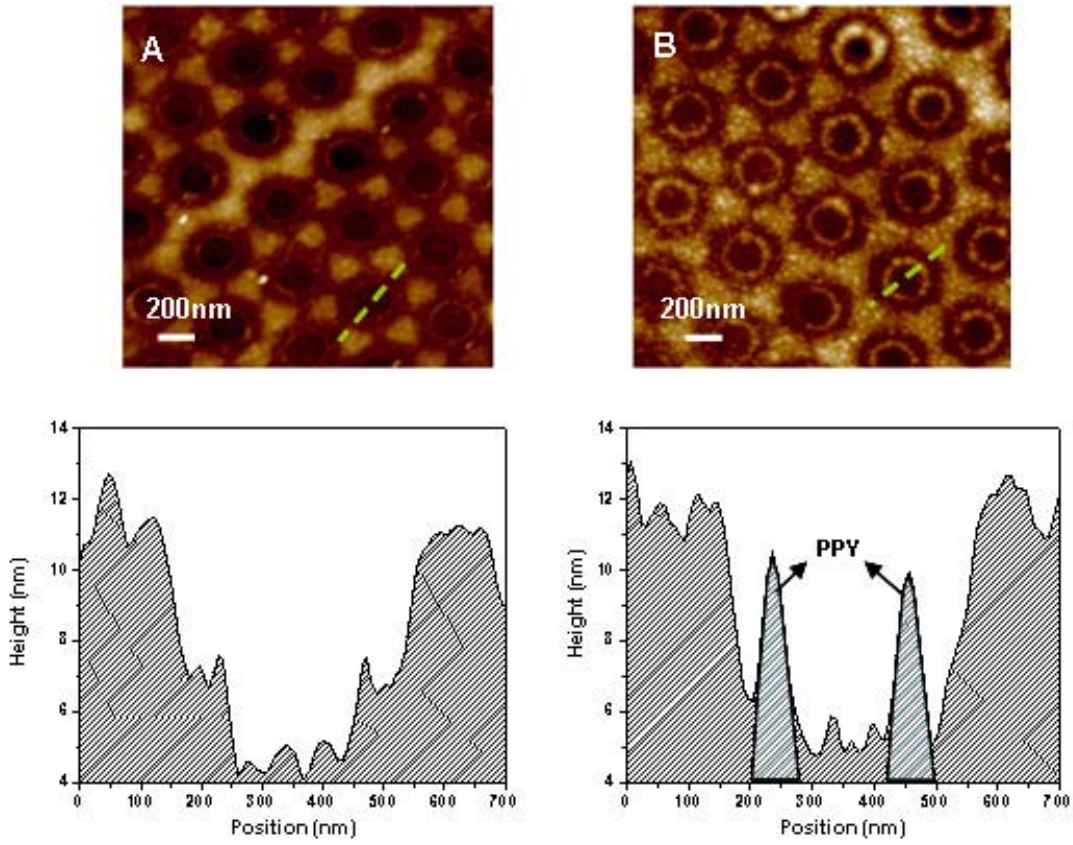

Figure 6.10 – Comparison of the nanoarray (10 seconds SiOx) A) before and B) after the PPy spotting.

7 SPRi studies of an immunoreaction using Nanoarrayed Polypyrrole surfaces

This chapter presents the study of the effect of a surface containing nanoarrays of PPy modified with proteins, on SPRi detection of immunoreactions based on proteins and peptides. The nanoarrayed surface present bio-detectors immobilised on PPy spots that permits to control bio-recognition reactions at nano-scale. This spatially controlled protein immobilisation is expected to create an optical grating during the recognition step thanks to the substantial increase of biomolecule thickness in the PPy nano areas. This thickness increase creates the optical contrast between the biomolecules and PBS. In this study was monitored the immunoreaction between OVA and anti-OVA; casein and anti-casein; and peptide C131-150 (Hepatitis C virus fragment) and anti-C131-150 were monitored. The results obtained with the nanoarrays were compared to uniformly functionalised PPy micro-spots. The effect of the nano-structured PPy surface on the immunoreaction efficiency was assessed using SPR imaging instrument (SPRi-LAB+ from GenOptics).

7.1 Nanoarray based on SiOX /PPy

The fabrication methods of the nanostructured surfaces used in this chapter are described in chapter 6. This section describes the results obtained in SPRi bio-detection using PPy nanoarrays distributed on a SiOx matrix of 10nm thickness. The results were compared with a uniform PPy functionalized surface.

The PPy growth on these surfaces was performed by the copolymerisation of pyrrole and pyrrole modified with peptides (Altergen, France) or pyrrole modified with proteins (prepared by using NHS functionalised pyrrole, INSERM, Grenoble). Table 7.1

summarises the concentrations of the pyrrole modified with the different biomolecules and the role of each biomolecule in the bioassay.

Biomolecule	Concentration µM	role
Ova	10	Bio-detector
Casein	10	Control for Ova assay
Peptide C131-150	100	Bio-detector
Peptide E2/5	100	Control for C131-150 assay

Table 7.1 - Type of biomolecules micro-spotted on the surface and corresponding concentration and role in the bioassay.

The electrocopolymerisation was performed in triplicate for each biomolecule species as well as for unmodified PPy that worked as negative control. Figure 7.1 presents the schematics of the spotting on the nanoarrayed surface. The same type of spotting distribution was performed on the uniform PPy spotted surface.

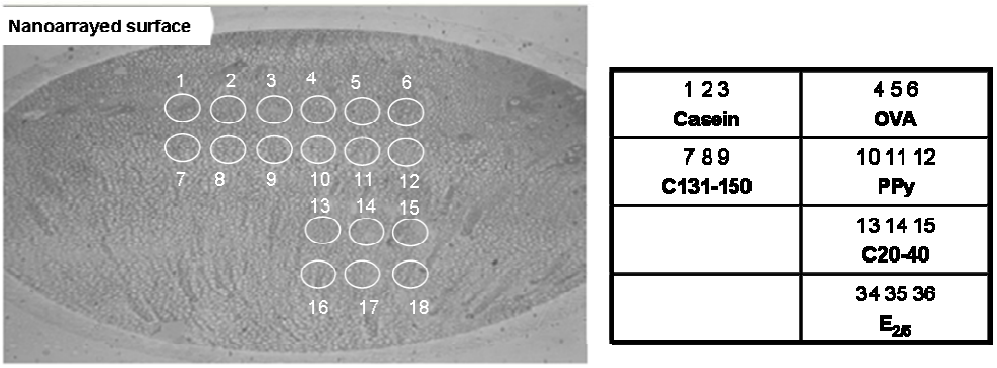

Figure 7.1 - Schema of the PPy spots on the SPR chip (SPRi image provided by the CCD camera).

Before starting the SPRi experiment, the reflectivity curves were plotted for all the different spots in order to choose the optimized working angle. Figure 7.2 shows the reflectivity curves measured for the nanostructured and for the uniform chip. The curves corresponding to the spots of nanoarrayed surfaces have different shapes which may be associated to a lack of homogeneity of the deposited PPy. The curves of the nanoarrayed surfaces present less pronounced dip of reflectivity, which related to a lower sensitivity of detection, thus affecting negatively the performance of the system.

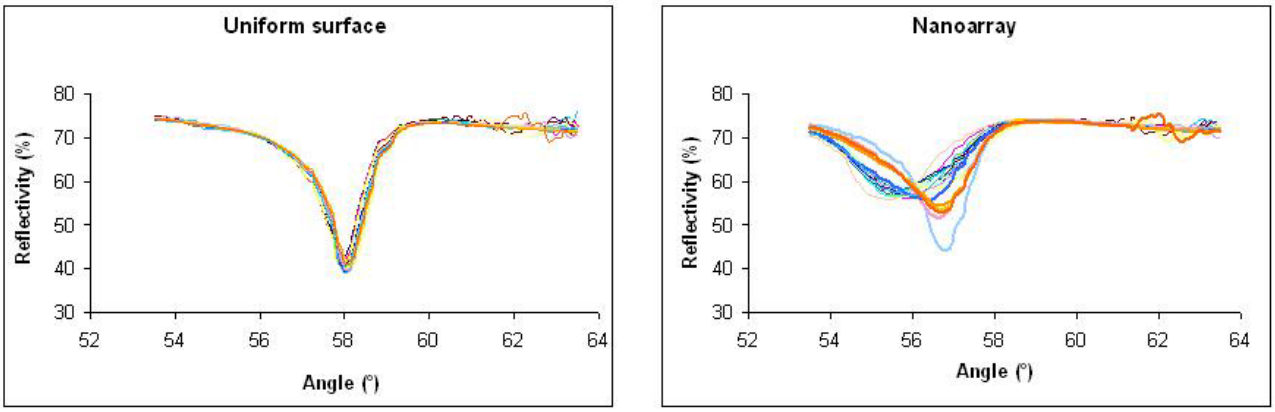

Figure 7.2 - Plasmon curves obtained for the nanoarray and uniform PPy surface.

The SPR measurements started by passing phosphate buffer saline (PBS) (10mM pH =7.4) with 40µl/min of flow rate until obtaining a stable signal that was considered as initial base line. All the biomolecule solutions were prepared using the PBS solution (with 0.01% NaN_3) and added with the same flow rate. The different solutions were injected in a 200µl loop and after were pulled into the cell chamber by the PBS buffer.

The bioassay was based on the bio-interaction between the proteins or peptides immobilised in the PPy matrix and their specific antibody. Before the bio-recognition step the surface was blocked with BSA. (Figure7.3)

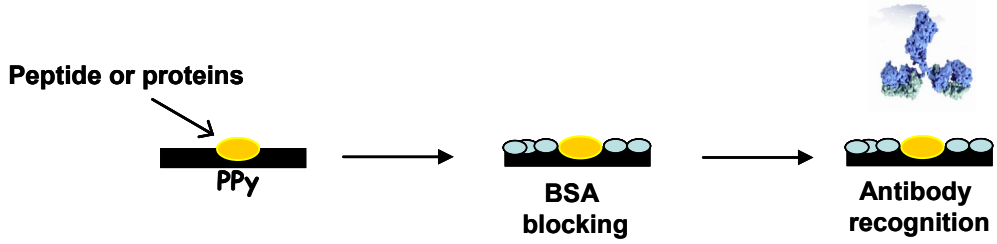

Figure 7.3 - General schema of the bioassay.

The first step of the SPRi measurement consisted in the unspecific binding sites blocking of the surface with a BSA solution (1% in PBS) during 10 minutes. Unbounded BSA molecules were removed by injecting Glycine HCl (0.1M pH=2.3) during 10minutes followed by an injection of Tris Buffer (20mM, pH 9.6) with Urea (4mM) and EDTA (20mM) during 5 minutes (Figure 7.4).

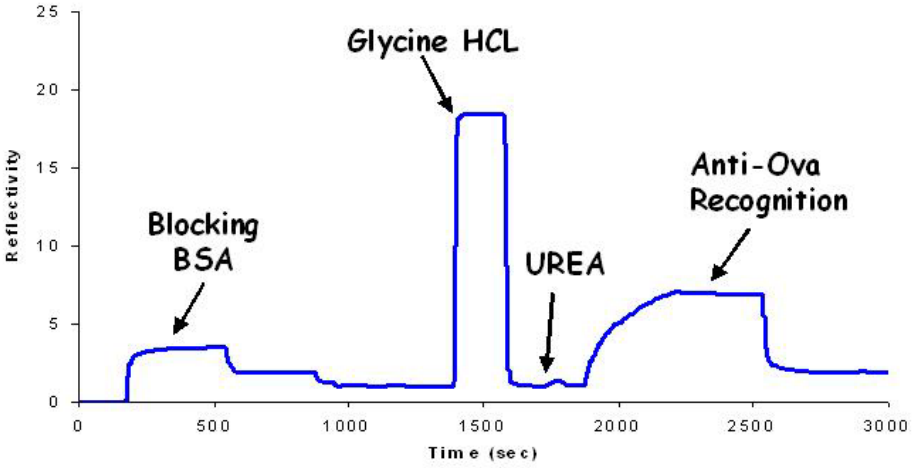

Figure 7.4 - Reflectivity change during different steps of the SPRi experiment. This sensogram is correspondent to a PPy-Ova spot in the nanoarrayed surface.

After these initial steps the recognition of the anti-Ova (Rockland) (Figure 7.4) and of anti serum anti-C131-150 (Neosystem) was performed using different concentrations. This step was performed by injecting a mixture of the two antibodies, making the detection of

both bio-interactions in simultaneous. After each recognition step, the chip was regenerated with Glycine HCl and Urea (as done after BSA blocking). The regeneration with these solutions was successful bringing the SPRi signal to the initial base line and giving the possibility to reuse the sensor to detect the various concentrations using the same chip several times.

In these experiments the background noise (signal of the various controls) was similar for both surfaces. In all the experiments performed the background noise was around 15 to 20 % of the specific signal. To calculate the real specific signal, the background noise was subtracted from the specific signal of recognition of the analyte.

Figure 7.5 presents the signals obtained in the recognition reaction of anti-C133-150 for both nanostructured and uniform surfaces after the subtracting of the background noise. The serum concentration is represented in dilution equivalents, where one equivalent corresponds to a dilution of 1:2500 of the original serum.

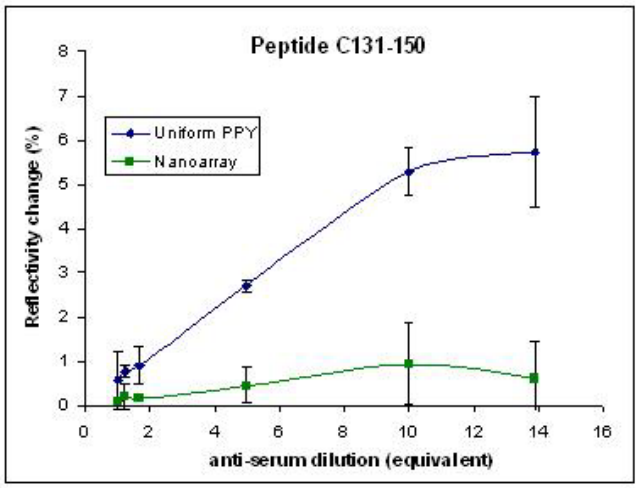

Figure 7.5 - SPRi signals of anti C131-150 detection on nanoarrayed and uniform PPy surface.

The measured signals are higher in the case of the uniform PPy surface for all the studied concentrations.

Figure 7.6 presents the results obtained after subtracting the background noise to the specific signal of recognition of anti-Ova. In these experiments the background noise was similar for both surfaces and was around 5 to 10 % of the specific signal.

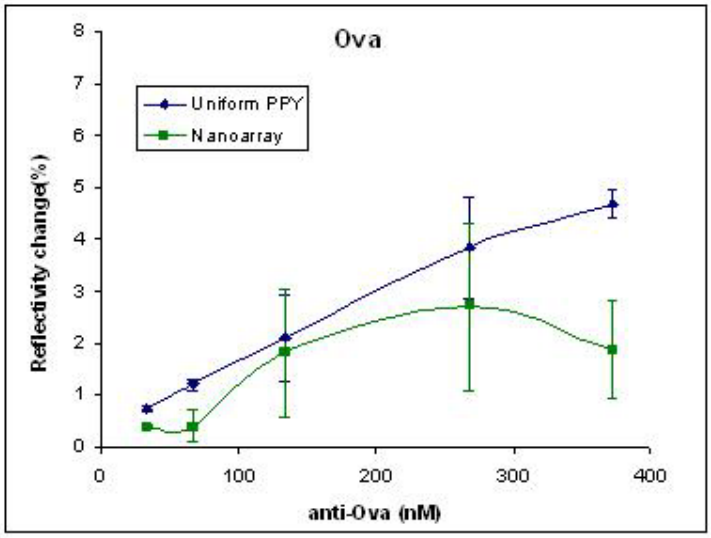

Figure 7.6 - SPRi signals of anti-Ova detection on nanoarrayed and uniform PPy surface.

Again, the signal is higher for the uniform surface for all concentrations and at low concentrations the difference between the two surfaces signals decreases.

Nevertheless, since the PPy nanoarray surface presents a lower bio-active surface (< 8% of total area since the PPy grows as a ring (Figure 7.9), the obtained signals are higher than expected as compared to the homogenous area with the same properties. The normalisation of the signal to the PPy area (considering 8% PPy active area on the nanoarray) (Figure 7.7) shows that the nanoarray is much more efficient in the detection of the bio-interactions, in particular for the Ova assay. This efficiency improvement is explained by the better availability of the bio-detector on the nanoarray surface as already discuss in chapter 5. It should be as well noticed as well that the plasmon curves

for the nanoarray were not the ideal ones for good detection sensitivity which demonstrates further efficiency of the nanoarray .

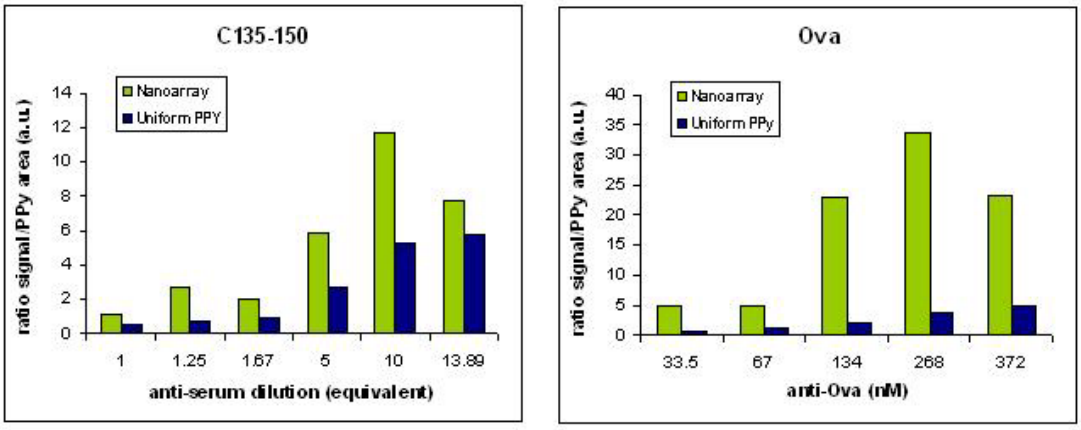

Figure 7.7 - Ratio signal/PPy area for the two surfaces obtained in the two different bio-interactions. The PPy area on the nanoarray was considered 8%.

The SPR signal in the nanoarray was not amplified as expected by the presence of the grating on the surface. Since the topology is the same the organothiols nanoarray (where we have higher signal in absolute) should lead to the same enhancement effect on the signal of detection. The reason for this different behaviour could be attributed to lack of homogeneity between the plasmon curves and the low dip in reflectivity, and to the complexity of the system. The surface presents an array with material with similar thickness (PPy has around 10nm high) and with a complex refractive index contrast (n_{SiOx}= 1.47 and $n_{PPy+\ proteins}$ = 1.817 + i.1.55) (Chen 2006; Khalil 2004). Since the PPy grows with a cylindrical form (Figure 7.8), PBS (n_{PBS} = 1.33) will fill the interior of the cylinder at the beginning of the experiment and thus the complexity of the optical contrast increases even more. The surface has a contrast of 4 different refractive indexes. This complexity seems not to induce an optical grating probably because the

combination of the refractive indexes of PBS, PPy and proteins is not enough different from the SiOx refractive index.

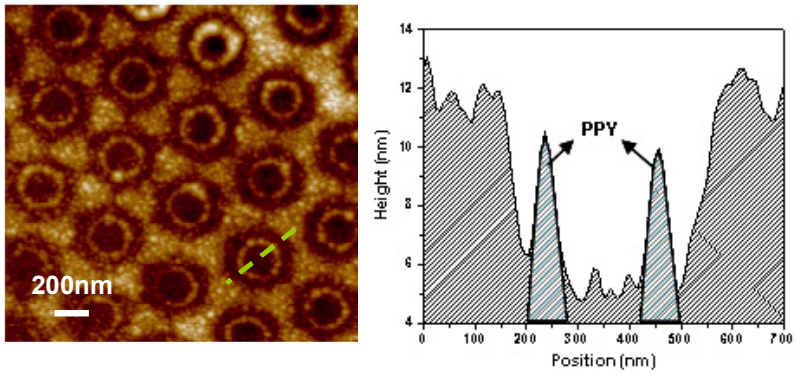

Figure 7.8- AFM topographic image of the PPy growth in the nanoarray (vertical scale 0-20 nm) and profile along the green line.

Nevertheless, the recognition step should induce antibodies immobilisation above the holes thus creating a PBS protein optical contrast. However this optical contrast is not pronounced since after the blocking step, BSA covers the SiOx matrix so the periodic grating is created with BSA and anti-ova or anti-C131-150 which are biomolecules having very similar refractive index and size (Figure 7.9).

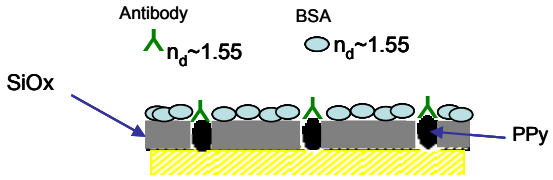

Figure 7.9 - Schema of the biomolecules distribution on the nanoarray surface during the bio-interaction.

To avoid this situation, the SiOx matrix should be passivated with a non bio-adhesive layer in order to impede BSA adsorption and create the optical contrast. The next section describes SPRi experiments using the nanoarray with the SiOx matrix passivated with plasma polymerised PEO.

7.2 Nanoarray based on PEO /PPy

To avoid the deposition of BSA on the SiOx layer as described in chapter 7.1, the nanoarray was prepared by covering the SiOx matrix with 10 nm PEO layer deposited by plasma processes. This new characteristic on the nanoarray will prevent BSA adsorption in between the spot and should improve the optical contrast necessary to induce the coupling of the surface plasmon with the grating on the surface (Figure 7.10).

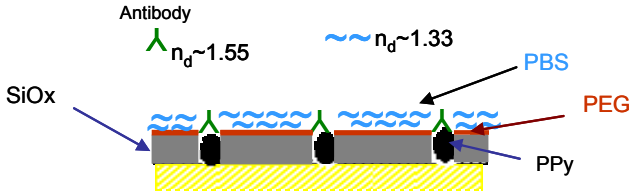

Figure 7.10 – Schema of the biomolecules distribution on the nanoarray surface with PEO layer during the bio-interaction.

The PPy growth on the nanoarrayed surfaces and uniform surfaces were performed by the copolymerisation of pyrrole and modified pyrrole as described in chapter 7.1. Table 7.2 summarises the concentrations of the pyrrole modified with the different biomolecules and the role of each biomolecule in the bioassay.

Biomolecule	Concentration µM	role
Ova	10	Control for Casein assay
Casein	10	Bio-detector
Peptide C131-150	100	Bio-detector
Peptide E2/5	100	Control for C131-150 assay

Table 7.2- Type of biomolecules micro-spotted on the surface and correspondent concentration and role in the bioassay.

As in previous experiments the electrocopolymerisation was performed in triplicate for each biomolecule species and for unmodified PPy (negative control).

Before starting the SPRi experiment, the reflectivity curves were plotted for all spots in order to choose the optimum working angle. The curves obtained for the nanoarray presented a lack of homogeneity and low reflectivity dip. In these conditions again the sensitivity of detection will be negatively influenced.

The SPRi experiment started with the initial steps described in chapter 7.1 followed by the recognition of anti- serum anti- αcasein (Neosystem) and anti serum anti-C131-150 (Neosystem). The regeneration was performed using Glycine HCl and Urea after each recognition step as before.

Figure 7.11 presents the results obtained in the detection of anti-C131-150 for both types of surfaces after subtracting the background signal. In this case the background signal for the nanoarray was very high (from 40 to 60%) and for uniform surfaces was less than 10%. The serum concentration is represented in dilution equivalents (1 equivalent corresponds to a dilution of 1:2500). It is clearly seen that the PEO layer does not lead to any improvement for the detection of the anti-C131-150, the obtained signals are similar than the one obtained without PEO (>1%). This low signals can be related to a low peptide accessibility due to their small size. Indeed, the peptides are embedded within the PPy matrix that is deposited in the nano-hole. The small size of the peptides limits the accessibility of the antibody to the binding sites.

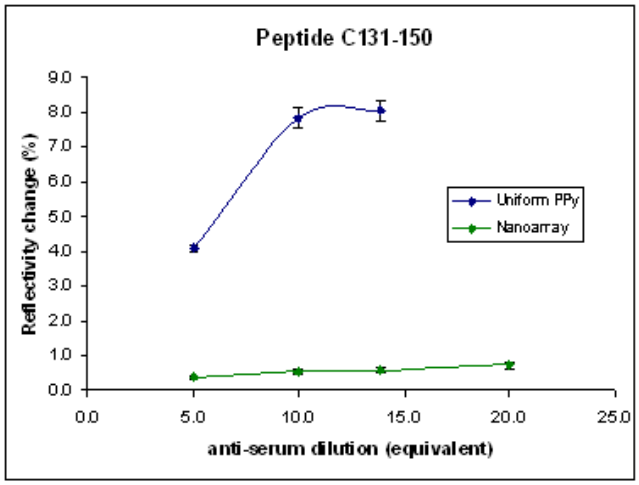

Figure 7.11- SPRi signals of anti C131-150 detection on nanoarrayed and uniform PPy surface.

The signals related with the anti-Casein recognition after background subtraction are summarized in figure 7.12. In this case the background signal for the nanoarray (2 to 5%) was lower than for the uniform surface (around 8%). The signal obtained with the nanoarray is very similar to the one obtained with the uniform surface. Clearly the PEO layer improves the specificity of the bio-reaction and improves the signal as compared to the previous results obtained with the same type of nanoarray without PEO layer. It should be noticed that in this case the area of gold available on the surface is 6% which is even slightly lower that in the case of the nanoarray described in chapter 7.1.

Even if in this case the bio-reaction was done with a biomolecules different than before, the size of the biomolecules is similar and so the accessibility and thickness increase was the same. The affinity of the reaction can be an issue, but comparing the results with the uniform surface results, it is clear that the improvement in the detection is not related with bio- affinity increase.

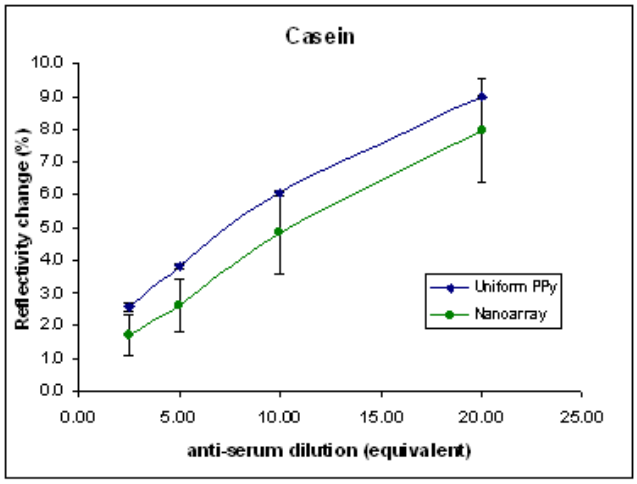

Figure 7.12- SPRi signals of anti-casein detection on nanoarrayed and uniform PPy surface.

Figure 7.13 presents the ratio between the detection signal and PPy area for the two bioassays. In the two cases the efficiency is better for the nanoarray, but in the case of the Casein assay this efficiency is much higher.

In this case the higher signals obtained cannot be explained simply by a better availability of the bio-detector, but probably by an amplification of the signal related to the surface plasmon interaction with the grating of optical contrast on the surface (Figure 7.10). Nevertheless the effect is lower than the one obtained with the organothiols surfaces, which can be related to the fact that some of the interaction takes place inside the holes and so not all of the immobilised antibodies are contributing to the increase of protein thickness that contrasts with the PBS on the interface.

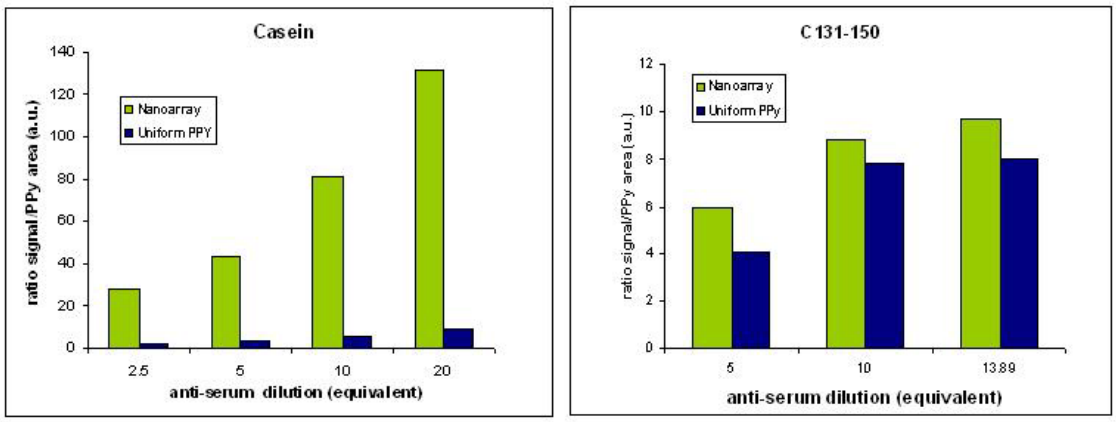

Figure 7.13- Ratio signal/PPy area for the two surfaces obtained in the two different bio-interactions. The PPy area in the nanoarray was considered 6%.

The results presented in this chapter show that the nanoarray of PPy are promising to improve the bio-detection in SPRi. The passivation of the SiOx matrix with PEO induces the creation of the optical grating in the interface during the recognition step, creating signal amplification. The application of a secondary antibody in the bioassay following a sandwich assay route could be a solution to increase the biomolecules thickness and thus create a proper grating for signal amplification. Nevertheless the complexity of the optical contrast presented in the starting surface creates some limitations to obtain the ideal refractive index contrast to induce high amplification.

References

Agheli, H., Malmstrom, J.,Larsson, E. M.,Textor, M.,Sutherland, D. S., **(2006)**. "Large area protein nanopatterning for biological applications." *Nano Letters* 6(6): 1165-1171.

Andreu, A., Merkert, J. W., Lecaros, L. A., Broglin, B. L., Brazell, J. T., El-Kouedi, M. **(2006)**. "Detection of DNA oligonucleotides on nanowire array electrodes using chronocoulometry." *Sensors and Actuators, B: Chemical* 114(2): 1116-1120.

Arrigan, D. W. M. **(2004)**. "Nanoelectrodes, nanoelectrode arrays and their applications." *Analyst* 129(12): 1157-1165.

Baird, C. L., Myszka, D. G. **(2001)**. "Current and emerging commercial optical biosensors." *Journal of Molecular Recognition* 14(5): 261-268.

Baralia, G. G., Pallandre, A., Nysten, B., Jonas, A. M. **(2006)**. "Nanopatterned self-assembled monolayers." *Nanotechnology* 17(4): 1160-1165.

Barnes, W. L. **(2006)**. "Surface plasmon-polariton length scales: A route to sub-wavelength optics." *Journal of Optics A: Pure and Applied Optics* 8(4): S87-S93.

Barnes, W. L., Dereux, A., Ebbesen, T. W. **(2003)**. "Surface plasmon subwavelength optics." *Nature* 424(6950): 824-830.

Barnes, W. L., Preist, T. W., Kitson, S. C.,Sambles, J. R. **(1996)**. "Physical origin of photonic energy gaps in the propagation of surface plasmons on gratings." *Physical Review B - Condensed Matter and Materials Physics* 54(9): 6227-6244.

Beamson, G., Briggs, D. **(1992)**. *High Resolution XPS of Organic Polymers*. NY, John Wiley and Sons.

Benahmed, A. J., Ho, C. M. **(2007)**. "Bandgap-assisted surface-plasmon sensing." *Applied Optics* 46(16): 3369-3375.

Bilitewski, U. **(2006)**. "Protein-sensing array formats and devices." *Analytica Chimica Acta* 568: 232-247.

Bizet, K., Gabrielli, C., Perrot, H. **(1999)**. "Biosensors based on piezoelectric transducers." *Analusis* 27(7): 609-616.

Blättler, T., Huwiler, C., Ochsner, M., Städler, B.,Solak, H., Vörös, J., Michelle Grandin, H. **(2006)**. "Nanopatterns with bioiogical functions." *Journal of Nanoscience and Nanotechnology* 6(8): 2237-2264.

Born, M., Wolf E. **(1965)**. *Principles of Optics*. NY, Pergamon Press.

Bosch, M. E., Sánchez, A.J.R., Rojas, F.S., Ojeda, C.B. **(2007)**. "Recent development in optical fiber biosensors." *Sensors* 7: 797-859.

References

Bretagnol, F., Ceriotti, L., Lejeune, M., Papadopoulou-Bouraoui, A.,Hasiwa, M.,Gilliland, D.,Ceccone, G.,Colpo, P.,Rossi, F. **(2006 A)**. "Functional micropatterned surfaces by combination of plasma polymerization and lift-off processes." *Plasma Processes and Polymers* 3(1): 30-38.

Bretagnol, F., Lejeune, M., Papadopoulou-Bouraoui, A., Hasiwa, M., Rauscher, H., Ceccone, G., Colpo, P., Rossi, F. **(2006 B)**. "Fouling and non-fouling surfaces produced by plasma polymerization of ethylene oxide monomer." *Acta Biomateriallia* 2(2): 165-172.

Bretagnol, F., Valsesia, A., Sasaki, T., Ceccone, G., Colpo, P., Rossi, F. **(2007)**. "Direct nanopatterning of 3D chemically active structures for biological applications." *Advanced Materials* 19(15): 1947-1950.

Cagnini, A., Palchetti, I.,Lionti, I.,Mascini, M.,Turner, A. P. F. **(1995)**. "Disposable ruthenized screen-printed biosensors for pesticides monitoring." *Sensors and Actuators, B: Chemical* B24(1 -3 pt 1): 85-89.

Chaubey, A., Pande, K. K.,Singh, V. S.,Malhotra, B. D. **(2000)**. "Co-immobilization of lactate oxidase and lactate dehydrogenase on conducting polyaniline films." *Analytica Chimica Acta* 407: 97-103.

Chen, G. Y. J., Uttamchandani, M., Zhu, Q., Wang, G.,Yao, S. Q. **(2003)**. "Developing a strategy for activity-based detection of enzymes in a protein microarray." *ChemBioChem* 4(4): 336-339.

Chen, Y., Jin, G. **(2006)**. "Refractive index and thickness analysis of natural silicon dioxide film growing on silicon with variable-angle spectroscopic ellipsometry." *Spectroscopy* 21(10): 26-31.

Chien, F. C., Chen, S. J. **(2006)**. "Direct determination of the refractive index and thickness of a biolayer based on coupled waveguide-surface plasmon resonance mode." *Optics Letters* 31(2): 187-189.

Chinowsky, T. M., Grow, M. S., Johnston, K. S., Nelson, K., Edwards, T., Fu, E., Yager, P. **(2007)**. "Compact, high performance surface plasmon resonance imaging system." *Biosensors and Bioelectronics* 22(9-10): 2208-2215.

Choi, D. G., Jang, S. G., Kim, S., Lee, E., Han, C. S.,Yang, S. M. **(2006)**. "Multifaceted and nanobored particle arrays sculpted using colloidal lithography." *Advanced Functional Materials* 16(1): 33-40.

Clark, L. C., Lyons, C. **(1962)**. "Electrode systems for continuous monitoring in cardiovascular surgery." *Ann. NY Acad. Sci.* 102: 29-45.

Cole, R. M., Baumberg, J. J., De Garcia Abajo, F. J., Mahajan, S., Abdelsalam, M., Bartlett, P. N. **(2007)**. "Understanding plasmons in nanoscale voids." *Nano Letters* 7(7): 2094-2100.

Collings, A. F., Caruso, F. **(1997)**. "Biosensors: Recent advances." *Reports on Progress in Physics* 60(11): 1397-1445.

References

Cooper, M. A. **(2006)**. "Optical biosensors: where next and how soon?" *Drug Discovery Today* 11(23-24): 1061-1067.

Coughlin, S. S. **(2002)**. "Future challenges for research on diagnostic tests: Genetic tests and disease prevention." *Journal of Epidemiology and Community Health* 56(5): 335-336.

Cox, W. G., Singer, V. L. **(2004)**. "Fluorescent DNA hybridization probe preparation using amine modification and reactive dye coupling." *BioTechniques* 36(1): 114-122.

Cuypers, P. A., Corsel, J. W., Janssen, M. P.,Kop, J. M.,Hermens, W. T.,Hemker, H. C. **(1983)**. "The adsorption of prothrombin to phosphatidylserine multilayers quantitated by ellipsometry." *Journal of Biological Chemistry* 258(4): 2426-2431.

D'Agostino, R. **(2005)**. "Process control and plasma modification of polymers." *Journal of Photopolymer Science and Technology* 18(2): 245-249.

D'Agostino, R., Favia, P., Oehr, C.,Wertheimer, M. R. **(2005)**. "Low-temperature plasma processing of materials: Past, present, and future." *Plasma Processes and Polymers* 2(1): 7-15.

D'Orazio, P. **(2003)**. "Biosensors in clinical chemistry." *Clinica Chimica Acta* 334(1-2): 41-69.

Demers, L. M., Ginger, D. S., Park, S. J., Li, Z., Chung, S. W. Mirkin, C. A. **(2002)**. "Direct patterning of modified oligonucleotides on metals and insulators by dip-pen nanolithography." *Science* 296(5574): 1836-1838.

Demers, L. M., Park, S. J., Andrew Taton, T., Li, Z., Mirkin, C. A. **(2001)**. "Orthogonal assembly of nanoparticle building blocks on dip-pen nanolithographically generated templates of DNA." *Angewandte Chemie - International Edition* 40(16): 3071-3073.

Dintinger, J., Klein, S.,Bustos, F.,Barnes, W. L.,Ebbesen, T. W. **(2005)**. "Strong coupling between surface plasmon-polaritons and organic molecules in subwavelength hole arrays." *Physical Review B - Condensed Matter and Materials Physics* 71(3): 1-5.

Drummond, T. G., Hill, M. G., Barton, J. K. **(2003)**. "Electrochemical DNA sensors." *Nature Biotechnology* 21(10): 1192-1199.

Du, Y. J., and,Brash, J. L. **(2003)**. "Synthesis and Characterization of Thiol-Terminated Poly(ethylene oxide) for Chemisorption to Gold Surface." *Journal of Applied Polymer Science* 90: 594-607.

Egitto, F. D. **(1990)**. "Plasma etching and modification of organic polymers." *Pure Applyed Chemistry* 62: 1699-1708.

Ekanayake, E. M. I. M., Preethichandra, D. M. G., Kaneto, K. **(2007)**. "Polypyrrole nanotube array sensor for enhanced adsorption of glucose oxidase in glucose biosensors." *Biosensors and Bioelectronics* 23(1): 107-113.

References

Ekins, R. P. **(1998)**. "Ligand assays: From electrophoresis to miniaturized microarrays." *Clinical Chemistry* 44(9): 2015-2030.

Eurobarometer. (2008). "Eurobarometer 69, PUBLIC OPINION IN THE EUROPEAN UNION."

Evans, S. D., Urankar, E., Ulman, A.,Ferris, N. **(1991)**. "Self-assembled monolayers of alkanethiols containing a polar aromatic group: effects of the dipole position on molecular packing, orientation, and surface wetting properties." *J. Am. Chem. Soc.* 113.

Fan, X., White, I. M.,Shopova, S. I.,Zhu, H.,Suter, J. D.,Sun, Y., **(2008)**. "Sensitive optical biosensors for unlabeled targets: A review." *Analytica Chimica Acta* 620(1-2): 8-26.

Flink, S., Van Veggel, F. C. J. M., Reinhoudt, D. N. **(2000)**. "Sensor functionalities in self-assembled monolayers." *Advanced Materials* 12(18): 1315-1328.

Frederix, F. **(2004 A)**. The use of Self-Assembly for the realisation of immunosensor interfaces and detection systems. *K.U.Leuven*. Leuven. PhD

Frederix, F., Bonroy, K., Reekmans, G.,Laureyn, W., Campitelli, A., Abramov, M. A., Dehaen, W., Maes, G. **(2004 B)**. "Reduced nonspecific adsorption on covalently immobilized protein surfaces using poly(ethylene oxide) containing blocking agents." *Journal of Biochemical and Biophysical Methods* 58(1): 67-74.

Gates, B. D., Xu, Q., Love, J. C., Wolfe, D. B., Whitesides, G. M. **(2004)**. Unconventional nanofabrication. *Annual Review of Materials Research*. 34: 339-372.

Gates, B. D., Xu, Q., Stewart, M., Ryan, D., Willson, C. G., Whitesides, G. M. **(2005)**. "New approaches to nanofabrication: Molding, printing, and other techniques." *Chemical Reviews* 105(4): 1171-1196.

Geissler, M., Xia, Y. **(2004)**. "Patterning: Principles and some new developments." *Advanced Materials* 16(15 SPEC. ISS.): 1249-1269.

Gerard, M., Chaubey, A.,Malhotra, B. D. **(2002)**. "Application of conducting polymers to biosensors." *Biosensors and Bioelectronics* 17(5): 345-359.

Ginger, D. S., et al. **(2003)**. "The Evolution of Dip-Pen Nanolithography." *Angewandte Chemie - International Edition* 43(1): 30-45.

Ginzton, E. L. **(1986)**. "Atomic Force Microscope." *Physical Review Letters* 56: 930 - 933

Glass, R., Möller, M. Spatz, J. P. **(2003)**. "Block copolymer micelle nanolithography." *Nanotechnology* 14(10): 1153-1160.

Goddard, J. M., Hotchkiss, J. H. **(2007)**. "Polymer surface modification for the attachment of bioactive compounds." *Progress in Polymer Science (Oxford)* 32(7): 698-725.

References

Goldstein, J. I., Newbury, D.E., Echlin, P., Joy, D.C., Romig, A.D., Lyman, C.E., Fiori, C., Lifshin, E. **(1992)**. *Surface Analysis by Auger and X-ray Photoelectron Spectroscopy Scanning, Electron Microscopy and X-Ray Microanalysis*. New York, Plenum Press.

Gramsbergen, J. B., Leegsma-Vogt, G., Venema, K., Noraberg, J.,Korf, J. **(2003)**. "Quantitative on-line monitoring of hippocampus glucose and lactate metabolism in organotypic cultures using biosensor technology." *Journal of Neurochemistry* 85(2): 399-408.

Grosjean, L., Cherif, B., Mercey, E., Roget, A., Levy, Y., Marche, P. N., Villiers, M. B., Livache, T. **(2005)**. "A polypyrrole protein microarray for antibody-antigen interaction studies using a label-free detection process." *Analytical Biochemistry* 347(2): 193-200.

Guedon, P., Livache, T., Martin, F.,Lesbre, F.,Roget, A., Bidan, G.,Levy, Y. **(2000)**. "Characterization and optimization of a real-time, parallel, label-free, polypyrrole-based DNA sensor by surface plasmon resonance imaging." *Analytical Chemistry* **72**(24): 6003-6009.

Guilbault, G. G., Montalvo Jr, J. **(1969)**. "Sensitized cation selective electrode." *Analytical Chemistry* 41(13): 1897-1899.

Guilbault, G. G., Montalvo Jr, J. G. **(1969)**. "A urea-specific enzyme electrode [43]." *Journal of the American Chemical Society* 91(8): 2164-2165.

Guimard, N. K., Gomez, N., Schmidt, C. E. **(2007)**. "Conducting polymers in biomedical engineering." *Progress in Polymer Science (Oxford)* 32(8-9): 876-921.

Haddour, N., Cosnier, S.,Gondran, C. **(2005)**. "Electrogeneration of a poly(pyrrole)-NTA chelator film for a reversible oriented immobilization of histidine-tagged proteins." *Journal of the American Chemical Society* 127(16): 5752-5753.

Hamley, I. W. **(2003 A)**. "Nanostructure fabrication using block copolymers." *Nanotechnology* 14(10): R39-R54.

Hamley, I. W. **(2003 B)**. "Nanotechnology with soft materials." *Angewandte Chemie - International Edition* 42(15): 1692-1712.

Hauge, P. S. **(1980)**. " Recent developments in instrumentation in ellipsometry." *Surface Science* 96: 108-140.

Hegemann, D. **(2006)**. "Plasma polymerization and its applications in textiles." *Indian Journal of Fibre and Textile Research* 31(1): 99-115.

Heister, K., Johansson, L. S. O., Grunze, M., Zharnikov, M. **(2003)**. "A detailed analysis of the C 1s photoemission of n-alkanethiolate films on noble metal substrates." *Surface Science* 529(1-2): 36-46.

Hibbins, A. P., Sambles, J. R., Lawrence, C. R. **(2002)**. "Excitation of remarkably nondispersive surface plasmons on a nondiffracting, dual-pitch metal grating." *Applied Physics Letters* 80(13): 2410.

References

Hoa, X. D., Kirk, A. G., Tabrizian, M. **(2007)**. "Towards integrated and sensitive surface plasmon resonance biosensors: A review of recent progress." *Biosensors and Bioelectronics* 23(2): 151-160.

Homola, J. **(2006)**. *Surface Plasmon Resonance Based Sensors*. Berlin-Heidelberg, Springer.

Homola, J. **(2008)**. "Surface plasmon resonance sensors for detection of chemical and biological species." *Chemical Reviews* 108(2): 462-493.

Homola, J., Yee, S. S.,Gauglitz, G. **(1999)**. "Surface plasmon resonance sensors: review." *Sensors and Actuators B: Chemical* 54(1-2): 3-15.

Ito, T., Okazaki, S. **(2000)**. "Pushing the limits of lithography." *Nature* 406(6799): 1027-1031.

Jordan, C. E., Corn, R. M. **(1997)**. "Surface Plasmon Resonance Imaging Measurements of Electrostatic Biopolymer Adsorption onto Chemically Modified Gold Surfaces." *Anal. Chem.* 69(7): 1449-1456.

Jordan, C. E., Frutos, A. G., Thiel, A. J., Corn, R. M. **(1997)**. "Surface Plasmon Resonance Imaging Measurements of DNA Hybridization Adsorption and Streptavidin/DNA Multilayer Formation at Chemically Modified Gold Surfaces." *Anal. Chem.* 69(24): 4939-4947.

Khalil, S., Bansal, L., El-Sherif, M. **(2004)**. "Intrinsic fiber optic chemical sensor for the detection of dimethyl methylphosphonate." *Optical Engineering* 43(11): 2683-2688.

Kim, S. J., Gobi, K. V., Harada, R., Shankaran, D. R., Miura, N. **(2006)**. "Miniaturized portable surface plasmon resonance immunosensor applicable for on-site detection of low-molecular-weight analytes." *Sensors and Actuators B: Chemical* 115(1): 349-356.

Kissinger, P. **(2005)**. "Biosensors-a perspective." *Biosensors and Bioelectronics* 20: 2512-2516.

Kitson, S. C., Barnes, W. L., Sambles, J. R. **(1996)**. "Full Photonic Band Gap for Surface Modes in the Visible." *Physical Review Letters* 77(13): 2670.

Koehne, J., Li, J., Cassell, A. M., Chen, H., Ye, Q., Ng, H. T., Han, J., Meyyappan, M. **(2004)**. "The fabrication and electrochemical characterization of carbon nanotube nanoelectrode arrays." *Journal of Materials Chemistry* 14(4): 676-684.

Krämer, S., Fuierer, R. R., Gorman, C. B. **(2003)**. "Scanning probe lithography using self-assembled monolayers." *Chemical Reviews* 103(11): 4367-4418.

Krishnamoorthy, S., Himmelhaus, M. **(2008)**. "Confinement-Induced enhancement of Antigen-Antibody interactions within binary nanopatterns to achieve higher efficiency of on-chip Immunosensors." *Advanced Materials* 20: 2782-2788.

References

Kurosawa, S., Park, J. W., Aizawa, H., Wakida, S. I., Tao, H.,Ishihara, K. **(2006)**. "Quartz crystal microbalance immunosensors for environmental monitoring." *Biosensors and Bioelectronics* 22(4 SPEC. ISS.): 473-481.

Lange, U., Roznyatovskaya, N. V., Mirsky, V. M. **(2008)**. "Conducting polymers in chemical sensors and arrays." *Analytica Chimica Acta* 614(1): 1-26.

Laschi, S., Fránek, M., Mascini, M. **(2000)**. "Screen-Printed Electrochemical Immunosensors for PCB Detection." *Electroanalysis* 12(16): 1293-1298.

Law, W.-C., Markowicz, P., Yong, K.-T., Roy, I., Baev, A., Patskovsky, S., Kabashin, A. V., Ho, H.-P., Prasad, P. N. **(2007)**. "Wide dynamic range phase-sensitive surface plasmon resonance biosensor based on measuring the modulation harmonics." *Biosensors and Bioelectronics* 23(5): 627-632.

Lee, J. H., Kopecek, J., Andrade, J. D. **(1989)**. "Protein-resistant surfaces prepared by PEO-containing block copolymer surfactants." *Journal of Biomedical Materials Research* 23(3): 351-368.

Lee, K. B., Kim, E. Y., Mirkin, C. A., Wolinsky, S. M. **(2004)**. "The use of nanoarrays for highly sensitive and selective detection of human immunodeficiency virus type 1 in plasma." *Nano Letters* 4(10): 1869-1872.

Lee, K. B., Park, S. J., Mirkin, C. A., Smith, J. C., Mrksich, M. **(2002)**. "Protein nanoarrays generated by dip-pen nanotithography." *Science* 295(5560): 1702-1705.

Leggett, G. J. **(2006)**. "Scanning near-field photolithography - Surface photochemistry with nanoscale spatial resolution." *Chemical Society Reviews* 35(11): 1150-1161.

Leopold, M. C., Black, J. A., Bowden, E. F. **(2002)**. "Influence of gold topography on carboxylic acid terminated self-assembled monolayers." *Langmuir* 18: 978-980.

Lercel, M. J., Craighead, H. G., Parikh, A. N., Seshadri, K., Allara, D. L. **(1996)**. "Sub-10 nm lithography with self-assembled monolayers." *Applied Physics Letters* 68(11): 1504-1506.

Li, H., Wu, N. **(2008)**. "A large-area nanoscale gold hemisphere pattern as a nanoelectrode array." *Nanotechnology* 19(27).

Li, J., Ng, H. T., Cassell, A., Fan, W., Chen, H., Ye, Q., Koehne, J., Han, J., Meyyappan, M. **(2003)**. "Carbon Nanotube Nanoelectrode Array for Ultrasensitive DNA Detection." *Nano Lett.* 3(5): 597-602.

Li, L., Hitchcock, A. P., Robar, N., Cornelius, R., Brash, J. L., Scholl, A., Doran, A. **(2006)**. "X-ray microscopy studies of protein adsorption on a phase-segregated polystyrene/polymethyl methacrylate surface. 1. Concentration and exposure-time dependence for albumin adsorption." *Journal of Physical Chemistry B* 110(33): 16763-16773.

Lieberman, M. A., Lichtenberg, A. J. **(1994)**. *Principles of plasma discharges and materials processing* New York, Wiley.

Lim, J. H., Ginger, D. S., Lee, K. B., Heo, J.,Nam, J. M., Mirkin, C. A. **(2003)**. "Direct-write dip-pen nanolithography of proteins on modified silicon oxide surfaces." *Angewandte Chemie - International Edition* 42(20): 2309-2312.

Lisboa, P., Gilliland, D., Ceccone, G.,Valsesia, A.,Rossi, F. **(2006)**. "Surface functionalisation of polypyrrole films using UV light induced radical activation." *Applied Surface Science* 252(13 SPEC. ISS.): 4397-4401.

Liu, L., Jia, N. q, Zhou, Q., Yan, M. m, Jiang, Z. y **(2007)**. "Electrochemically fabricated nanoelectrode ensembles for glucose biosensors." *Materials Science and Engineering C* 27(1): 57-60.

Livache, T., Bazin, H., Caillat, P., Roget, A. **(1998)**. "Electroconducting polymers for the construction of DNA or peptide arrays on silicon chips." *Biosensors and Bioelectronics* 13(6): 629-634.

Livache, T., Guedon, P., Brakha, C., Roget, A., Levy, Y., Bidan, G. **(2001)**. "Polypyrrole electrospotting for the construction of oligonucleotide arrays compatible with a surface plasmon resonance hybridization detection." *Synthetic Metals* 121(1-3): 1443-1444.

Löfås, S., Johnsson, B. **(1990)**. "A novel hydrogel matrix on gold surfaces in surface plasmon resonance sensors for fast and efficient covalent immobilization of ligands." *Journal of the Chemical Society, Chemical Communications*(21): 1526-1528.

Love, J. C., Estroff, L. A., Kriebel, J. K., Nuzzo, R. G., Whitesides, G. M. **(2005)**. "Self-assembled monolayers of thiolates on metals as a form of nanotechnology." *Chemical Reviews* 105(4): 1103-1169.

Lucarelli, F., Tombelli, S., Minunni, M., Marrazza, G., Mascini, M. **(2008)**. "Electrochemical and piezoelectric DNA biosensors for hybridisation detection." *Analytica Chimica Acta* 609(2): 139-159.

Luong, J., Male, K., Glennon, J. **(2008)**. "Biosensor technology: Technology push versus market pull." *Biotechnology Advances* 26: 492-500.

Luppa, P. B., Sokoll, L. J., Chan, D. W. **(2001)**. "Immunosensors-principles and applications to clinical chemistry." *Clinica Chimica Acta* 314: 1-26.

Lupu, A., Valsesia, A., Bretagnol, F., Colpo, P., Rossi, F. **(2007)**. "Development of a potentiometric biosensor based on nanostructured surface for lactate determination." *Sensors and Actuators B: Chemical* 127(2): 606-612.

Malmsten, M., Emoto K., Van Alstine, J.M. **(1998)**. "Effect of Chain Density of Protein Adsorption by Poly(ethylene glycol) Based Coatings." *Journal of Colloid and Interface Science* 202: 507-517.

Mannelli, I., Minunni, M., Tombelli, S., Wang, R., Spiriti, M. M., Mascini, M. **(2005)**. "Direct immobilisation of DNA probes for the development of affinity biosensors." *Bioelectrochemistry* 66(1-2 SPEC. ISS.): 129-138.

References

Mascini, M., Del Carlo, M.,Minunni, M.,Chen, B.,Compagnone, D. **(2005)**. "Identification of mammalian species using genosensors." *Bioelectrochemistry* 67(2 SPEC. ISS.): 163-169.

Meadows, D. **(1996)**. "Recent developments with biosensing technology and applications in the pharmaceutical industry." *Advanced Drug Delivery Reviews* **21**(3): 179-189.

Meziani, T., Colpo, P.,Rossi, F. **(2001)**. "Design of a magnetic-pole enhanced inductively coupled plasma source." *Plasma Sources Science and Technology* 10(2): 276-283.

Minunni, M., Mannelli, I.,Spiriti, M. M.,Tombelli, S.,Mascini, M. **(2004)**. "Detection of highly repeated sequences in non-amplified genomic DNA by bulk acoustic wave (BAW) affinity biosensor." *Analytica Chimica Acta* 526(1): 19-25.

Minunni, M., Mascini, M., Guilbault, G. G.,Hock, B. **(1995)**. "The quartz crystal microbalance as biosensor. A status report on its future." *Analytical Letters* 28(5): 749-764.

Moerner, W. E. **(2007)**. " Single-molecule chemistry and biology special feature: New directions in single-molecule imaging (12596-12602) DOI: 10.1073/pnas.0610081104)." *Proceedings of the National Academy of Sciences of the United States of America* 104(39): 15584.

Moreno, J. D., Marcos, M. L.,Agulló-Rueda, F.,Guerrero-Lemus, R., Martín-Palma, R. J., Martínez-Duart, J. M., González-Velasco, J. **(1999)**. "Galvanostatic study of the electrodeposition of polypyrrole into porous silicon." *Thin Solid Films* 348(1): 152-156.

Muguruma, H. **(2007)**. "Plasma-polymerized films for biosensors II." *TrAC - Trends in Analytical Chemistry* 26(5): 433-443.

Mullett, W. M., Lai, E. P. C.,Yeung, J. M. **(2000)**. "Surface Plasmon Resonance-Based Immunoassays." *Methods* 22(1): 77-91.

Myszka, D. G. **(1997)**. "Kinetic analysis of macromolecular interactions using surface plasmon resonance biosensors." *Current Opinion in Biotechnology* 8(1): 50-57.

Myszka, D. G. **(1999)**. "Survey of the 1998 optical biosensor literature." *Journal of Molecular Recognition* 12(6): 390-408.

Nagaoka, S., Nakao, A. **(1990)**. "Clinical application of antithrombogenic hydrogel with long poly(ethylene oxide) chains." *Biomaterials* 11(2): 119-121.

Navani, N. K., Li, Y. **(2006)**. "Nucleic acid aptamers and enzymes as sensors." *Current Opinion in Chemical Biology* 10(3): 272-281.

Oh, B. K., Kim, Y. K., Park, K. W., Lee, W. H., Choi, J. W. **(2004)**. "Surface plasmon resonance immunosensor for the detection of Salmonella typhimurium." *Biosensors and Bioelectronics* 19(11): 1497-1504.

References

Paleček, E., Jelen, F. **(2002)**. "Electrochemistry of nucleic acids and development of DNA sensors." *Critical Reviews in Analytical Chemistry* 32(3): 261-270.

Park, J., Moon, J. **(2006)**. "Control of colloidal particle deposit patterns within picoliter droplets ejected by ink-jet printing." *Langmuir* 22(8): 3506-3513.

Park, S., Lee, G., Song, S. H., Oh, C. H., Kim, P. S. **(2003)**. "Resonant coupling of surface plasmons to radiation modes by use of dielectric gratings." *Optics Letters* 28(20): 1870-1872.

Parkin, M. C., Hopwood, S. E., Boutelle, M. G.,Strong, A. J. **(2003)**. "Resolving dynamic changes in brain metabolism using biosensors and on-line microdialysis." *TrAC - Trends in Analytical Chemistry* 22(9): 487-497.

Polzius, R., Schneider, T., Bier, F. F., Bilitewski, U.,Koschinski, W. **(1996)**. "Optimization of biosensing using grating couplers: Immobilization on tantalum oxide waveguides." *Biosensors and Bioelectronics* 11(5): 503-514.

Pretsch, E., Clerc, T., Seibl, J., Simon W. (1985). Tablas para la elucidacion estructural de compuestos organicos por metodos espectroscopicos, Editorial Alhambra,S.A.**:** H95.

Prime, K. L., Whitesides, G. M. **(1991)**. "Self-assembled organic monolayers: Model systems for studying adsorption of proteins at surfaces." *Science* 252(5010): 1164-1167.

Prime, K. L., Whitesides, G. M. **(1993)**. "Adsorption of proteins onto surfaces containing end-attached oligo(ethylene oxide): A model system using self-assembled monolayers." *Journal of the American Chemical Society* 115(23): 10714-10721.

Raiteri, R., Grattarola, M., Berger, R. **(2002)**. "Micromechanics senses biomolecules." *Materials Today* 5: 22-29.

Ramanavičius, A., Ramanavičiene, A., Malinauskas, A. **(2006)**. "Electrochemical sensors based on conducting polymer-polypyrrole." *Electrochimica Acta* 51(27): 6025-6037.

Rasooly, A., Jacobson, J. **(2006)**. "Development of Biosensors for cancer clinical testing." *Biosensors and Bioelectronics* 21: 1851-1858.

Ratner, B. D. **(1995)**. "Plasma deposition of organic thin films for surface modification." *Journal of Photopolymer Science and Technology* 8: 481-494.

Reiter, S., Habermüller, K., Schuhmann, W. **(2001)**. "A reagentless glucose biosensor based on glucose oxidase entrapped into osmium-complex modified polypyrrole films." *Sensors and Actuators B: Chemical* 79(2-3): 150-156.

Reviakine, I., Brisson, A. **(2001)**. "Streptavidin 2D crystals on supported phospholipid bilayers: Toward constructing anchored phospholipid bilayers." *Langmuir* 17(26): 8293-8299.

Ricci, F., Volpe, G., Micheli, L., Palleschi, G. **(2007)**. "A review on novel developments and applications of immunosensors in food analysis." *Analytica Chimica Acta* 605(2): 111-129.

Rich, R. L., Myszka, D. G. **(2007)**. "Higher-throughput, label-free, real-time molecular interaction analysis." *Analytical Biochemistry* 361(1): 1-6.

Rich, R. L., Myszka, D. G. **(2005)**. "Survey of the year 2004 commercial optical biosensor literature." *Journal of Molecular Recognition* 18(6): 431-478.

Rodriguez-Mozaz, S., López de Alda,M., Marco,M.,Barceló, D. **(2005)**. "Evaluation/Validation of Novel Biosensors in Real Environmental and Food Samples." *Talanta* 65: 291-297.

Rogers, K. R., Mascini, M. **(1998)**. "Biosensors for field analytical monitoring." *Field Analytical Chemistry & Technology* 2(6): 317-331.

Rosi, N. L., Mirkin, C. A. **(2005)**. "Nanostructures in biodiagnostics." *Chemical Reviews* 105(4): 1547-1562.

Saah, A. J., Hoover, D. R. **(1997)**. ""Sensitivity" and "Specificity" Reconsidered: The Meaning of These Terms in Analytical and Diagnostic Settings." *MEDICAL WRITINGS* 126 91-94.

Sandison, M. E., Cooper, J. M. **(2006)**. "Nanofabrication of electrode arrays by electron-beam and nanoimprint lithographies." *Lab on a Chip - Miniaturisation for Chemistry and Biology* 6(8): 1020-1025.

Sardella, E., Gristina, R., Senesi, G. S., D'Agostino, R., Favia, P. **(2004)**. "Homogeneous and micro-patterned plasma-deposited PEO-like coatings for biomedical surfaces." *Plasma Processes and Polymers* 1(1): 63-72.

Sauerbrey, G. **(1959)**. "Verwendung von Schwingquarzen zur Wägung dünner Schichten und zur Mikrowägung." *Zeitschrift für Physik* 155: 206-222

Schasfoort, R. B. M., Tudos, A. J. **(2008)**. *Handbook of Surface Plasmon Resonance*. Cambridge, RSC Publishing.

Shankaran, D. R., Matsumoto, K., Toko, K., Miura, N. **(2006)**. "Development and comparison of two immunoassays for the detection of 2,4,6-trinitrotoluene (TNT) based on surface plasmon resonance." *Sensors and Actuators B: Chemical* 114(1): 71-79.

Sheehan, P. E., Whitman, L. J. **(2005)**. "Detection limits for nanoscale biosensors." *Nano Letters* 5(4): 803-807.

Silverstein, R. M., Webster, F. X. **(1997)**. *Spectrometric Identification of Organic Compounds*. New York, Wiley & Sons

Silverton, E. W., Navia, M. A., Davies, D. R. **(1977)**. "Three dimensional structure of an intact human immunoglobulin." *Proceedings of the National Academy of Sciences of the United States of America* 74(11): 5140-5144.

Smith, R. K., Lewis, P. A., Weiss, P. S. **(2004)**. "Patterning self-assembled monolayers." *Progress in Surface Science* 75(1-2).

Sofia, S. J., Premnath, V., Merrill, E. W. **(1998)**. "Poly(ethylene oxide) grafted to silicon surfaces: Grafting density and protein adsorption." *Macromolecules* 31(15): 5059-5070.

Song, H. K., Toste, B., Ahmann, K., Hoffman-Kim, D., Palmore, G. T. R. **(2006)**. "Micropatterns of positive guidance cues anchored to polypyrrole doped with polyglutamic acid: A new platform for characterizing neurite extension in complex environments." *Biomaterials* 27(3): 473-484.

Spangler, B. D., Wilkinson, E. A.,Murphy, J. T.,Tyler, B. J. **(2001)**. "Comparison of the Spreeta® surface plasmon resonance sensor and a quartz crystal microbalance for detection of Escherichia coli heat-labile enterotoxin." *Analytica Chimica Acta* 444(1): 149-161.

Stewart, M. E., Mack, N. H., Malyarchuk, V., Soares, J. A. N. T., Lee, T. W., Gray, S. K., Nuzzo, R. G., Rogers, J. A. **(2006)**. "Quantitative multispectral biosensing and 1D imaging using quasi-3D plasmonic crystals." *Proceedings of the National Academy of Sciences of the United States of America* 103(46): 17143-17148.

Thévenot, D. R., Toth, K., Durst, R. A., Wilson, G. S. **(2001)**. "Electrochemical biosensors: Recommended definitions and classification." *Biosensors and Bioelectronics* 16(1-2): 121-131.

Tietje-Girault, J., Ponce de León, C., Walsh, F. C. **(2007)**. "Electrochemically deposited polypyrrole films and their characterization." *Surface and Coatings Technology* 201(12): 6025-6034.

Tokumitsu, S., Liebich, A., Herrwerth, S., Eck, W., Himmelhaus, M., Grunze, M. **(2002)**. "Grafting of alkanethiol-terminated poly(ethylene glycol) on gold." *Langmuir* 18(23): 8862-8870.

Tom-Moy, M., Baer, R. L., Spira-Solomon, D., Doherty, T. P. **(1995)**. "Atrazine measurements using surface transverse wave devices." *Analytical Chemistry* 67(9): 1510-1516.

Tombelli, S., Mascini, M., Turner, A. P. F. **(2002)**. "Improved procedures for immobilisation of oligonucleotides on gold-coated piezoelectric quartz crystals." *Biosensors and Bioelectronics* 17(11-12): 929-936.

Tombelli, S., Minunni, M. Luzi, E.,Mascini, M. **(2005)**. "Aptamer-based biosensors for the detection of HIV-1 Tat protein." *Bioelectrochemistry* 67(2): 135-141.

Tu, Y., Lin, Y., Yantasee, W., Ren, Z. **(2005)**. "Carbon nanotubes based nanoelectrode arrays: Fabrication, evaluation, and application in voltammetric analysis." *Electroanalysis* 17(1): 79-84.

Udd, E. **(1995)**. "An overview of fiber-optic sensors." *Review of Scientific Instruments* 66(8): 4015-4030.

References

Unsworth, L. D., Sheardown, H.,Brash, J. L. **(2005)**. "Protein resistance of surfaces prepared by sorption of end-thiolated poly(ethylene glycol) to gold: Effect of surface chain density." *Langmuir* 21(3): 1036-1041.

Unsworth, L. D., Tun, Z., Sheardown, H., Brash, J. L. **(2005)**. "Chemisorption of thiolated poly(ethylene oxide) to gold: surface chain densities measured by ellipsometry and neutron reflectometry." *Journal of Colloid and Interface Science* 281(1): 112-121.

Updike, S. J., Hicks, G. P. **(1967)**. "The enzyme electrode." *Nature* 214(5092): 986-988.

Valsesia , A. **(2008 A)**. Fabrication of nanostructured surfaces for the development of advanced biointerfaces. *Dipartimento di Fisica "A .Volta"*. Pavia, Università degli studi di Pavia. PhD.

Valsesia, A., Colpo, P., Mannelli, I., Mornet, S., Bretagnol, F., Ceccone, G., Rossi, F. **(2008 B)**. "Use of nanopatterned surfaces to enhance immunoreaction efficiency." *Analytical Chemistry* 80(5): 1418-1424.

Valsesia, A., Colpo, P., Meziani, T., Lisboa, P., Lejeune, M., Rossi, F. **(2006)**. "Immobilization of antibodies on biosensing devices by nanoarrayed self-assembled monolayers." *Langmuir* 22(4): 1763-1767.

Vogel, A. I. **(1961)**. *A text-book of pratical organic chemistry*. London and Colchester, Longmans.

Vörös, J., Blättler, T., Textor, M. **(2005)**. "Bioactive patterns at the 100-nm scale produced using multifunctional physisorbed monolayers." *MRS Bulletin* 30(3): 202-206.

Wang, J. **(2006)**. *Analytical Electrochemistry.* NY, Wiley-VCH.

Wedge, S., Giannattasio, A., Barnes, W. L. **(2007)**. "Surface plasmon-polariton mediated emission of light from top-emitting organic light-emitting diode type structures." *Organic Electronics: physics, materials, applications* 8(2-3): 136-147.

West, K., Jacobsen, T., Zachau-Christiansen, B., Careem, M. A., Skaarup, S. **(1993)**. "Electrochemical synthesis of polypyrrole: Influence of current density on structure." *Synthetic Metals* 55(2-3): 1412-1417.

Whelan, C. M., Ghijsen, J., Pireaux, J. J., Maex, K. **(2004)**. "Cu adsorption on carboxylic acid-terminated self-assembled monolayers: A high-resolution X-ray photoelectron spectroscopy study." *Thin Solid Films* 464-465: 388-392.

Whitesides, G. M., Ostuni, E., Takayama, S., Jiang, X., Ingber, D. E. (2001). Soft lithography in biology and biochemistry. Annual Review of Biomedical Engineering. **3:** 335-373.

Wilchek, M., Miron, T. **(2003)**. "Oriented versus random protein immobilization." *Journal of Biochemical and Biophysical Methods* 55(1): 67-70.

Wilson, G. S., Gifford, R. **(2005)**. "Biosensors for real-time in vivo measurements." *Biosensors and Bioelectronics* 20(12): 2388-2403.

Xia, Y., Whitesides, G. M. **(1998)**. "Soft lithography." *Angewandte Chemie - International Edition* 37(5): 551-575.

Yang, D. Y., Tsai, T. H., Cheng, C. H., Lee, C. W., Chen, S. H., Cheng, F. C. **(2001)**. "Simultaneous monitoring of extracellular glucose, pyruvate, lactate and glutamate in gerbil cortex during focal cerebral ischemia by dual probe microdialysis." *Journal of Chromatography A* 913(1-2): 349-354.

Yang, M., Qu, F., Lu, Y., He, Y., Shen, G., Yu, R. **(2006)**. "Platinum nanowire nanoelectrode array for the fabrication of biosensors." *Biomaterials* 27(35): 5944-5950.

Yang, S. M., Jang, S. G., Choi, D. G., Kim, S., Yu, H. K. **(2006)**. "Nanomachining by colloidal lithography." *Small* 2(4): 458-475.

Yasuda, H., Gazicki, M. **(1982)**. "Biomedical applications of plasma polymerization and plasma treatment of polymer surfaces." *Biomaterials* 3(2): 68-77.

Yasuda, H., Matsuzawa, Y. **(2005)**. "Economical advantages of low-pressure plasma polymerization coating." *Plasma Processes and Polymers* 2(6): 507-512.

Yasuzawa, M., Matsuki, T.,Mitsui, H.,Kunugi, A.,Nakaya, T. **(2000)**. "Properties of glucose sensors prepared by the electropolymerization of pyrroles containing phosphatidylcholine (II)." *Sensors and Actuators B: Chemical* 66: 25-27.

Yu, P., Wilson, G. S. **(2000)**. "An independently addressable microbiosensor array: What are the limits of sensing element density ?" *Faraday Discussions* 116: 305-317.

8 Conclusions

8.1 General Conclusions

Sensors based on biomolecular recognition are very promising tools for the development of advanced analytical devices. Nevertheless, biosensors do not generally have all the necessary performance to be applied extensively for very demanding domains such as early diagnostics and environment monitoring. To fulfil the performance requirements, it is necessary to develop highly sensitive, fast and low cost biosensor devices. This need has consequently created numerous research programs aiming at improving the sensitivity, specificity and limit of detection of biosensors. Among all components to optimize, the sensor surface chemistry represents one of the principal bottleneck since it must guaranty the bioactivity performance of the bio-detector on the transducer surface.

The aim of this thesis was to develop of advanced nanostructured surfaces to enhance SPRi detection sensitivity and performance.

The strategy chosen was based on nano-patterning of surfaces in domains having similar length scale as the ones of the biomolecules.

The first objective was to develop nanoarrays with bio-adhesive/non-adhesive nano-contrasts in order to induce selective immobilisation of proteins in the specific adhesive areas, improving their bio-activity.

The second objective was to use the 2D crystalline organisation nanoarrays for the creation of an optical grating at the interface of the SPRi chip, improving the sensitivity of detection of the instrument.

Nanoarrays have been fabricated by using organothiols chemistry and electrochemical copolymerisation of PPy functionalised with biomolecules.

In both cases the fabrication was based on colloidal lithography, a parallel fabrication method which presents many advantages such as flexibility, low cost and easy implementation. This technique uses nanoparticles as nano-masks during etching and

deposition processes Crystalline arrangements of the nanospheres on the surface is used to produce nanoarrays with lattices dependent on the colloids size.

The organothiols is a simple and fast method for producing a surface with a controlled chemistry and turns out to be an adequate material to create nanoarrays with chemical contrast. Organothiol nanoarrays with an adhesive/non-adhesive contrast were produced with 500nm beads . These nanoarrays were used to selectively immobilise proteins and functionalised nanoparticles, via electrostatic interaction, in the adhesive areas of the surface.

Nano-template with conductive nano-scale areas on an insulating matrix were also developed to grow PPy by electrodeposition on the specific conductive areas, thus creating PPy arrays. In the case of PPy nanoarray, the bio-detectors were covalently bonded to the pyrrole and grown together with the polymer during polymerisation, creating immediately protein functionalised-PPy domains.

Colloidal lithography and plasma processes combined with SAMs and electrochemical deposition of polymers demonstrated to be a successful approach to create different types of nanoarrays.

The behaviour of these surfaces during detection of immunoreactions by SPRi was studied as a function of their properties.

The results of the SPRi study demonstrate that the organothiols nanoarray improved the SPRi detection sensitivity of an immunoreaction as compared to a uniformly functionalised surface. This improvement is attributed to two reasons:

1) Improvement of the binding sites availability of the bio-detector on the surface which results in an increase of the efficiency of the bio recognition. This increased availability can be attributed to the reduction of the steric hindrance of the molecules thanks to the adhesive-non-adhesive pattern. Furthermore, the limited space available due to the confinement effect is expected to prevent proteins denaturation.

2) The creation of optical gratings that interact with SPRi detection improve the detection signal. The proteins immobilisation on the nanoarrayed surface creates a crystalline distribution of domains of different refractive index forming an optical grating above the gold film. The optical grating leads to a positive interaction with the surface plasmon wave.

This interaction is related to the fact that the lattice constant of the protein domains array is of the same order of magnitude as the surface plasmon wavelength (respectively 500 nm and 650 nm). The interaction results in high changes in the surface plasmon coupling conditions and induces higher reflectivity changes, which results in a better signal sensitivity.
PPy nanoarrays provided lower efficient amplification which is however improved when the matrix that surrounds the nano areas of PPy is covered with anti adhesive layer. The lower effect observed could be attributed to the poor optical contrast present on the surface due to a more complex geometry created during the nanoarray formation. Moreover, the geometry of the array could also create accessibility problems to the proteins to reach the bio-detector immobilised on the PPy matrix.
More generally, the results obtained indicate that SPRi detection performance can be improved by the rational functionalisation of the sensor surface with nanopatterns, characterised by spacing of the order of magnitude of the wavelength of the surface plasmon wave. Furthermore adhesive/non-adhesive nano-patterns induce better availability of the biomolecules on the surface improving the efficiency of the reactions.
The developed nanoarrays can be used as basis to solve different analytical problems where the analyte detection is based in immunoreactions. In addition the optimisation of the sensor like concentration of the bio-detector, concentration of the blocking should be handed value to the optical amplification.

8.2 Perspectives and future work

This thesis opens new perspectives for the development of high performance biosensors.

First it underlines the importance and potentiality of surface chemistry to enhance the sensitivity of detection. Nano-patterned surfaces were found to improve immunoreaction efficiency and reactive sites availability. The Plasmon coupling with the nanoarrays was found to be an efficient effect to increase the signal detected by almost an order of magnitude in the conditions tested.

However, many questions still need to be resolved. For instance, the ratio between the grating lattice constant and the light wavelength has to be better understood, in order to maximize the interaction between the grating and the surface plasmons. For our experimental conditions (810 nm), the optimum lattice constant should be around 300nm meaning that should be used 300nm nanoparticles for the colloidal lithography process. To change size of the colloids, the production steps have to be newly studied and optimized (smaller nanoparticles are more difficult to assemble on large surfaces with a good coverage). Maximising the interaction can also be achieved by maintaining the nanoarrays lattice constant at 500 nm and by increasing the wavelength toward infrared light. This would imply a modification of the optical set up and a different CCD camera for imaging.

Another interesting point is related to the plasmon coupling efficiency that can be achieved depending on the structure of the 2D array: it is expected that quadratic, cubic or center-faced cubic arrangement will lead to different coupling efficiencies.

An additional point for future development is related to the lithography technique used in this work. Colloidal lithography is widely used thanks to its easiness of implementation and low costs. Nevertheless, transferring this technique to industrial fabrication can be problematic because of poor reproducibility. Other nanofabrication techniques could be used to produce the nanoarrays, for instance a physical shadow mask for creating the pattern, but this technique is expensive when high resolution is required. Nano imprint lithography could also be possible when the technique has gained a better maturity.

Finally the application of different biomolecules immobilisation techniques or bio-assay formats can improve detection performance of the developed systems. For instance covalent binding can be a technique of choice to improve the robustness of the system based on organothiols and the use of sandwich assays could improve the signal of detection in the PPy based system due to an increase in biomolecules thickness and a better Plasmon coupling.

However, this work has demonstrated the interest of nanotechnology techniques for the development oh high sensitivity sensors. Even if many aspects are still to be clarified and the technique further optimised, the interest of nano-patterned surfaces is evident and we can expect this technique to be caught progressively in the future, due to the potential it represents in terms of cost and performance.